MICROSTRUCTURAL CHARACTERISTICS, WEAR AND CORROSION BEHAVIOUR OF HVOF AND HVAF SPRAYED CERMET COATINGS

Teză destinată obţinerii
titlului ştiinţific de doctor inginer
la
Universitatea Politehnica Timişoara
în domeniul ȘTIINȚA ȘI INGINERIA MATERIALELOR
de către

Ing. Iosif Hulka

Conducător ştiinţific:	prof.univ.dr.ing. Viorel Aurel Șerban
Referenţi ştiinţifici:	prof.univ.dr.ing Waltraut Brandl
	prof.univ.dr.ing. Ioan Vida-Simiti
	conf.univ.dr.ing. Ion Mitelea

Ziua susţinerii tezei: 25.01.2013

Seriile Teze de doctorat ale UPT sunt:

1. Automatică
2. Chimie
3. Energetică
4. Ingineria Chimică
5. Inginerie Civilă
6. Inginerie Electrică
7. Inginerie Electronică şi Telecomunicaţii
8. Inginerie Industrială
9. Inginerie Mecanică
10. Ştiinţa Calculatoarelor
11. Ştiinţa şi Ingineria Materialelor

Universitatea Politehnica Timişoara a iniţiat seriile de mai sus în scopul diseminării expertizei, cunoştinţelor şi rezultatelor cercetărilor întreprinse în cadrul şcolii doctorale a universităţii. Seriile conţin, potrivit H.B.Ex.S Nr. 14 / 14.07.2006, tezele de doctorat susţinute în universitate începând cu 1 octombrie 2006.

România, 300159 Timişoara, Bd. Republicii 9,
tel. 0256 403823, fax. 0256 403221
e-mail: editura@edipol.upt.ro

Foreward

The present thesis was elaborated during my activity at the Politehnica Univeristy Timișoara, in cooperation with Tampere Univeristy of Technology, Finland. It brings together accumulated knowledge on cermet coatings and wear and corrosion resistance of coaintgs.

The thesis adresses materials engineeris and all interested in knowing and understandig wear and corrosion resistant cermet coatings deposited on low carbon steel through High Velocity Oxygen Fuel and High Velocity Air Fuel spraying techniques. The deposition tecniques, tribological and corrosion mechanisms, morpholgy and properties of coatings, characterization and investigation of coatings are described and discussed. One aim of the thesis has been to bring together briefly the state of the art knowledge on modern thermal spraynig techniques and technology and study conventional and as well new tungsten carbide and chromium carbide powders and coaitings. It presents also the oportunity the deposit cermet coatings through High Velocity Air Fuel, as an economical alternative to High Velocity Oxygen Fuel thermal spraying technique.

I believe that the present thesis represents a solid scientific support for future research and industrial applications having as theme microstructural characteristic, wear and corrosion behaviour of cermet coatings deposited through High Velocity Oxygen Fuel and High Velocity Air spraying techniques.

Timişoara, Ianuarie 2013 Iosif Hulka

Acknowledgments

I would like to express my sincer gratitude to my scientific supervisors, Prof. Dr. Eng Vioarel-Aurel Șerban, Prof. Dr. Eng. Petri Vuoristo and Dr. Kari Niemi for their encuragment and guidance through the achievement of my PhD thesis, and for their invaluable suggestions and unwavering suport.

My honest gratefulness to Fincoat Oy, Finland and Mr. Mikko Kylmälahti for the thermal spray depositions, Andrea Milanti, Matikainen Ville, Niko Syren and Jussi Laurila for introducing me the equipment needed for my experiments at Tampere Univeristy of Technology.

And last but not least, I would like to thank Dr. Eng. Heli Koivuluoto for conducting the salt spray tests, Dr. Eng. Dragoș Uțu for his wise words and also many thanks to my friends and coleagues.

Hulka, Iosif

Microstructural Characteristics, Wear and Corrosion Behaviour of HVOF and HVAF Sprayed Cermet Coatings

Teze de doctorat ale UPT, Seria 11, Nr. 31, Editura Politehnica, 2013,
132 pagini, 120 figuri, 34 tabele.
ISSN: 1842-7855

ISBN: 978-606-554-610-3

Cuvinte cheie: Thermal spraying, HVOF, HVAF, cermet, WC/CrC based coatings, wear resistance, corrosion behaviour.

Rezumat,

The present thesis approaches an important domain of Materials Science and Engineering namely that of thermally sprayed WC and CrC cermet based coatings with high density, good adhesion to the substrate, reduced porosity and also a relatively reduced decarburisation level due to modern HVOF and HVAF thermal spraying techniques. This type of coatings have a wide range of application, especially in the past decade, in various industrial fields like aeronautics, automotive, petro-chemical, cellulose, energetics, chemical industry, etc. The deposited coatings aim to increase the lifetime of various components subjected to severe working conditions and also to recondition worn parts.

This work presents research studies conducted on cermet coatings like WC-10Co-4Cr, Cr3C2-25NiCr, Cr3C2-37WC-18M and WC-FeCrAl in order to obtain protective coatings deposited using the HVAF spraying process comparable in terms of microstructure, wear and corrosion resistance with coatings deposited using the HVOF spraying process but having as advantage a relativelly lower manufacturing cost due to the use of air as combustion gas.

CONTENT

List of Figures

List of Tables

CHAPTER I. LITERATURE REVIEW

1.1 Introduction to thermal spraying

Thermal spraying is a deposition technique in which molten, semi-molten or solid particles are deposited on a surface [1]. The new deposited coating, results from the impact of accelerated droplets on the substrate, where the particles flow into thin lamellar shapes, overlap and interlock as they are cooling down and solidify [2]. A device called spray gun or torch accelerates the particles. The feedstock material is in the form of stick (rod), wire and powder which is fed into the flame produced by the spraying gun. The high temperature and kinetic energy of the gun is obtained with burning mixtures of different fuel gases or kerosene with oxygen, or by using electrical power sources. According to S. Grainger and J. Blunt [3], there are several characteristic which distinguish thermal spray processes from weld-overlay. The applied coatings are much thinner than welded coatings, but also the coating thickness can be increased function of the spraying process. Substrate adhesion is dependent on the feedstock material and its properties and it can be characterized as a mechanical bounding compared to metallurgical bonding found in weld overlay coatings. Thermal spraying allows the deposition of almost all materials including ceramics, plastics, cermets and metals on a cold substrate in order to avoid distortion, metallurgical degradation or dilution of substrate. As a disadvantage of the process is the line-of-sight spraying which means that only the surfaces exposed to the spraying nozzle are covered. Also the size limitation is a problem, making difficult to spray small components, deep cavities, holes, and other surfaces with limited access to the gun. Due to new robot system the spraying guns can be manipulated in such a way that also components with a complex geometry can be deposited [3]. The thickness can be established function of used feedstock, spraying process, application and it is generated in multiple passes of the spraying gun.

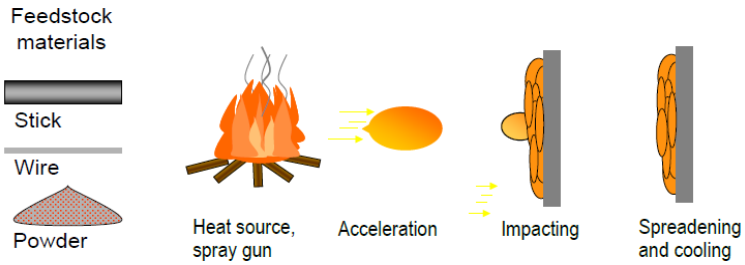

Figure 1.1 Schematics of thermal spraying presenting the heating of the feedstock material, acceleration of the particles and impact at the surface [4]

The thermal spraying has three major advantages. According to C. Robert and Jr. Tucker from Praxair Surface Technology, Inc. this advantages are: an extremely wide variety of materials that can be deposited; a second advantage is the ability of the process to apply coatings on a substrate without significantly heating it which allows the deposition of protective layers on finally machined, heat treated industrial components without changing the properties of the component and without inducing thermal distortion; the third advantage is the ability to strip and recoat worn or damaged components without changing the properties of the component [5].

1.2 Brief history of thermal spraying

Thermal spraying was invented by the Swiss Dr. Max Ulrich Schoop in the early 1900 after his study on lead cannon balls which adhered to vertical surfaces after firing. In figure 1.2 are presented Dr. Schoop and the first thermal spray system. In 1911 Scoop applied the first tin and lead coatings onto metal surfaces in order to improve corrosion performance [6]. In 1926, T.H. Turner and N.F. Budgen published a book named "Metal Spraying" which was one of the first books in this new developed field reedited in 1963 with a new title " Metal Spraying and the Flame deposition of ceramics and plastics" to reflect the shift from metals to other materials [7].

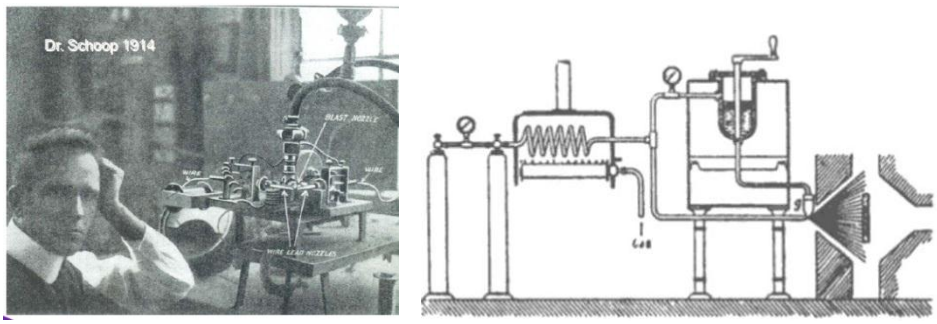

Figure 1.2 Dr. Schoop and the Schoop Process for the production of metallic coatings [8]

After the development of the first spray system in the next years the development of new processes was reatively lower and just after 1950 the spray sistems started to evolve and divide in a largy variety of new processes. In table 1.1 are presented the first pattents related to thermal spraying, classified according to acceptance date. One of the first and most important patternts in this field is entitled "*Improvements in or connected with the coating of surface with metal, applicable also for Soldering or Uniting Metals and other Materials (Master Patent for molten metal spraying)*" writen by M.U. Schoop. This work is basically the foundation of nowadays used - state of the art -thermal spray processes.

Table 1.1. Patents in thermal spray equipment and processes [8]

Patent No	Accepted Date	Authors	Title
UK 5.712	26.01.1911	M.U. Schoop	Improvements in or connected with the coating of surface with metal, applicable also for Soldering or Uniting Metals and other Materials (Master Patent for molten metal spraying)
1.002.721	05.09.1911	E.A. Mathers	Electric Arc Furnace Heater
UK 21.066	23.09.1912	M.U. Schoop	An Improuved Process of Applying of Metal or Metallic Compounds to Surfaces (Master Patent for powder metal spraying)
UK 28.001	29.05.1913	E. Morf	A method of producing bodie and coatings of glass and other substances (Master Patent for wire spraying)
1.262.134	09.04.1918	G. Stolle	Apparatus for Making Metallic Coatings
1.968.329	31.07.1934	D.D. Taylor	Metal spraying apparatus
2.858.411	28.10.1955	R.M Gage	Arc Torch and Process
2.858.412	28.10.1958	G.M. Giannini, A.C. Ducati	Plasma Steam Apparatus and Method
2.858.412	28.10.1958	J.S. Kane, C.W. Hill	Plasma flame generator

Figure 1.3 offers an overview about the development of thermal spray technology. It presents the applications and devices developed by entrepreneur or companies during the time, starting with the first spray system developed by Dr. Schoop until the newest spray systems which are used nowadays. A significant number of new patents ware developed in the field of plasma spraying after the development of Detonation Gun, by Union Carbide Corporation. The technological growth was attributed to the deposition of thermal barrier coatings based on stabilized zirconia.
A second growth occurred in the 1980s with the invention of vacuum plasma spraying and low pressure plasma spraying. Also, during that time the first high velocity oxygen fuel HVOF spray system, Jet Kote, was developed by Browning Engineering, Enfield, SUA [7]. The first cold gas sprays system and High Velocity Air Fuel systems were discovered also at the late 1980s. Since then further increase in the rate of technological innovations include new developed spray systems, new guns, feedstock feeders and more precise control units and new feedstock materials.

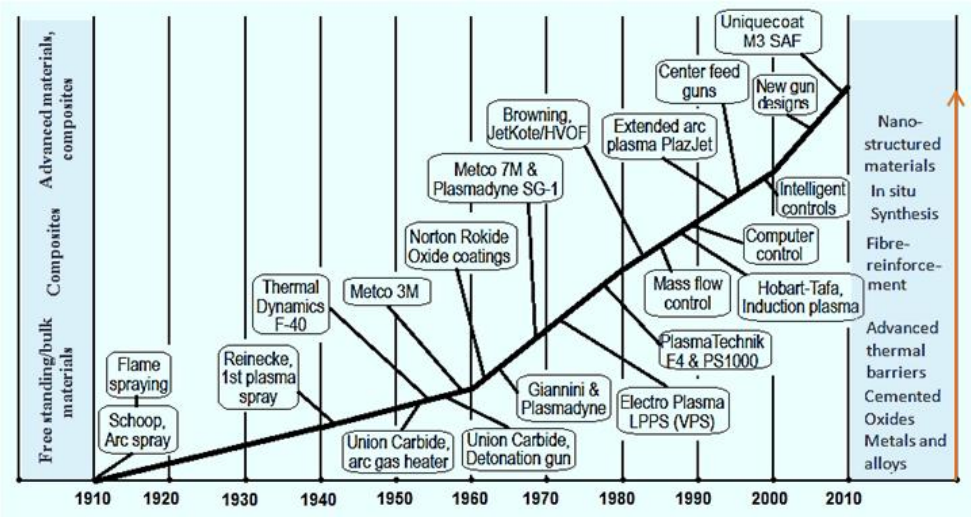

Figure 1.3 Thermal spraying milestones [9]

1.3 Classification of thermal spray processes

Based on the energy source, thermal spraying techniques can be classified into a few main groups: energy from molten liquid, energy from combustion of gases, kinetic energy, energy from electric discharge and energy from beans [10]. Each of this group encompasses many more subsets, and each subset has its own characteristic like velocity, enthalpy and temperature. This characteristics influence the quality and properties of the coatings and they are unique to each process. These include the adhesion of the coating to the substrate, porosity, intern-splat bonding, oxides, harness, brittleness and toughness.

It was demonstrated that for some thermally sprayed coatings, decarburization occurs during the spraying process that affects the microstructure reducing the hardness and the wear resistance of the deposited coating [8]. This fact is influenced by the spraying conditions like high temperatures, an oxidizing atmosphere and high cooling rates, which means that the coating is subjected to complex physical and chemical transformation during spraying. It is hard to say which one is the best spraying method among the presented techniques.

The selection of the proper spraying technique depends on application type, material to be coated, feedstock material, size and shape of component (there might be small samples which need protection which can be sprayed into special designed chambers or big parts like metallic bridges which need to be sprayed outside) , etc.

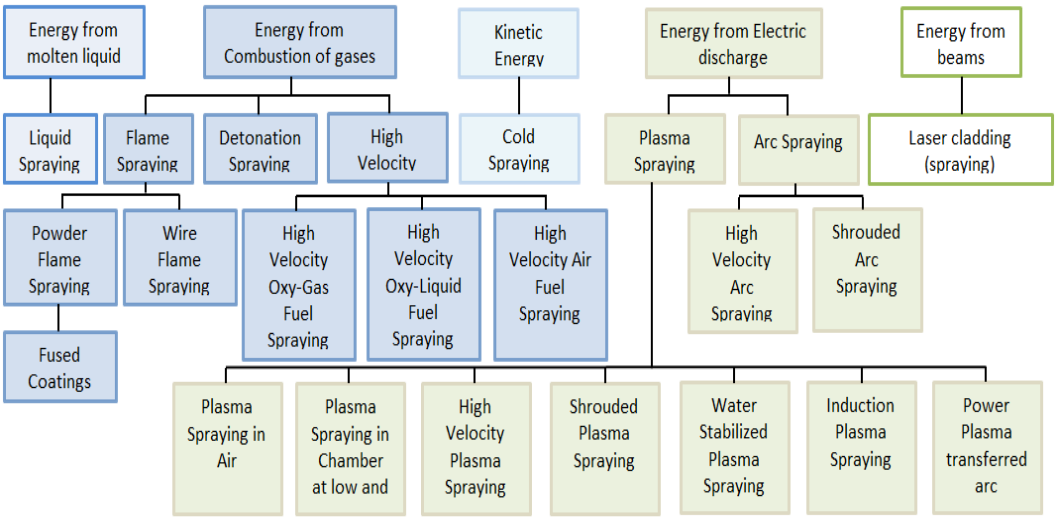

Figure 1.4 Classification of thermal spray processes according to various types of energy sources [10]

1.4 Thermal spraying equipment

When is about to produce thermal spray coatings there are few requirements regarding the necessary equipment. Every thermal spraying system is composed of three main groups of components. These groups are the core components, the handling system and the peripheral equipment (figure 1.5).
The core components are the "heart" of the system and are composed of the spray gun, control unit, powder feeder, power supply and the feedstock material.
The handling system includes the gun manipulator, work-piece manipulator and handling controller. The gun manipulator might be a robot, an automated device or in some cases the gun might be manipulated by hand by a qualified operator. The peripheral equipment includes a sound proof cabin, cooling unit, filter and exhaust system.

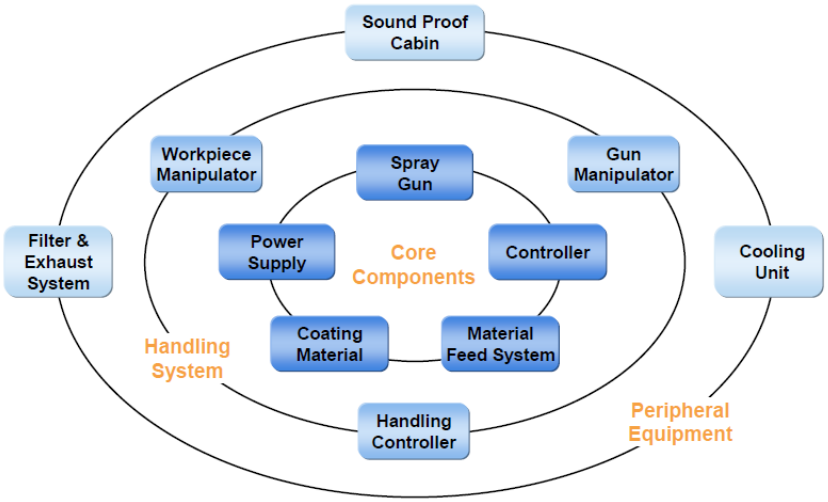

Figure 1.5 Key elements in thermal spray process (courtesy of Sulzer Metco)

1.5 The structure of thermally sprayed coatings

Thermal spraying processes allow building up coatings from the rapid solidifying droplets which are flattened from striking the substrate. A typical structure for a coating is a pancake-like structure as it is illustrated in figure 1.6. The microstructure of thermal spray coatings might include unmelted particles, porosity, cracks forming an inhomogeneous structure which allows the aggressive corrosion agents to reach the substrate by penetrating the protective layer [12]. Ceramic coatings contain cracks due to relaxation of stress after spraying and the metallic coatings usually contain oxides due to the oxidation process which took place during spraying [13]. The oxidation is caused because the hot particles are exposed to air atmosphere, which results in oxide layers at splat boundaries [12]. The porosity found in the coatings is divided in three groups according to Kulkami et al., into globular pores, interlamelar pores and intrasplat cracks [14]. Globular pores are formed by the incomplete melting or fast solidification of the particles. Interlamelar pores are formed by a reduced cohesion between the splats and they are parallel to the coated substrate. Intrasplat cracks are formed by the stress relaxation during the cooling process due to a different coefficient of thermal expansion and they are characterized by the perpendicular position to the splat interface [15, 16, 17]. The difference between the pores is attributed to the melting stage and the thermal spray processes used for the deposition. According to Pawlowski, the porosity in coatings is in the range of 1 up to 23%; the difference being caused by the feedstock material and deposition process.
According to [1] there are several mechanisms of coating-substrate adhesion like mechanical interlocking, physical bounding and chemical-metallurgical bonding. If the spraying process has a relatively low velocity the adhesion between the coating and substrate depends on the mechanical interlocking formed due to roughness of the substrate and solidification of the droplet, except when VPS or LPPS spraying is used to deposit the coating [18]. Yang, noticed that the adhesive strength can be

enhanced with the improvement of the melting degree of spray particles and increasing the roughness of the substrate [19].

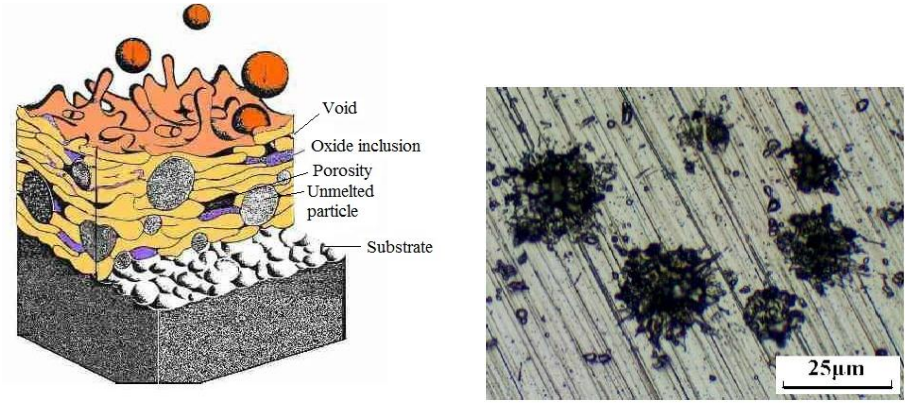

Figure 1.6 Characteristics of thermally sprayed coatings structure [20] and the morphology of HVOF deposited WC-Co splats [19]

Factors which might affect bonding of the coating might be the cleanliness and surface roughness of substrate, thermal energy, cooling rate, and droplets velocity, physical and chemical properties of the feedstock material.
In thermal sprayed coatings residual stresses are always present and they cannot be avoided, especially when the coatings contain composite materials with different mechanical and thermo-physical properties [21]. During spraying tensile or compressive stresses are formed within the coating. This stresses have different underlying mechanism. During the quick cooling process the coating solidifies very fast and this develop quenching stresses. This stresses are always tensile and depends on the coefficient of thermal expansion of the coating and the temperature difference between the splats and already deposited coating. Thermal stresses occur during cooling due to a different coefficient of thermal expansion between coating and substrate. Quenching and thermal stresses are tensile or compressive type, depending on the difference in thermal expansion behavior and Young's modulus [22, 23]. Other stresses are caused due to the phase transformation because the volume changes during this process [21].

1.6 State of the art in thermal spraying

In last years, energy and environmental issues have been becoming larger and larger. To meet this circumstances industrial equipment are required to have higher operation efficiency and their components are subjected to severe operating conditions like high corrosion, wear conditions or high temperature. In many cases the components meet a combination of the mentioned conditions. Operation and maintenance costs are required to cut back against the backdrop of energy prices [24]. Thermal spray coatings have high potentials to manufacture coatings which are suitable to severe operation conditions and in many cases at lower cost than the bulk materials. Thermal barrier, corrosion and wear resistant, medical coatings are manufactured using thermal spraying processes.

In this chapter the most common thermal spray processes are summarized and their operating principle is presented as well as the state of the art in mater of new equipment, materials and applications are briefly presented.

1.6.1 Atmospheric Plasma Spraying (APS)

Plasma spraying is used in industrial applications for producing thermal barrier, wear and corrosion resistant, abrasion resistant coatings and others in order to protect the substrate expending their lifetime and increasing performances [2]. The plasma state develops when a high voltage arc is formed between two electrodes in a plasma forming gas, as it is explained in figure 1.7. The electric arc is formed between an anode and a cathode. Due to the pressure of the gas the arc temperature increases ionizing the gas. The flame temperature is in the range of 15.000-20.000 °C, depending on the spraying system and gas used [9]. The powder particles are injected into the jet at the nozzle exit. The powder particles after melting into the high temperature jet, impact de substrate and build up the coating. The process is simple, based on continuous particle impact onto the substrate. Parameters as powder temperature and velocity affect the properties of the deposited coatings [25]. The deposition rates are higher compared with other spraying processes but the disadvantages are the complexity of the process and the relatively high cost [1, 26].

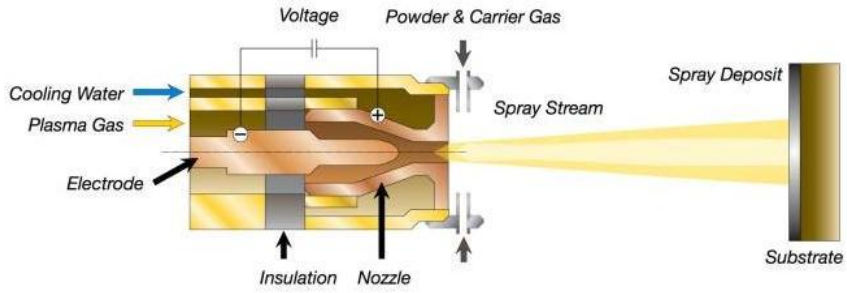

Figure 1.7 Schematic diagram of APS process

Energy sources for plasma systems are usually dc, electric arcs or RF (radio frequency or induction coupled plasma) discharges [9].

ProPlasma HP is an APS gun design by Saint-Gobain, which reaches very high levels of productivity with reduced energy requirements, lowering cost of operation and reducing powder waste. The gun runs with a conventional plasma system with a single powder source and it can be used from 30 kW up to 65 kW, allowing deposition rates up to 3-4 times higher than conventional plasma guns. The gun is suitable for dense wear resistant coatings, TBCs and it runs with Ar-H_2, Ar-He or Ar-H_2-He. The gun is under patent pending [27]. The gun basically is a modified conventional gun which was modified to increase deposition efficiency at high feed rates with low electrode wear and reduced energy consumption [28].

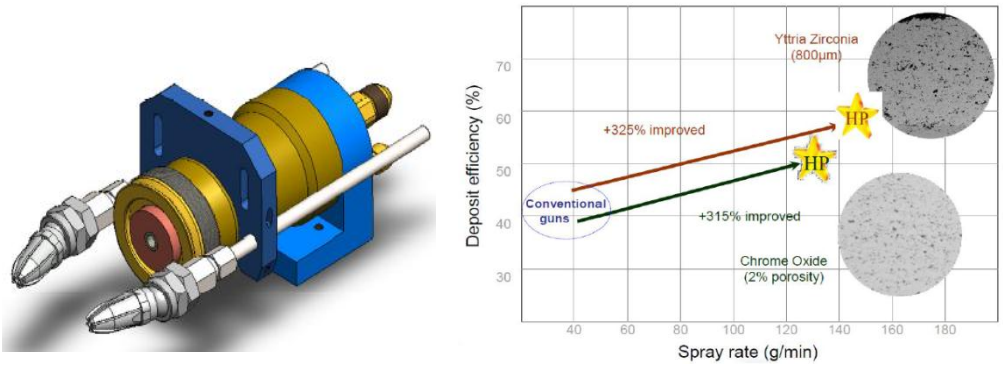

Figure 1.8 ProPlasma HP spraying gun and improved spray rates for Ytria-Zirconia and Chrome Oxide (courtesy of Saint Gobain)

Axial III Plasma spray torch is a three anode three cathode plasma spray torch with axial injection developed for powder feedstock. The plasma streams converge at a poin where the powder feedstock is injected into the gun, ensuring that the powder is melted uniformly in the plasma jet. In that point, where the powder is injected the acceleration trough the nozzle starts and the feedstock powder do not touch the nozzle during spaying. The gun uses an electrical power in the range of 50-150 kW and the deposition velocities are close to HVOF spraying [29].

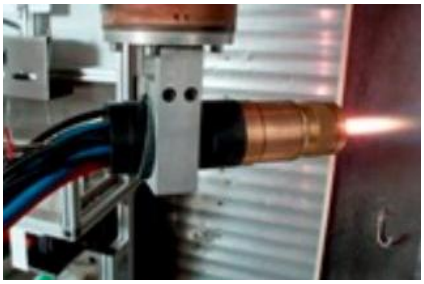

Figure 1.9 Axial III plasma spray torch (courtesy of Mettech Corporation)

Single cathode plasma guns used in conventional plasma spraying have as disadvantages like instability and drifting of the plasma arc which results in relatively low deposition efficiency combined with a relatively short life time of electrodes, 10 to 30 hours facts which lead to higher operational costs [30,31,32]. To improve coating productivity Sulzer Metco developed the TriplexPro 210 plasma gun.

TriplexPro 210 is a universal plasma spray gun with three essential design elements, cascaded arc chamber, divided arc current and standard exchangeable nozzle. The advantages of the gun are the high voltage with lower amperage operation, reduction in voltage oscillation, the influence of gas flow and type of arc behavior were eliminated, uniform heating of the plasma gas, less erosion of the

anode and reduce spray process costs because it uses low helium or helium free gases like Ar, Ar-N_2, Ar-N_2 [33].

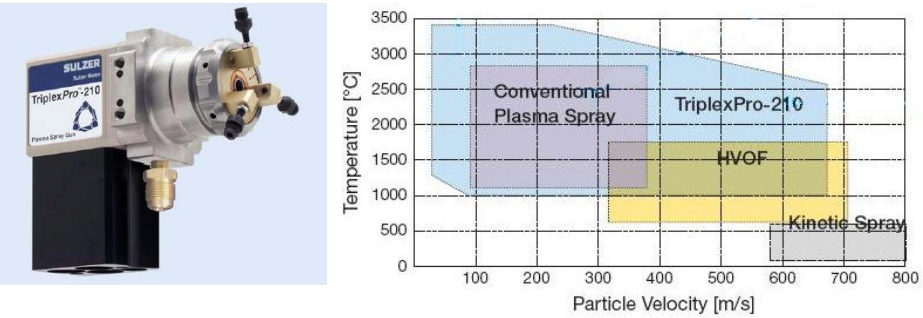

Figure 1.10 TriplexPro-210 Plasma Gun and spray rates (courtesy of Sulzer Metco)

For industrial applications there is also few plasma guns used for coatings deposition like SG 100 and SG 200 manufactured by Praxair, the 3 MB, 9MB, F4 and SM-F210 manufactured by Sulzer Metco, ProPlasma manufactured by Saint Gobain, etc.

Materials and applications

According to the literature there are many materials which might be deposited using the plasma spraying method, like: Al, Al-SiC, Al_2O_3, YSZ, Y-TiAl, TiAlCrYN, Ti-Al-Ag [34, 35, 36], usually ceramic or materials which require high melting temperature for spraying. As an innovative application for the process is the deposition of YSZ in solid fuel cells [35]. For gas turbine engines due to high operation temperature, approximate 1300 °C, materials with high melting point are required, like perovskite with the complexes $Ba(Mg_{1/3}Ta_{2/3})O_3$ (BMT) and $La(Al_{1/4}Mg_{1/2}T_{1/4})O_3$ (LAMT) [37]. In general the process is used to deposit thermal barrier and wear resistant coatings which require high melting temperatures.

1.6.2 Flame spraying

The process is the oldest spraying technique among thermal spray processes. The feedstock material is continuously fed in the spraying plum where it is melted and accelerated in the atomized gas jet. Acetylene, propane and MAPP are the most common gasses used for combustion mixtures with air which is the atomization gas. The temperature of the gas jet is above 2600 °C and its velocity is below 100 m/s. Due to process parameters the coatings present a high level of porosity [38, 39]. Adjusting the fuel/oxygen ratio an oxidizing or reducing flame might be obtained function of the feedstock material and required application. Most common systems use acetylene as the main fuel in mixtures with oxygen generating the highest combustion temperatures among the other spraying fuels which might be used in the combustion process [9]. The process might be divided in two categories function of feedstock material type in: wire flame and powder flame spraying [2].

In wire flame spraying the gun includes the drive unit with a motor and drive rollers for feedstock feeding. The process is slower and relatively has a higher operational cost due to the processes gases but as an advantage it can be mentioned that the processes is portable and is used to apply corrosion protective coatings. The schematics of wire flame spraying are presented in figure 1.11.
In powder flame spraying there is no atomizing air stream. Excepting the lack of atomizing air stream the process is similar to wire flame spraying. The droplets are atomized in the flame jet and projected towards the substrate. The productivity of the process is lower compared to wire flame spraying and the porosity in the deposited coatings has a quite high level.

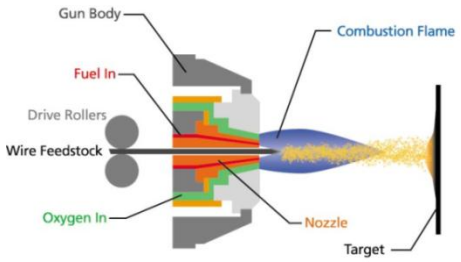

Figure 1.11 Principle of wire flame spraying (courtesy of Hyden Corporation)

The Top Jet 2 is a wire flame spray gun designed for manually handling for overhaul and anti-corrosion protections. It is suitable for deposition of metal wires, core wires or flexi-cords. The lightweight gun it makes easier to spray complicated shapes by hand. It is equipped with an interchangeable air motor depending on the feedstock material and process temperature; fast air motor for low melting point for metal spraying and slow air motor fir high melting point for metal and flexi-core spraying. It is suitable to deposit copper alloys, nickel alloys, steels, molybdenum, aluminum, tin, babbit, etc. under wire form and Nialide, NiCrAlY, alumina, spinel, Zirconia, chromium oxide etc. under flexi-cord form [27].

The 5P II is an economical lightweight hand held spraying gun unique in the industry due to build in powder canister which uses a gravimetric feeding system. It is suitable to surface repairs, corrosion and wear protection and dimensional restoration. It is suitable for the deposition of self-fluxing alloys, self-bonding materials, steels, stainless steels, bronze, aluminum and nickel alloys. It uses acetylene or hydrogen for combustion, but last one is used for finer powders [33].
Several guns used in industrial applications are: Sulzer Metco 10/11/12/14 E with wire, SNMI SN-TOP-Jet with wire, Castolin DS 8000 with powder, Praxair PF 71 with powder, Sulzer Metco 6P II with powder, etc.

Materials and applications

Flame spraying is used to apply metallic and non-metallic powders, metal wires, ceramic rods and polymers. It is used for the deposition off YSZ, Al_2O_3 (for high temperature abradable applications), Mo coatings, stainless steel [40], Al_2, Zn, Al/Zn alloys. Nowadays the composite polymer structures with polymer coatings or substrates gas gained interest [41, 42] with applications in aircraft industry due to

reduced weight and high strength [43]. There are also studies regarding the deposition of metallic coating on polymer substrate, like Al-12Si [44].

Figure 1.12 Top Jet 2 wire (courtesy of Saint Gobain Coating Solutions) and 5P II powder (courtesy of Sulzer Metco) flame spray guns

1.6.3 High Velocity Oxy-Fuel spraying

High velocity oxy-fuel (HVOF) spraying process is characterized by a flame velocity up to 2000 m/s, which can project in its gas stream powder particles at high velocities up to 800 m/s, usually between 600-650 m/s. During the spraying process the powder particles might be heated up between 1600 °C and 2200 °C [45]. In the HVOF spraying process oxygen and fuel are mixed and burnet in the combustion chamber of the spraying gun at high flow rates and pressure, up to 12 bar [46]. The fuels which can be used for the burning mixture might be hydrogen, propane, propylene, ethylene, acetylene, natural gas or kerosene, depending on the spraying system.

High velocity oxygen fuel spraying is relatively a new spraying process in which the hypersonic velocity of the flame shortens the interaction time between the powder particles and flame. The high kinetic energy acquired by the powder particles ensures a good cohesion between particles and substrate and between splats allowing the deposition of coatings with reduced porosity with high hardness and density [11].

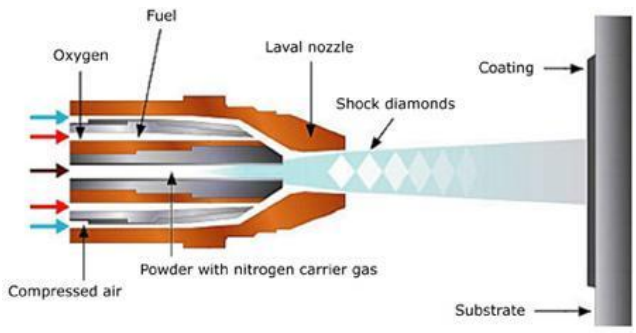

Figure 1.13 Schematic diagram of HVOF process

The 5220 HVOF gun due to a unique design is a high pressure spraying gun which allows the deposition of high quality coatings. The high pressure in the combustion chamber is up to 8.2 bar, compared to other thermal spray guns which are limited to pressures in the range of 2-5.4 bar. A particular advantage of the gun is the high velocity (gas velocities up to 2.19 m/s), coatings with higher hardness and reduced oxide content. The combustion chamber of the gun is monitored to keep under control the pressure to ensure a stable, clean and uniform combustion of gasses. The feedstock powder is injected radially in the lower pressure area of the converging-diverging nozzle which promotes better powder mixing, even heating and higher particle velocities. It operates with kerosene mixed with a typical fuel gas for HVOF spraying. The gun is reliable to the next generation coating system, the JP 8000, which includes a sophisticated PLC based, mass flow controlled management system [47].

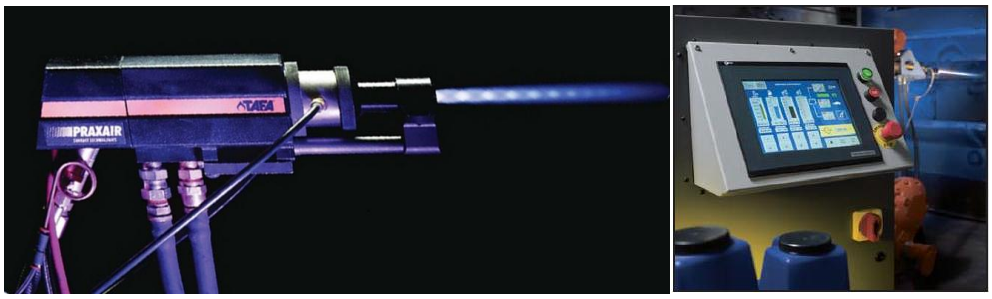

Figure 1.14 5520 HVOF gun and TAFA JP-8000 high pressure spraying system (courtesy of Praxair Surface Technologies)

The CJS gun is a flexible HVOF gun based on a sophisticated radial powder injection with adaptable nozzle configuration function of powder type. It is a high pressure with a combustion chamber pressure up to 25 bar. The jet temperature is controlled by a kerosene-oxygen system while a hydrogen-oxygen system controls the jet speed. The gun might be connected to the CPF – Fine Arts - powder feeder which works based on a vibration system that fluidizes even micro-fine powder with particles under 10 μm [48].

Figure 1.15 CJS gun and CPF powder feeder (courtesy of Thermico GmbH & Co KG)

Apart from the newest spray guns presented previously other commercially available HVOF guns are Diamond Jet, Diamond Jet Hybrid, HV-2000, Jet Kote, JP 5000, OSU, Met Jet II [49].

Materials and applications

The process is used to deposit corrosion, erosion, wear resistant, medical, high temperature resistant coatings. Among the materials deposited, WC and Cr_3C_2 (in Ni, Cr, Co or alloys of these elements) based coatings are the most widely applied [49, 50]. Other materials deposited via HVOF process are: Inco 718 (Ni base super-alloy), Triboloy 800 (Co based coatings), and high temperature oxidation resistant MCrAlY, titanium alloys [51], and refractory metals like Mo, etc. [52].

1.6.4 Activated combustion High Velocity Air Fuel spraying

The HVAF spraying process is similar to HVOF process. There are some differences like the use of air instead of oxygen in a mixture with a fuel gas such as propane, propylene or natural gas which allows the spraying system to operate at lower process temperatures. The lower process temperature, below 1600 K [53], makes the process similar to cold spraying due to the advantages of solid state particle spraying. The presence of oxides in the coating is also reduced. The deposited coatings have higher density with compressive residual stress, high hardness and reduced oxides [54].
The M3 gun developed by Uniquecoat, operates at particle velocities of 600-700 m/s and uses air for internal cooling. The non-clogging nozzle can operate a longer time without being necessary to replace it. The gun might operate with natural gas which offers a cost reduction of the process providing good deposition efficiency. There are different type of nozzles which might be used in the spraying process, depending on the feedstock powder and spraying system: manual or robotic [55].

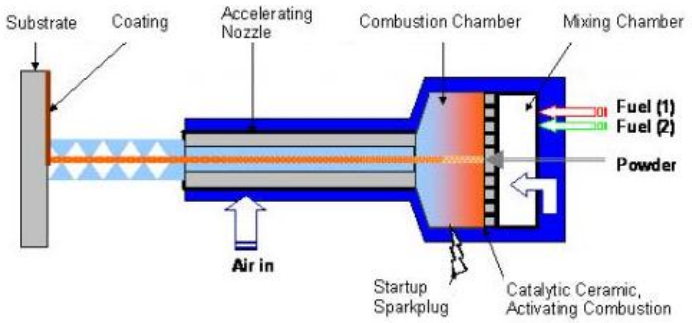

Figure 1.16 Schematic diagram of HVAF process

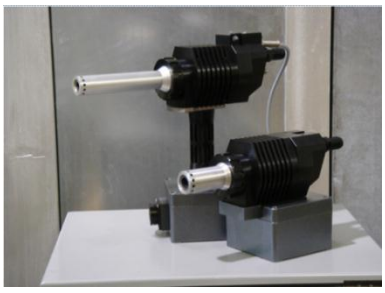

Figure 1.17 M2 AC-HVAF gun (courtesy of Uniquecoat)

Supersonic Air Fuel Spraying is a patent pending thermal spray technology, a successor to AC-HVAF spraying, and producing particle velocities of 1000-1200 m/sec. The higher kinetic energy of the solid particle which are projected towards the substrate, leads to a better adhesion and cohesion between splats. The coatings have improved physical and mechanical properties and high hardness. The process basically raises the coatings quality compared to AC-HVAF spraying [55].

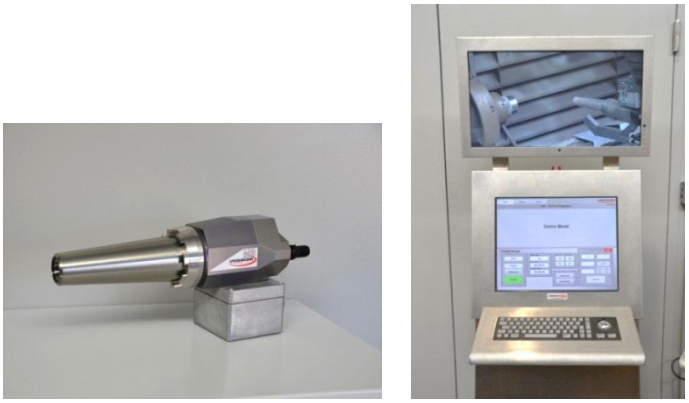

Figure 1.18 M3 Supersonic SAF gun and Ultracoat control system with live video feed of spray process (courtesy of Uniquecoat)

Other HVAF equipment: HVAF Flame wire arc gun (courtesy of Uniquecote), AcuKote Guns (courtesy of Kermetico, Inc.) suitable for HVAF spraying and also for surface preparation via grit blasting.

Materials and applications

The HVAF and SAF spraying systems are used for deposition of carbides, cermets, metals and metal alloys to protect different components, vessels and structures against corrosion, erosion and wear [55]. HVAF deposited WC-Co coatings increase the wear behavior of piston rods against Al-Ni-Bronze alloys in landing gears [54]. Austenite stainless steel for improving corrosion resistance on the surface of steel parts [53]. Oil and gas industry for applications on valve gates, valve balls and stems, pump shafts, sleeves, packing nuts, cartridges, compressor rods, etc. [56].

1.6.5 High velocity arc spraying HV-ARC

The process uses two metallic wires as feedstock materials which are electrically charged. At the gun nozzle the two wires are brought together and due to the opposing charges an electric arc is created which atomize the molted material. The droplets are projected onto the substrate by means of pressurized air. The process has high deposition efficiency and it is suitable for applications in civil and municipal structures (steel structures, bridges, marine coatings, etc.) Typical operating ranges are 15 to 400 A, 50 to 250 A dc and 400-1500 A dc in few units for corrosion coatings. The open circuit voltage is around 40 V dc [9]. Using older arc spraying technologies some applications are restricted due to a lower cyclic stress of the substrate and the coating has a lower bond strength and increased porosity compared to other thermal spray processes [2] but in the meantime it is a fast and cheap processes [57]. The process allows the deposition of every electrically conducting feedstock wire. Particle velocities might reach 150 m/s during spraying and 8-20 kg/h deposition rate, depending on the feedstock material [1, 58]. A schematic presentation of arc spraying is presented in figure 1.19.

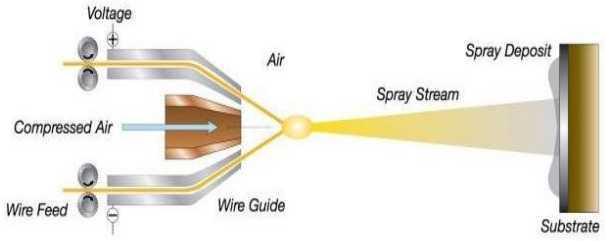

Figure 1.19 Schematic diagram of arc spraying

Figure 1.20 TAFA 9935 arc spray gun and CoArc spray system (courtesy of Praxair Surface Technologies)

Several arc spray guns used for industrial application are: Praxair Tafa 8830/8835/9000, Praxair BP 400, Sulzer Metco Smart Arc, Arc Jet 95, AT-400, IMC 95, etc.

Materials and applications

The materials used for spraying are limited to conductive materials that can be formed into wires [9]. The feedstock powder might be used as wires or cored wires (which consist of a tubular metallic shell with powder in the core). Arc spraying is used to recover blades of hydraulic turbines with cavitation wear loss and to deposit new alloys with erosion and cavitation resistance. Cavitation resistance Fe-Mn-Cr-Si on AISI 1020 [57], corrosion resistance coatings manufactured using Zn, Al, Zn/Al (85/15) deposited on steel substrates [59], Fe and Ni based cored wires: FeCrBSiMn and NiCrBSi [60], FeNi deposition on Ni substrate [21] are a few new materials and applications of arc spraying process.

1.6.6 Suspension spraying

Spraying of suspensions represent a group of thermal processes representing innovative technology which use high velocity and plasma guns to deposit coatings with fine microstructure using as feedstock material powders with fine particles, usually in the range of 5-10 μm and even finer which cannot be used in conventional powder feeders [61, 1]. The process evolved during the past ten years and offers new opportunities in the field of thermal spraying. During the spraying process the liquid from the slurry evaporates after the injection in the flame/plasma jet, the solid particles agglomerate, melt and impact the substrate to build up the coating [62, 63]. The process enables to deposit coatings with fine surfaces but thinner due to the fact that the process requires higher combustion energy to evaporate the liquid. The slurry might be injected using an atomizer or a nozzle.
Usually the suspension sprayed coatings are manufactured using a conventional HVOF, HVFS or plasma gun and a suspension powder feeder is used to inject the fine powder into the flame/plasma jet. In figure 1.21 the principle of HVOF suspension spraying is presented.

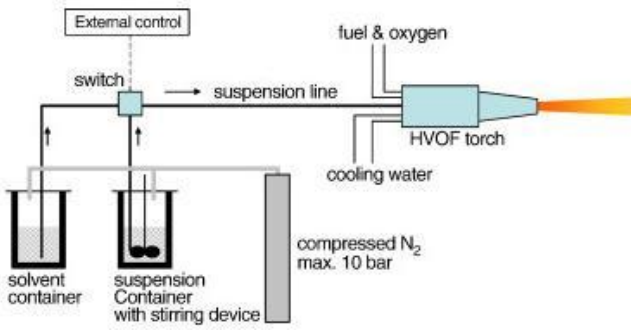

Figure 1.21 Schematic diagram of HVOF suspension process

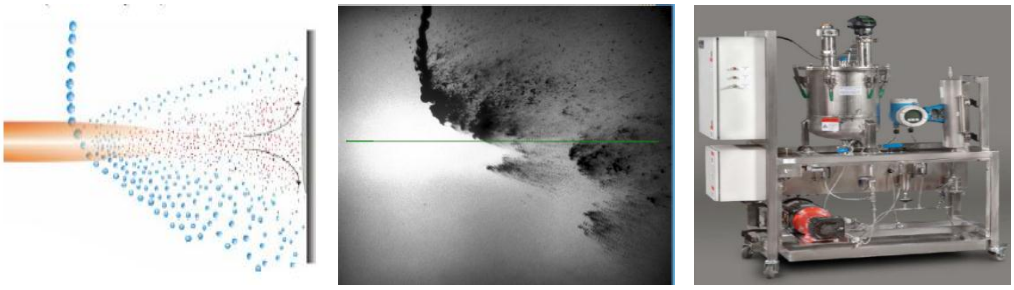

Figure 1.22 Nano/submicron powder partciles flow in the plasma jet and Mettech NanoFeed 750 suspension feeder

For the suspension preparation usually water, ethanol and pentanol are used. The properties of the liquids are summarized in table 1.2.

Table 1.2 Physical properties of liquids used in suspension spraying [64]

	Surface tension [N/m]	Viscosity [kg/(m*s)]	Enthalpy of Vaporisation [kJ/mol]	Energy of combustion [MJ/kg]
H_2O	72.88	1.0	40.65	-
C_2H_6O	22.55	1.19	38.6	29
$C_5H_{12}O$	25	4.0	44.36	35

The liquids are different regarding their physical properties which control the atomization during spraying. Water and ethanol have similar viscosity but the surface tension of water is almost four times higher. There are also similarities between the surface tension of ethanol and pentanol but the viscosity of the former one is almost four times higher than viscosity of ethanol. From the previous table it can be noticed that all liquids differ regarding the energy released during spraying.
In order to prepare the suspension, the powder is reduced to finer grades, using for example the ball milling process. In case of YSZ, for example, the suspension is prepared using 20% powder, 40% water and 40% ethanol [62, 65, 61]. J. Puranen et al. [66] studied $MnCo_2O_4$ ceramic coatings deposited via SPPS, using two different solvents: water and deionized water plus ethanol with a 50/50 ratio.
The properties of the suspension are strongly influenced by particle size, powder chemistry, weight percent powder addition, powder to solvent ratios and solvent type.

Materials and applications

The process is used to deposit very fine powders and nano-structured powders with improved mechanical properties or electric properties, which cannot be deposited with conventional powder feeders [1].
High velocity suspension spraying is used to deposit nano-oxides and also bioceramics.
Some of the common powders deposited using these processes are: TiO_2, Cr_2O_3, YZS and Hydroxyapatite [67]. Wittmann et al. [68] deposited composite coatings

composed of 316L stainless steel powder in combination with WC nanoparticles using a plasma torch. The nano-oxides deposited by plasma spraying might exhibit fine grain size with high porosity levels which make the coatings suitable for applications as electrochemical electrodes in devices like solid oxide fuel cells, lithium ion batteries, ultra capacitors and sensors. According to Golozar et al. [69], ultra-capacitors electrodes, were coated using α-MoO_3 (molybdenum trioxide). Suspension plasma sprayed coating might be deposited onto the surface of hot extrusion tools by spraying $Ti_{n-2}Cr_2O_{2n-1}$ type powders to increase the tools performances [25].

1.6.7 Cold Spraying

The beginning of cold gas spraying started in the early 1980s in Russia, at the Institute of Theoretical and Applied Mechanics of the Siberian Branch of the Russian Academy of Science, while a model was subjected to a supersonic two phase flow in a wind tunnel [70]. Compared to other spraying methods, in cold spraying the particles are in solid state before they reach the substrate which allows the process to be used even at room temperatures, fact that is impossible in other spraying methods. By cold gas spraying there is no need to melt the feedstock powder which eliminates unwanted chemical reactions such as oxidation or other phase changes which took place in other thermal spraying processes [71]. Due to the high velocity and low temperature the powder particles suffer plastic deformation and strongly adhere to the substrate [72]. The powder particles usually in the range of 1-100 μm, are accelerated to high speed in the range of 400-1200 m/s by the supersonic gas [70, 73]. The powder particles after the impact with the substrate highly deform forming ring-type material jets around the particle impact zone [74]. In order to increase particle velocity the gas is preheated to increase gas viscosity [75]. The process allows manufacturing dens coatings with low porosity and low oxygen content [74].

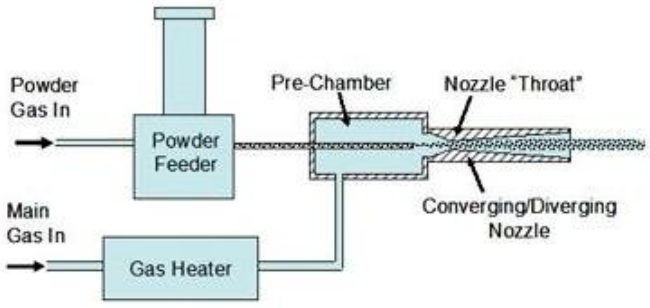

Figure 1.23 Schematic diagram of cold spray process [76]

Cold spraying is divided into two different processes according to the pressure level in high pressure cold spraying (HPCS) and low pressure cold spraying (LPCS) processes.

High pressure cold spraying

The process operates at high pressures, up to 40 bar and the jet temperature can reach 800°C. In the process, the high pressurized gas is heated in the gas heater. In the nozzle the gases are mixed with the axially injected powder and high velocity is generated due to the converging-diverging shape. The supersonic velocity is created in the diverging part of the nozzle.
A typical cold spraying system is the Kinetiks 4000 presented in figure 1.24. The system is composed of a heater, control cabinet, spraying gun – Active Jet, and a high pressure powder feeder. The control cabinet uses a heating powder from 17 to 47 kW. The heater uses helium as process gas and generates temperatures up to 450 °C. The powder feeder is a PF 4000 Confort which fed the powder at high pressure. With the Active Jet spray gun a maximum temperature of 800 °C can be reached at 30 bar using helium as process gas. It works also with nitrogen.

Figure 1.24 Active Jet cold spray gun and Kinetics 4000/47 cold gas spray system (courtesy of Sulzer Metco)

Usually pure metals and metal alloy are used as feedstock for HPCS under powder form, like: Al, Ni, Cu-Sn, Cu, Ti, Ni-20Cr, Al-Al_2O_3, Inconel 718 (nickel based superalloy), Al-Ni-Ce (amorphous aluminum) etc. [74, 71,77, 78].

Low pressure cold spraying

In LPCS the feedstock powder is not melted in the gun but is kinetically deposited on the substrate at low temperature. The pressure in the process is up to 10 bar and the temperature varies from room temperature up to 650 °C. The adhesion to the substrate is solid state bounding. Subsequent particle collision plastically deforms the previous deposited particles, and in this way they adhere to the already deposited layer. The process works with reduced consumption of compressed air and power consumption, it is an environmental friendly process and it is portable equipment. In figure 1.25 a modern low pressure cold spray system is presented. The spraying system is compact equiped with GDS spray gun. The control unit includes air pressure and air temperature control. The operating pressure of the compresses air can be controled by pressure regulator. The powder feeder alows quice change of powders. The gun includes air heater and supersonic exchangeble nozzle [79].

Figure 1.25 GDS gun and DYMET 413K low pressure cold spray system (courtesy of Dymet Technology)

With the LPCS process powder mixtures based on Al_2O_3, SiC ceramics mixed with Al, Cu, Zn, Pb etc. can be deposited. The role of ceramics is to keep the nozzle clean and to compact the coating by mechanical hammering [79, 80].

Materials and applications

Since 2002 when the process was limited to applications which involved the deposition of copper and aluminum nowadays with cold spraying can be deposited a wide range of metals for different applications like magnetic and electrically conducting coatings for sensors, thermally conducting coatings, electrically conducting coatings to reduce contact resistance [81]. Cold gas process might be used to repair aluminum molds, restoration of corrosion defect on different components, sealing of holes in the aluminum case, filling the casting defects, corrosion protection at welding lines, restoration of copper coatings, sculptures or parts [79].

1.6.8 Laser spraying (cladding)

Laser cladding is a process which allows the deposition of metallic or ceramic coatings using a laser beam as the heat source. The process is situated somewhere between thermal spray processes and deposition welding processes, it is not quite common at the moment and still require a lot of technical know-how but it has the ability to produce dense and coatings with very good adhesion to the substrate [82]. The laser cladding process is similar to thermal spraying because it has an energy source to melt the powder feedstock which is deposited to a substrate. The difference is that it uses a concentrated laser beam as the heat source, the metallurgical bond is superior to thermal spray coatings and the lake of porosity is a characteristic of the process [83].

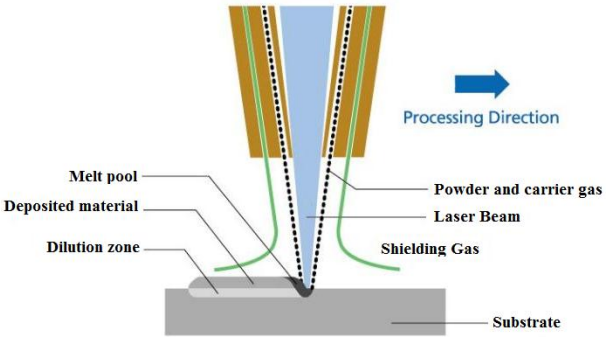

Figure 1.26 Schematic diagram of laser cladding process (courtesy of Hayden Corporation)

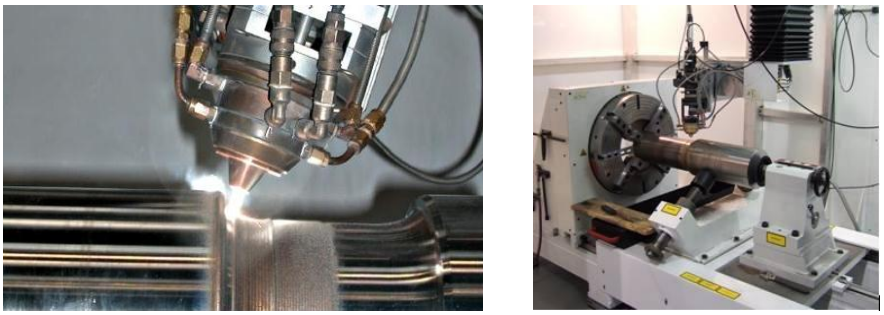

Figure 1.27 Laser cladding gun and laser cladding system (property of Laser Cladding Technology Ltd. and Thermal Spray Depot)

Materials and applications

Laser cladded coatings might find applications in extremely high wear applications, down-hole tools for oil and gas drilling, hard valves and seats, agricultural size reduction tooling, etc. [84]. High temperature abradable NiCrAlY coatings, according to Bardi et al., might be clad on components for gas turbines, which withstand temperatures greater than 900 °C [85]. Zhenda et al. used a 3 kW CO_2 laser to clad WC-Ni composite coating with superior wear resistance on mild steel [86]. Another new powder, FeNiW, it was found out that is suitable in depositions on casting molds in aluminum industry improving the erosion and corrosion resistance of the molds [82].

1.7 Surface pre-treatment

Surface preparation includes surface treatments which change the properties of the surface and cleaning, which reduces the surface contamination or unwanted matter from a surface. One important goal of surface preparation is to produce a homogeneous surface. Surface modification can include roughening or smoothing or by activating a polymer surface by plasma treatment [87]. For thermal sprayed components the surface preparation is a very important step which requires lot of attention [88]. The adhesion of thermally sprayed coatings depends critically on the

conditions of the surface before spraying [89]. In order to increase the adhesion of the coating with the substrate it is necessary to make the surface rough enough prior spraying. It is well known that the adhesion of coating depends on anchoring effect, formation of the fusion layer, Van der Waals forces, and diffusion of elements. Among these mechanisms the anchoring effect is the most important [90]. A proper surface preparation is required to avoid coating stripping. If surface preparation is not done properly consequences like substantial investment, considering labor and overhead expenses might take place. According to Hare [91] the goals of surface preparation are:

- to ensure a uniform substrate that it is closed as possible to the theoretical model designed by the design engineer
- to ensure adhesion by removing contaminants and foreign matter from the steel surface and freeing up reactive sites on the metal surface
- to increase adhesion by increasing the real surface area per apparent surface area

1.7.1 Cleaning

The first step in preparing a substrate for thermal spraying is to remove contaminants such as rust, scale, oil, paint, moisture etc. [9]. The selection of proper cleaning and surface preparation technique depends on the nature of surface and the intended coating or surface treatment technique. According to ASM Committee [92] there are several factors which must to be considered when is about to select a cleaning method:

- identification and characterization of the soil to be removed
- identification of the substrate to be clean
- establish the degree of cleanliness required
- establish the capabilities of the available facilities
- determine the impact of the process on the environment
- calculate the cost of the process
- material handling factors, etc.

The selection of a cleaning method depends on the degree of cleanliness requires and the further operation which needs to be performed. Solvent, solvent vapor degrease, emulsion soak, alkaline soak, alkaline electro-clean with acidic cleaning and ultrasonic cleaning are methods which are used to obtain a clean surface.

Cleaners

The selection of the proper cleaning method depends on mechanics of the cleaning action. The conventional cleaning methods are classified function of typical solvents used in the cleaning process [92]:

- Solvent cleaning uses typical solvents like: trichloroethylene, methylene chloride, toluene and benzene. The solvent can be applied by swabbing, tank immersion, spray or solid stream flushing and vapor condensation;
- Emulsion cleaning uses water or water solvent based solutions like kerosene and water containing emulsifiable surfactant;

- Alkaline cleaning may employ physical and chemical actions. The cleaners are a mix of surfactants, sequestering agents, saponifiers, emulsifiers and chelators;
- Saponification is a chemical reaction which splits an ester into its acid and alcohol moieties an irreversible induced hydrolysis. The process takes place in a alkaline cleaner;
- Electrolitic cleaning might be anodic (reverse cleaning) or chatodic (direct cleaning) in which an electrical current is imposed on the part to produce gassing in the part surface to release the unwanted matter;
- Abrasive cleaning uses small particles projected by compressed air or water towards the part which needs to be cleaned. The contaminants are removed doe to the impact force;
- Acid cleaning uses acids which dissolves oxides. Several acids used in the process are hydrochloric, sulfuric and nitric acids;
- Ultrasonic cleaning involves sound waves at a very high frequency trough liquid alkaline, acid, or organic solvent cleaners.

1.7.2 Blasting

Blasts cleaning next to grinding and polishing are mechanical cleaning processes used to remove oxides, corrosion products and millscale. Grinding and polishing consist in abrading the surface using felted, cotton or other abrasive based wheels or belts until they become smooth. Polishing is to decrease the surface roughness after grinding process. It is accomplished by abrading the surface with fine abrasives progressively decreasing to sub-micron sized [93].
Blast cleaning is an erosion process from the point of view of material removal. As a tribological system it can be considered a removal of material due to the action of impinging solid particles [94]. The process is one of the most frequently used methods for roughening the surface before thermal spraying.
According to ISO 12944-4 (1998) blast cleaning methods are classified in the following way:

- Wet abrasive blast cleaning;
- Dry abrasive blast cleaning;
- Moisture injection abrasive blast cleaning.

Abrasives

For industrial application there are many types of abrasive media but the most used ones are: copper slag, coal boiler slag, garnet, olivine, silica sand, hematite, iron slag, nickel slag, staurolite, steel grit, steel shot [94].
A blasting media must have the following general attributes in order to be successful [95]:

- Low health risk including low levels of dangerous contaminants (ex: asbestos, arsenic, etc.);
- Low dusting level under normal usage conditions;
- High rates of production and cleaning, without damaging the work piece;
- Durability of the media (collection, reclamation and reuse);

- Appropriate grain shape and size for desired application;
- Low environmental impact during storage, use and disposal.

According to the international standard ISO 11124 – "Preparation of steel substrates before application of paints and related products – Specification for metallic blast-cleaning abrasives" there are 4 types of metallic abrasives:

- Chilled-iron grit
- High-carbon cast-steel shot and grit
- Low-carbon cast-steel shot
- Cut steel wire

According to the international standard ISO 11126 – "Preparation of steel before application of paints and related products – Specification for non-metallic blast-cleaning abrasives" there are 9 types of non-metallic abrasives:

- Silica sand
- Cooper refinery slag
- Coal furnace slag
- Nickel refinery slag
- Iron furnace slag
- Fused alumina oxide
- Olivine sand
- Staurolite
- Garnet

Gould and Wilson classified the abrasive medias in four general types:

- Natural minerals (e.g. silica sand, garnet, olivine);
- Manufactured media (e.g. steel shot, glass grit, alumina, plastic beads, solid carbon dioxide, sodium bicarbonate);
- Mineral slag (e.g. copper slag, nickel slag, iron slag and coal slag);
- Organic media (corn cobs, nut shells, starch grains).

Table 1.3 Abrasive media characteristics [95]

Abrasive	**Composition**	**Mohs Hardness**	**Density (gms./cu. cm)**	**Dusting/ Recycling**
Silica sand (BQ)	Crystalline Silica	7	1.6	Low/No
Staurolite/Zircon	Iron Aluminium Silicate	7.5	2	Mod/No
Garnet(Almandite)	Iron Aluminium Silicate	7.5	2	Low/Yes
Olivine	Iron Silicate	6.5	1.9	High/No
Hametite	Iron Oxide	6	2.3	Mod/Yes
Copper slag	Iron Silicate Glass	6	1.6	Mod/No
Nickel slag	Nickel Iron Glass	6	1.6	High/No
Iron slag	Iron Silicate Glass	6	1.6	High/No
Coal boiler slag	Calcium, Iron Silicate Glass	6	1.4	High/No
Steel/Grit Shot	Iron	6	2.2	Low/Yes
Baking Soda	Sodium Carbonates	2-3	1.1	High/No
Crushed Glass	Alkaline Silicate Glass	6	1.6	High/No
Organic Media	Variuos	2-3	0.6-1	N/A/No

Variables that modify the geometry of the surface include the size, shape, and hardness, chemistry of the abrasives and density, etc. [9, 96, 97].
Size – the physical size is measured in mesh. The larger the mesh number, the smaller the abrasive grains. Depending on size, the larger particle will cut deeper.
Shape – The shape of the abrasive media will determine the roughness and speed during the blasting. Abrasives with sharp, irregular and angular shapes will cut faster the surface by removing particles form the substrate and increasing roughness while spherical and rounded particles are used to clean components without removing material from the substrate.
Hardness – The hardness will influence the cleaning speed, the amount of dust and breakdown of grains.
Recyclability – in order to be reused, the abrasive media must be collected and cleaned. Reusing the grit several times depends on the abrasive's hardness, resiliency, retention of shape, the amount of removed material, and the overall efficiency of the collection and cleaning process.
Density - The bigger the density of the grit the impact energy is larger, having as result an increased roughness.
Embedment – grit embedment depend on impact angle and abrasives type. A maximum embedment value occurs at a 90^0 impact angle. Brittle grit can suffer extreme breakdown forming fine abrasive particles which smear over the surface. The over-blasting process, increase the contamination level due to additional grit embedment.
Consumption rate –is given by the weight of abrasive used divided by the area cleaned. Parameters which influence the consumption rate are: the abrasive type, nozzle and pressure used for the blasting process.
Dust generation –due to impact strength and fracture resistance of the abrasive media dust generation occur when breakdown of abrasive media took place.
Cost – abrasive cleaning can be performed outdoor or in a blasting cabinet. The abrasive media used in outdoor applications cannot be reused, therefore cheap material like sand or slag is recommended. The more expensive abrasive media is used in cabinets and it can be reused. The most used abrasives for surface preparation before thermal spraying are presented in table 1.5.

Table 1.4 Abrasives used for grit blasting before thermal spraying [98]

Abrasive	**Trade-name**	**Composition**
Silicon Carbide	-	SiC
Brown Fused Alumina	BFA	Al_2O_3-TiO_2 97/3
White Fused Alumina	WFA	Al_2O_3 < 99%
Zirconia Alundum	Alundum ZF	Al_2O_3-ZrO_2 75/25

Silicon carbide – is an artificial abrasive used for blasting but it is not suitable for coatings application due to the reactivity at high temperature with various substrates and coating materials.
Aluminium Oxide – it is one of the most used blasting media for coatings applications. The grit usually is used in a brown form when it is manufactured by fusing bauxite and it can be found in many grades. There are also grades with low content of iron (white and pink alumina) [99]. It is a recyclable media used on non-ferrous metals, steel, stainless steel because it does not contaminate the surface.
Alumina zirconia - is made of zirconium oxide and aluminum oxide fused under carefully controlled conditions to produce a chemically inert abrasive alloy. The

abrasive reduces wear on interior nozzle surfaces because it only fractures on direct impact. Alumina zirconia grains consist of fine primary Corundum and an Alumina-Zirconia eutectic crystalline structure. This structure allows for one of the most durable abrasive materials in industry [100].

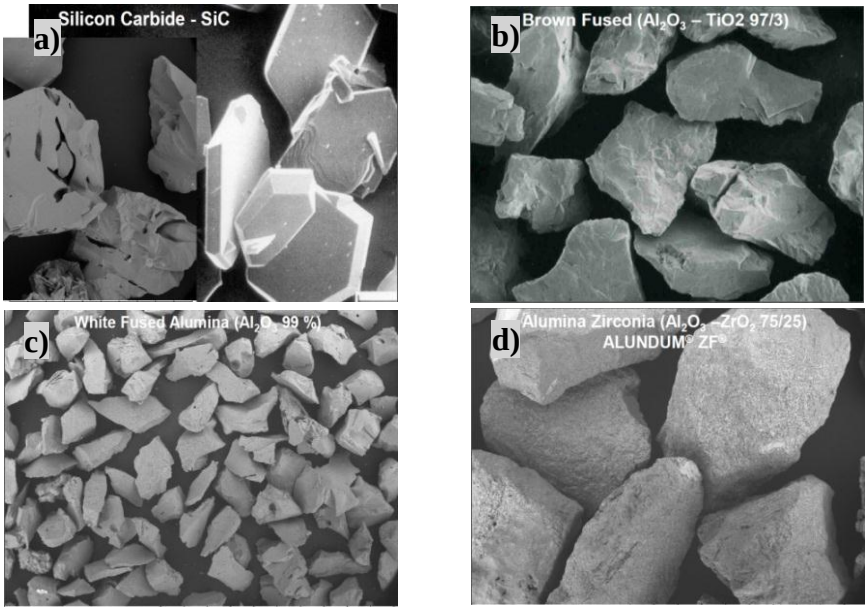

Figure 1.28 Morphology of a) SiC, b) BFA, c) WFA, d) Alundum ZF (courtesy of Saint-Gobain)

Table 1.5 Physical properties of abrasive used to activate the surface prior to thermal spraying [101]

Abrasive	**SiC**	**BFA**	**WFA**	**Alundum ZF**
Colour	black	brown	white	grey
Hardness HV	2651	2141	2243	1937
Density [g/cm_3]	3.2	3.92	3.96	4.3
Melting point [°C]	2300	2000	2090	1900

Surface activation requirements (courtesy of Sulzer Metco):

- The surface needs to be free of greases, oil or other foreign elements that can contaminate the grit;
- The air needs to be clean and dry at constant pressure;
- It is required to use the most appropriate grit for the surface preparation;
- The grit size needs to be kept within closed limits;
- Recycled grit needs to be free of dust and the size maintained;
- The blasting equipment needs to ensure optimum performance.

1.7.3 Masking

The process is used in order to protect areas which shall not be treated. For masking there are several methods for protection: using liquid compounds, tapes, rubber or plastic inserts, polymers, metals sheets. Masking tapes can be manufactured using glass fabrics with silicon and adhesives, aluminum laminated foil with silicone and adhesives.

1.8 Surface post-treatments

The sprayed coatings by thermal spraying usually are subjected to different surface treatments in order to change the coatings microstructure, density, enhance bond strength, reduction of oxides, reduction of internal stress, etc. According to J. R. Davis there are three methods used after thermal spraying to enhance the coatings properties [9]:

- Chemical and physical treatments like sealing, aluminizing and chromizing;
- Thermal treatments like fusion, heat treatments, diffusion, laser glazing and hot isostatic pressing;
- Mechanical treatments like machining, grinding, shot pinning and polishing.

Among the above mentioned methods only the sealing treatment will be presented in details due to the newer technique and materials available.

1.8.1 Sealing

When coated parts are subjected to liquids or gases due to the porosity present in the microstructure and environmental exposure the corrosion process is activated. If the coatings are not protected this may cause the degradation of the coating and finally the degradation and replacement of the component. Sealants are applied to eliminate permeability of deposited coatings against liquids or gases. In some cases is used only to reduce the permeability depending on the work environment of the coated component. They are applied on coatings as a post-treatment to enhance their properties being applied like water-borne or organic liquids over the as-sprayed or ground coatings [102].

Figure 1.29 Application of sealers on thermally sprayed coating

Under liquid form the sealant penetrates into the coating pores (found on the coating surface), sealing them. Depending on the sealant type, baking is required. The sealants in most cases do not affect the coating thickness. Depending on the sealant type and application there are sealants used for permanent or temporary protection. Functional sealants prolong life of the coating even of the coating is worn due to the fact that they penetrate the coating [102].

Table 1.6 Frequently applied sealants [102]

Sealant	Temp. limit. [°C]	Solubility			Chemical resistance		
		H_2O	Alcohol	Acetone	Strong acids	Oxidizing acids	Caustics
Silicone	510	None	None	Soluble	Excellent	Good	Poor
Alumina	1150	Soluble	Soluble	Soluble	-	-	-
Phenolic epoxy	300	None	None	Soluble	Fair	Poor	Excellent
Fluorinated Ethylene Propylene	344	None	None	None	Excellent	Good	Excellent
Flouro-elastomer	300	None	None	Soluble	Good	Fair	Excelent
Furfuryl Alcohol	149	None	None	Soluble	Excellent	Poor	Excellent
Polyurethane	149	None	None	Soluble	Excellent	Poor	Excellent

All coatings have a certain degree of porosity which might go up until 15% in the case of porous coatings. The interconnected pores may be present in the coating from the top until the substrate which may damage the sprayed coating. Sealers are used to fell the pores and to improve the service lifetime of the coatings.
Low viscosity sealers are used because they are rapidly absorbed by the pores. Sealers are applied at low film thicknesses like 75 μm or even less. Also is necessary to pay attention when selecting the sealer because their chemistry must be compatible with the chemical composition of the coating. Some resin based sealers may saponify if they are applied on zinc coating due to the alkalinity of the zinc [1].

1.9 Safety issues

Common health and hazards associated to thermal spray processes are presented briefly below and include:
Dust, gases, vapors and airborne inhalation might cause pulmonary diseases like asthma, pneumoconiosis, hyperplasia (enlargement of an organ due to enlargement of cell number), embolus, RADS (reactive airway dysfunctions syndrome), skin and eye damage, etc. Also they represent a high explosion risk. In order to avoid ricks the spray operators should wear appropriate respirators. If highly toxic materials are used for the coatings than a spray cabin is required. Ventilation systems are required.
Noise can cause hearing impairment, tension, slow reaction time, nervousness. All spraying processes are generating high level of noise, more than 110 dB and the

level increase function of spraying process, when the normal noise level is 70 dB. The noise level might be reduced using spray cabins which are lined with sound absorbing materials. Earplugs and earmuffs are required for the operator protection.
Radiation – ultraviolet, bright visible and infrared radiation – they cause temporary or permanent damage to the eyes. They increase the risks of conjunctivitis, cataract, and lesion. As a protection against radiation there are several methods like increasing the distance from the radiation source, use special glasses or robot handling system and spray cabinets.
Electric Shock - due to high DC voltages and amperages during wire arc spraying the operator is exposed to severe electrical hazards. To avoid any ricks ground protection, electrical outlets with ground fault circuit interrupters, equipment cleaning, etc. are required [103].
Ventilation systems are required to provide adequate air flow in the spraying cabin to avoid accumulation of combustibles or explosive gases and remove them as well fumes, reaction by-products, heat and dust particles. In the thermal spray area is necessary to remove paper, oils, cleaning solvents, paints, wood and any inflammable materials [104].
All protection against hazardous risks needs to be considered and the spraying process needs to be effectuated according to national and international standards and lows specially designed for thermal spraying activity.

1.10 Effects of wear and corrosion

The progressive deterioration of different metallic parts due to wear and corrosion is an unavoidable fact of life. These processes are materialized in the daily activities in: *loss of production* – if a damaged part needs replacement or repair, the whole plant may shut down for a while; *reduction of efficiency* – the damages caused by wear and corrosion reduce the efficiency of a power plant; *product contamination* – the fine debris and corrosion products might contaminate products in the food processing industry; *costs associated with design* – wear and corrosion decisions are a part of the engineering design process and they do not need to cause delays because it will damage the profitability of the process; *costs associated with novel solutions* - it means that the project manager needs to choose the right solution between a standard solution with unexpected problems or to attempt a novel solution which might lead to extra operational costs (usually the new solutions are used if they offer a better/cheaper solution) [105]. Wear and corrosion often combined cause aggressive damage in all industries such as mining, chemical processing, pulp and paper, energy production, mineral processing etc., and might cause disaster when is about metallic bridges, constructions, chemical containers, nuclear plants, etc. It is necessary to protect the metallic components exposed to wear and corrosion and to perform maintenance and overhaul periodically in order to avoid disasters and extra operational costs.

1.10.1 Wear

Wear represents the surface damage or material removal from one or two solid surfaces brought in contact under sliding, impact motion or rolling. Generally speaking wear occurs through surface interaction trough asperities. Wear as friction is a system response influenced by the operation conditions. Wear is undesirable in almost all industrial applications such as seals, gears, cams, bearings, etc. In an optimal tribological system the removal of material due to wear is a very slow, steady and continuous process [106]. One of the biggest challenges in solving wear problems is to anticipate the type/types of wear at which a component will be subjected [107]. According to Burwell [108] the wear mechanisms are classified in five groups and they are presented briefly below.

Abrasive wear occurs when hard particles roll or slide under a certain pressure and cut the surface and involves progressive loss of material. This type of wear is defined by ASTM as the process in which hard particles or protuberances are forced against a surface and move along with it [107]. The loss rate depends on the characteristics of the surfaces brought in contact, the abrasive between the surfaces, speed of contact and environmental conditions. Abrasion wear is categorized function of contact type and might be *open two-body, closed two-body, open three-body and closed-three body* wear. Also abrasion is characterized as being *low stress* – occurs when the abrasive remains relatively intact; *high-stress* – occurs when abrasive particles are being crushed; and *gouging* – occur when a larger abrasive will groove the material that is not properly hardened [109].

Adhesive wear or micro-welding occurs when the asperities from one surface come in contact with asperities from other surface. Due to the friction between the two surfaces a micro-welding occur between those asperities which cause wear debris. The wear debris will act as an abrasive media between the surfaces enhancing the wear process, deteriorating faster the surfaces [110].

Erosive wear occurs when solid particles with high hardness and/or high velocity hit and damage a surface. The degree of degradation depends on the structural characteristics and properties of the material also if the material is brittle, ductile, if the process takes place at high temperature, etc. [111]. Erosion wear might be classified according to the environment and erodent particles in the following way:
- solid particle erosion represents material loss from the surface material as a result of repeated impact of small and tough particles. This type of wear is very dangerous in industrial application such as turbines, pipelines, valves, fluidized bed combustion systems, etc. [110]. The process is also useful in applications like sandblasting, roughening, abrasive jet cutting.
- liquid impingement erosion is a progressive loss of material from a surface due to continuous striking of liquid drops or jets. The jet/drop strikes generate impulsive contact pressure on the surface higher compared to those produced by steady flows. In advanced stage the process is characterized by jagged surface, composed of sharp pits and peaks [107, 112].
- cavitation erosion – *cavitation* is a development of vapor structures in a fluid flow which takes place at almost same temperature caused by a local pressure drop in the flow [113]. The process is characterized by the repeated nucleation, growth and violent collapse of cavities or bubbles in the liquid. Cavitation erosion is characterized by the mechanical degradation of materials due to cavitation in

liquids. The liquid microjets formed during the process hit very severe the surface causing deformation followed by material removal [109].
-slurry erosion is a progressive loss of surface material by a mixture of abrasive particles in a liquid. The slurry is usually water but might be also a liquid with a certain consistency which can be easily pumped. The particles are in suspension in the liquid and pumped, strike the surface with high velocity [109].

Erosion corrosion occurs from the combined action of wear and chemical attack due to fluid motion. This type of corrosion is harmful to coatings that passivate by forming a protective surface film. If the coating is not able of continuously reforming the protective film the corrosion might be severe. Soft metal, like copper and lead are susceptible to this kind of wear. Surface grooves and waves characterized by the flow of the fluid are characteristic of erosion-corrosion. The nature of the fluid and its velocity strongly influence the corrosion behavior. The process is characteristic in piping, elbows and changes in the pipe diameter. Propellers, turbine blades, pumps, etc. are susceptible to this type of wear [114].

Surface fatigue wear occurs usually in sliding friction between two surfaces due to cyclic loading which involves tension and compression causing cracks. The cracks develop along the sliding direction starting at the surface and continuing in the material. At a certain depth a pit is formed due the cracks. The process develops slowly but the expansion rate is very fast [115].

Corrosive wear – occur when the wear takes place in a corrosive environment. It is also known as chemical wear. If the process takes space in air it is called oxidative wear because the most dominant corrosive medium in the atmosphere is oxygen. Due to oxygen a thin layer of oxides form on the surface of components and if the process is combined with sliding wear the oxide layer is peeled and the debris products act as an abrasive. The process sometimes prevent the contact between components reduce the formation of adhesion wear which is much severe. This type of wear is important in industries such as mining, chemical processing, mineral processing, etc. [116].

1.10.2 Corrosion

Corrosion is a destructive and unintentional chemical or electrochemical reaction of a metal with the environment. In economic term it was found out that only the corrosion prevention and protection cost 5% of an industrialized nation's income [114]. Most common forms of corrosion are presented by Fontana and Greene [117] and they are divided in eight types: uniform corrosion, pitting, crevice corrosion, erosion corrosion, hydrogen damage, stress corrosion and selective leaching. This classification was incomplete due to the fact that the inspection was based on visual characteristics of the morphology of attack. A more complex classification was established by the ASM Committee [118] and the classification is presented below:

General corrosion also called uniform corrosion is the simplest and most common form of corrosion. This type of corrosion is characterized by metal loss due to chemical attack or dissolution of metallic parts into metallic ions. When the corrosion takes place at high temperature the metallic loss combines with other element rather than its oxidation to a metallic ion. The combination with oxygen

forms metallic oxides resulting loss of material under flakes form which return to nature damaging the components [119].

Atmospheric corrosion is the reaction of usually a metal and its atmospheric environment. It is the oldest type of corrosion recognized and the atmosphere is the most usual environment [120]. It might be classified as dry, wet and dumb function of atmospheric contaminants and their variables.
Galvanic corrosion occurs when a metal/alloy is coupled to another metal/alloy or conducting nonmetal in the same electrolyte [121].

Other forms of general corrosion are:

- Stray-current corrosion
- General biological corrosion
- Molten salt corrosion
- Corrosion in liquid metal
- High temperature corrosion
- Oxidation
- Sulfidation
- Carburization

Localized corrosion – a particular characteristic is the corrosion damage produced localized instead of being spread uniformly over the surface. This form of wear is much more aggressive and the material is penetrated faster at specific areas [118]. Based on common features it might be classified as follows:

- Filiform corrosion
- Crevice corrosion
- Pitting corrosion
- Localized biological corrosion

Metalurgically influenced corrosion it is especially influenced by *chemical composition* such as alloying elements, impurities; *metallurgical properties* such as metallic phases and metallic joint; and *fabrication procedures* such as heat treatment, lamination or welding [122]. It might be classified in the following way:

- Intergranular corrosion
- Dealloying corrosion

Mechanically assisted degradation is defined as any type of degradation that involves simultaneously wear and corrosion [123]. This form of degradation might be classified in:

- Erosion corrosion
- Fretting corrosion
- Cavitation and water drop impingement
- Corrosion fatigue

Environmentally induced cracking takes place due to metals or intermetallic compounds exposure to their environment. It is characterized by slow and stable

crack extension with a predictable growth rate. If the cracks propagate rapidly unpredictable catastrophic fracture occurs [123]. It might be classified as follows:

- Stress corrosion cracking
- Hydrogen damage
- Liquid metal embrittlement
- Solid metal induced embrittlement

CHAPTER II HVOF AND HVAF SPRAYING

2.1 High Velocity Oxygen Fuel

The process is one of the newest thermal spraying methods and it was invented in the early 1980s by James Browning [124]. The process uses thermal and kinetic energy for melting the feedstock powder and to accelerate de particles toward a desired surface. The fuel is burnet with oxygen at a high pressure generating a high velocity jet. For HVOF spraying the usually fuel gases are acetylene, kerosene, hydrogen, methacetylane-propadiene mixture. The ration of the gas flow strongly influences the flame temperature. If the burning fuel consist of acetylene and oxygen the temperature might reach 3170 °C while using an oxygen propylene mixture the flame temperature reach a temperature around 2900 °C [125]. Usually the temperature varies between 2500 °C and 3200 °C depending on the fuels. Depending on the jet temperature in the process the feedstock material is partially or totally melted during spraying. The jet temperature, the melting degree and dwell time are important parameters of the spraying process. Due to the high pressure generated within the combustion chamber of the spraying gun hypersonic velocities are generated. Function of spraying velocity the HVOF systems are classified in three groups such as first, second and third generation. In the first systems the combustion of fuels with oxygen generated a jet velocity in the range of 1800-2000 m/s at a powder level of 80 kW. In the third generation the powder level is in the range of 100-200 kW [17].

2.2 Activated Combustion High Velocity Air Fuel

The process is a recently developed spraying technology for deposition of metallic, carbide and cermet coatings being applied in many industrial fields to provide protection against corrosion, erosion and wear [126]. The specific of the process is that the feedstock powder particles are heated below their melting point and accelerated at velocities above 700 m/s. The high speed reduces the dwell time of the particles reducing the thermal deterioration and particle oxidation [127]. The process uses for combustion compressed air mixed with a fuel has which might be propane, propylene, natural gas or MAPP [55]. The combustion process is activated by a hot wall from the burning chamber, which contains a high temperature catalyst. This offers the advantage of stable air fuel combustion. The process is described by Verstak and Baranowsky as a "solid particle" spraying process due to relatively low combustion temperature and high velocities [128]. The Supersonic Air Fuel produces very high spray jets with speeds up to Mach 3 and particle velocities in the range of 1000-1200 m/s. Due to an increased kinetic energy the powder particles produces high contact pressures at impact leading to a better adhesion to the substrate and cohesion reducing also the porosity within the coatings and increasing the hardness [55].

2.3 Comparison of HVOF and HVAF thermal spraying

The main difference between the both processes is the relationship between the thermal and kinetic energy which influence the flame temperature and particle velocity. Typical parameters are presented in table 2.1.

Table 2.1 Characteristics of HVOF [17, 9] and HVAF spraying [55]

Spraying process	Flame temperature [°C]	Particle velocity [m/s]	Spray rates (for carbides)
HVOF	2500-3200	650-800	Up to 14 Kg/h
HVAF	~2000	700-1200	Up to 30 Kg/h

Due to the oxygen used in the combustion process HVOF produces higher flow velocity compared to HVAF process. This results in a higher temperature in the flame jet which causes the oxidation of the feedstock particles during dwell time. The HVOF process uses high pressure guns cooled usually with water to produce the combustion gases which are accelerated trough a "de Laval" type nozzle to reach the supersonic speed. In the HVAF gun the fuel and compresses air are supplied in two steps, first the air is supplied for combustion and after the air cools down the flame. Due to supplied fuel the HVAF gun has a much complex design and allows the compressed air supplied to provide a stable and efficient combustion and cooling down the gun simultaneously. The HVAF gun is designed in such a way to achieve a stable and complete combustion of gases, to generate the required temperature in order to melt the feedstock material and obtain high has velocity able to project the droplets towards the substrate. The relatively low temperature in the HVAF process allows a precise heating of the feedstock material compared to conventional thermal spray processes such as plasma or HVOF which have higher jet temperatures. The material fusion and dissolution is significantly reduced. The coatings obtained by HVAF process are manufactured at higher velocities and preset compressive stresses due to high velocity impact of the feedstock particles. If both processes uses the same fuel mixed with air in case of HVAF process and oxygen for HVOF spraying then the adiabatic flame temperature for the stoichiometric mixture of gases will be around 3000 °C for HVOF and 2000 °C for HVAF. In the HVAF process the flame is diluted by the compressed air which reduces the temperature inside the gun and protects the gun against overheating [129]. Genliang et all., used the two dimensional computational fluid dynamics method to calculate the flame characteristics in the fuel region of HVOF and HVAF processes using ideal conditions and gases. Figure 2.1 illustrates the axial velocity and temperature in the guns and outside the guns. Figure 2.1 proves that the temperatures in the gun and outside the gun are lower for the HVAF process. In the HVOF process the under-expended gas will expend in the atmosphere which significantly increase the jet speed and lower the flame temperature while the HVAF process will exhibit the opposite. From the simulation it can be also noticed that both flames have supersonic speed [130].

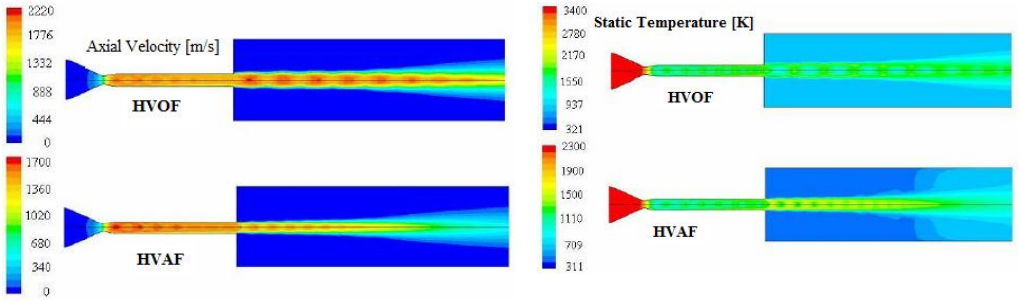

Figure 2.1 Axial velocity distribution and Static temperature distribution [130]

According to Thorpe and Richter there are specific particles conditions related to HVOF spraying in air, compared to plasma spraying and arc spray processes, such as reduced dwell time, reduced mixing with ambient air, lower ultimate temperature and higher particle energy upon impact [131]. In table 2.2 are presented also the advantages of HVOF spraying compared to plasma or arc spray processes.

Table 2.2 HVOF advantages compared to plasma and arc guns [131,132]

Coating benefit	**Main causes**
Higher density	Higher impact energy
Improved corrosion	Less trough porosity
Higher Hardness	Less carbide degradation
Better wear resistance	Harder, tougher coatings
Higher bond and cohesive strength	Improved particle bonding
Less unmelted particles content	Better particle heating
Great chemistry retention	Reduced dwell time
Thicker coating	Less residual stress
Smoother surface	Higher impact energy

The HVAF process temperature is lower compared to HVOF process, around 2000 °C [9] but even lower temperatures, around 1500 °C, were reported [133]. From the literature [126-128] and thermal spray systems manufacturers [102, 55] it might be concluded that the HVAF process have similar or even better characteristics than HVOF process. Unfortunately only a few materials were deposited by both processes and compared. Due to the newer process technique, HVAF spraying is not that much studied than HVOF spraying. It might be noticed that there is a lack of research and information related to HVAF spraying and there are only few materials sprayed and compared to HVOF process, and usually this materials are WC, CrC, Ni and Fe based coatings [134-137]. The HVAF process has the capability to produce superior coatings without oxidation or decarburization effects compared to HVOF [134, 138, 139].

2.4 HVOF and HVAF fuels

In high velocity thermal spraying usually propane, propylene, hydrogen, acetylene and ethane are used as fuel gases. The gases used in the spraying processes can considerably influence the quality of the coating. The gas purity level in high velocity spraying is around 2.8 minimum, quality which is uniformly defined by international standards and specifications recognized all over the world [140]. Hydrogen is one of the gases which offers a maximum reproducibility when is required unlike propane and natural gases while their quality is not subjected to regional and seasonal fluctuations which can easily conduct to different results [141].
In table 2.3 are presented general information according to Voronetski and Belashchenko, regarding the available fuels used in HVOF/AF systems. The combustion parameters were calculated using the supposition that heat losses were absent in the combustion chamber of the gun and the stoichiometry ratio was = 1.

Table 2.3 Properties of gaseous hydrocarbon fuels [142, 2]

Flame parameter	Propane C_3H_8	Propylene C_3H_6	Methane CH_4	MAPP C_3H_4	Hydrogen H_2	Kerosene C_9H_{20}
$T_{C\ at\ 0.1}$, K	3094	3150	3052	3195	3076	3109
$T_{C\ at\ 0.5}$, K	3310	3380	3261	3435	3296	3335
λ, W/(m*K)	0.3	0.29	0.32	0.28	0.46	0.28
E_K, kg/(m*sec2)	369, 230	372, 416	368, 705	335, 296	366, 125	370, 915
HP, W/m	993	980	1043	962	1516	934
Q_g, MJ/kg	50.45	49	63.6	59.454	120.5	42.9
W, m/s	1849	1840	1892	1845	2287	1828
ρ, Kg/m^3	0.108	0.11	0.103	0.985	0.07	0.111
T, K	2632	2671	2602	2701	2634	2642

In the previous table, $T_{C\ at\ 0.1}$ is the combustion temperature at atmospheric pressure, $T_{C\ at\ 0.5}$ represents the combustion temperature at 0.5 MPa combustion pressure, λ represents the thermal conductivity of combustion products, E_K specific kinetic energy at the nozzle exit, HP represents the heat potential characterizing the efficiency of heat transfer from combustion products to spraying powder particles. Q_g is a heat value/kg fuel and W, ρ, T are the velocity, density and temperature of combustion products.
According to the values presented in the table there are little differences in the combustion temperature at 0.1 and 0.5 MPa, kinetic energy, density, temperature, heat transfer when is about using the mentioned gasses in HVOF/AF processes. When is about to select a gas for the spraying process is necessary to pay attention at the cost, availability, safety issues and the composition of the fuel. In comparison with the conventional hydrocarbon fuels hydrogen has with approximately 50% better heat transfer which might cause undesirable phase transformation for example in WC based carbide coatings [142].

2.5 Process map

The gasses used for spraying, spraying system, feedstock powder, droplets velocity, particle temperature and substrate are important parameters in thermal spraying and they affect strongly the quality of the coating. Particle velocity, dwell time, particle temperature, spraying distance influence the deposition efficiency, spray rate and microstructure of the coating. It is very important to know the process parameters in order to make easier the spraying process comprising them in so called *process maps.* To a better understanding of spraying parameter special tool are developed to help building up the process map. This map might have two meaning such as optimization and mapping of in-flight process conditions of the feedstock particles with a different melting range of the particles, or finding the influence of splat structures and substrates on the final structure and properties of the deposited coatings [17]. Sampath et all., classified this maps as *First order map* and *Second order map* [48], schematically illustrated in figure 2.2.

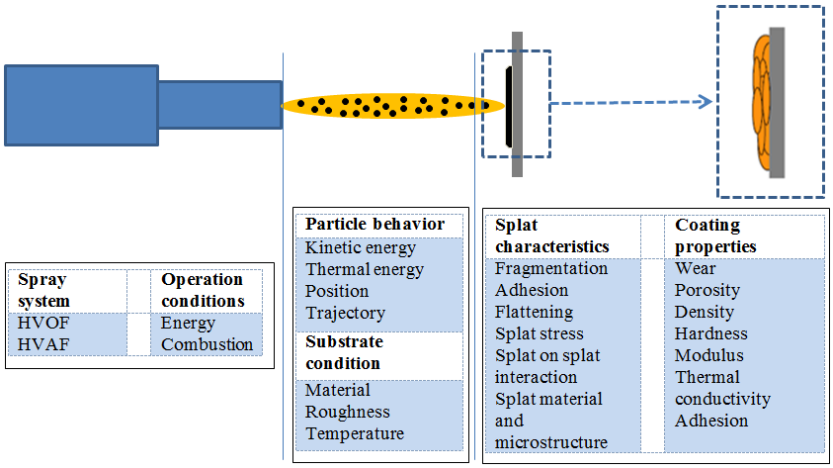

Figure 2.2 Schematic overview of process maps; First order map including: Spray system, Operation conditions and Particle behavior; Second order map including: Splat characteristic and Coating properties [48, 17]

According to [48] single tools are used to build up the process map such us: a) in-flight diagnostics (the velocity and temperature of the feedstock droplets are measured during spraying); b) splat studies (droplet melting, spreading and solidification is studied individually) and c) droplet/surface or droplet/coating interaction (the temperature of the surface is studied due to splat morphology, deposit microstructure and properties). On-line diagnostic methods tool are used to measured thermal spray properties such as enthalpy, particle temperature and velocity, particle size and total particle flux. Splat studies are carried out to understand the relationship between particles during spraying and coating microstructure [17]. The process map is recommended for any type of thermal spraying technique for a better understanding and repeatability of the process.

2.6 Materials for HVOF and HVAF thermal spraying

Thermally sprayed coatings might be classified according to material chemistry and type, morphology, particle size distribution spray process and application [9]. All powders used for thermal spray application might be divided into two main groups: composite powders and refractory compounds [143]. Thus they might be classified according to their chemical composition in [2]:

Metals and alloys: aluminum, aluminum-zinc, copper, nickel aluminum alloys, nickel chromium alloys, etc.

Ceramics: aluminum oxide, chromium oxide, hydroxyapatite, titanium oxide, zirconia, etc.

Intermetallics: nickel-aluminum

Composite and blends: aluminum-silicon-polyester, molybdenum-nickel-chromium-boron-silicon, nickel graphite, tungsten carbide based powders, borides, chromium carbide based powders etc.

Polymers: nylon, polyester, polyamide, etc.
Cermets can be manufactured as composites and blends.

Materials used to improve wear and corrosion

Most used materials for wear and corrosion applications deposited by HVOF spraying are presented below in table 2.4. HVAF spraying due to similar characteristics compared to HVOF process might be used to spray the same materials. One of the most common material for wear and corrosion resistance is WC-10Co-4Cr which is also one of the oldest powders developed for thermal spray applications [144].

Table 2.4 Summary of HVOF/HVAF materials used for wear and corrosion applications [102, 145]

Type of coating	Material (balance and wt%)
Composite coatings for wear and corrosion applications	Tungsten Carbide Cobalt Chrome (WC-10Co-5Cr, WC-10Co-4Cr) Tungsten Carbide Cobalt (WC-12Co, WC-17Co) Tungsten Carbide Chrome Carbide Nickel ($WC-20Cr_3C_2-7Ni$) Chrome Carbide Nickel Chrome (Cr3C2-NiCr) Moly Boride Cobalt Chrome (MoB-45CrMo-30Co) Nickel Aluminide Alumina (NiAl-Al2O3) Iron Aluminide Alumina (FeAl-Al2O3)

Hardface metal coatings for wear and corrosion applications	Stainless steel 430SS (Fe-0.4Cr-15Cr) Hard Steel (Fe-2C-3Si-3.3B-6Ni-14Cr) Armacor M (Ni-1Mn-1Si-6B-45Cr) Stellite 1 and 6 (Co-1C-12W-30Cr/Co-1C-4W-30Cr) Tribaloy T400 and T800 (Co-3.4Si-28Mo-17Cr/Co-2.6Si-26Mo-8.5Cr) Nickel Chrome Tungsten Boron (Ni-0.8Co-4Si-3B-9W-15Cr) Nickel Boron (Ni-4Si-2B)
Metallic alloy coatings for corrosion applications	Hasteloy C276 (Ni-5Fe-4W-16Mo-15.5Cr) Inconel 625/622/718 (Ni-2.3/2.3/18.5Fe-3.5/-/5Nb-9/14/3Mo-21.5/20.5/18Cr) Nickel Chrome (Ni-0.6Si-0.5Ti-45.5Cr) NiCrAlY (Ni-Y-10Al-22Cr) NiCoCrAlY (Ni-0.6Y-4Ta-23Co-8.5Al-20Cr) G 195 (Co-0.5Y-8Al-32Ni-21Cr) Iron Chrome (Fe-0.002C-3Si-36Cr) Titanium (99.5 Ti) Monel 400 (Ni-1Mn-Fe-32Cu)

Powder manufacturing methods

Even if the powders have identical chemical composition and size distribution but manufactured by different suppliers might have different morphologies due to different manufacturing processes. If the same powders are coated with different spraying processes structural variations occur. The powder morphology varies from spherical to irregular/blocky. The irregular shapes might have cubic like structures mixed with needles like structure while blocky particles are dense and exhibit an elongation ratio close to unity [146]. The flowability of the powder is a very important characteristic and it is influenced by the powder morphology. The presence of pores might be noticed in spherical particles and also in irregular shape particles but not that much in blocky powders which are dense. The homogeneity of powder particles is another important factor besides the oxidation level during manufacturing and density. There are many methods for powder production, pressed in details in [2, 146] thus according to the manufacturing method the powders might be divided as follows:

- Atomized powders
- Fused and crushed powders
- Milled and sintered powders
- Milled powders
- Mechanical alloyed and milled

- Spray dried powders
- Powders manufactured trough cladding process
- Powders manufactured trough sol-gel process
- Powders manufactured trough spheroidization

Applications

HVOF applications are used in many industrial applications due to favorable economic factors and process characteristics. The process usually is used to deposit wear and corrosion resistant coatings but also thermal resistant coatings. Some HVOF applications are:

- Pulp and paper industry: highly stressed components, recycled process-water tanks, cooling chambers, pumps, valves, cylinders, retention towers, revolving elements, press rolls, pressing nips, steam heaters, calender rolls, etc.
- Aerospace coatings: landing gears, flaps, tracks, fan, different components in compressors, turbine,
- Industrial gas turbines: inlets, exhaust and casting components such as shafts, bearings, miscellaneous contact points, etc.
- Automotive industry: piston rings, valves, cylinder bores, hydraulic parts, swash plates, brake disks, shifter forks, synchronizing rings, etc.
- Oil and petrochemical industry: sub-sea ball valves, seals, drills, etc.
- Other applications: deposition on mandrel, extruders, tracks, mixer parts, shredding components, hard-facing granular rotors, coatings on knife edges, etc. [147].

Nowadays the HVAF process is used in several applications to enhance components resistance against wear and corrosion. Some of these applications are [126]:

- Power generation industry: corrosion resistant coatings on furnace waterwall of pulverized coal and waste-to-energy boilers; erosion-corrosion resistant coatings on waterwall of circulating fluidized bed combustion boilers; erosion resistant coatings on coal impellers of circular burners, corrosion on high temperature wear resistant coatings on different gas turbine components
- Pulp and paper industry: wear resistant coatings on dryer cans and calendar rolls of paper machines; corrosion resistant coatings on furnace waterwall and floor of black liquor recovery boilers;
- Textile industry: wear resistant coatings on aluminum clutch hubs of wiring machines; friction coating on housing and hubs of brakes
- Film making industry: wear resistant and functional coatings on process rolls
- Steel works: wear and corrosion resistant coatings on sink roll in zinc galvanizing, wear resistant coatings on process rolls; erosion-corrosion resistant coatings onto a hood of oxygen blowing furnace; wear resistant coatings on hearth rolls of annealing furnace
- Hard chrome alternative in machine building, plastic extrusion, hydraulic compounds, printing industries.

CHAPTER III. AIM OF THE STUDY

The aim of the study was to obtain good quality coatings with high wear and corrosion resistance properties with minimized decarburization process, comparable to HVOF coatings, obtained at lower manufacturing costs.
Objectives – the study aims to develop a range of cermet coatings like WC-CoCr, CrC-NiCr, CrC-WC-18M and WC-FeCrAl with good wear and corrosion resistance properties deposited by HVAF spraying comparable to HVOF coatings. The coatings are expected to have similar of even better microstructure, wear and corrosion properties than HVOF coatings and might be obtained at lower manufacturing costs.
Activities – characterize the microstructure, wear and corrosion behavior of HVOF and HVAF deposited coatings by mean of microstructural investigations, porosity quantification, hardness and roughness measurements, wear resistance via rubber wheel abrasion, pin-on disk tests, corrosion resistance via open cell potential measurements, salt spray tests and finally compare the results.

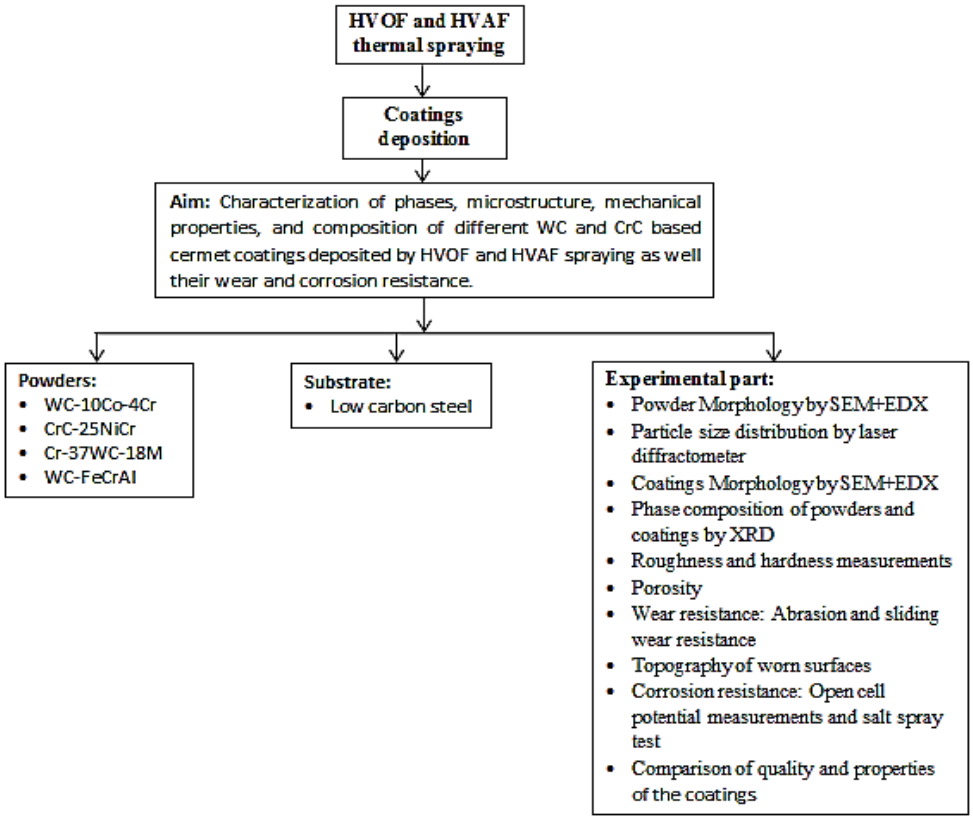

Figure 3.1 Schematic representation of the experimental part

CHAPTER IV. METHODS

4.1 Blasting

In order to increase the roughness of the substrate and to enhance the bonding strength between the coatings and substrate brown fused alumina was used as an abrasive media. Brown fused alumina is manufactured from the electric arc furnacing and refinement of bauxite ore to purity up to 95% +aluminum oxide content [148]. The morphology of the grit is characterized by tough irregular, blocky and dense grains with sharp edges able to remove easily material from the substrate's surface, with high grinding efficiency.

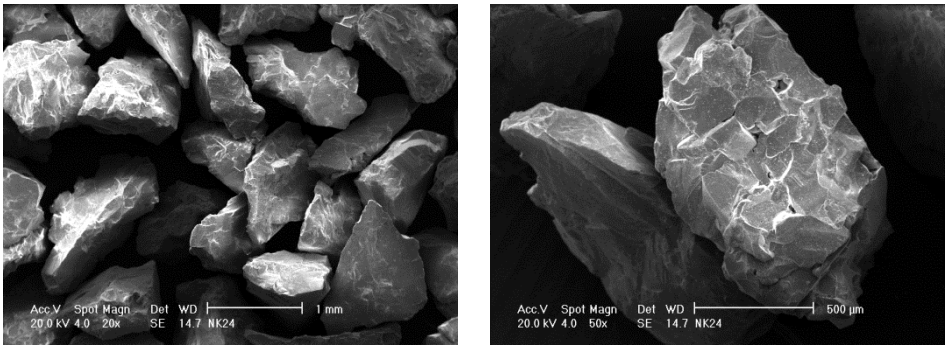

Figure 4.1 Morphology of brown fused alumina

According to the manufacturer the brown fused alumina grit has the typical chemistry presented in Table 4.1.

Table 4.1 Typical brown fused alumina chemistry [27]

Chemistry	Percentage [%]	Chemistry	Percentage [%]
Al_2O_3	95.46 min	TiO_2	2.57 max
SiO_2	0.76 max	CaO	0.19 max
Fe_2O_3	0.44 max	MgO	0.26 max
Na_2O	0.02 max	MnO_2	0.11 max

The 24 grit abrasive particles were sprayed against the substrate to remove contaminants and roughening the surface at blasting pressure of 4 bar. The blasting distance was about 200 mm and a 90° blasting angle to the substrate.

4.2 Spraying methods

A large number of different HVOF and HVAF systems have been developed during last decades and are used nowadays for coatings deposition in different industrial fields. In this study one of the most popular HVOF system was used, the Diamond Jet Hybrid 2700 system, manufactured by Sulzer Metco (Westbury, NY, USA). The HVOF coatings were deposited at Tampere University of Technology, Finland. The HVAF coatings were manufactured using an AC-HVAF M2 system (UniqueCoat, Ashland, Virginia, USA), deposited at Fincoat Oy, Riihimäki, Finland.

4.2.1 HVOF spray system

For the HVOF spraying the Diamond Jet Hybrid 2700 thermal spray gun was used. The gun is a third generation one and provides particle velocities up to 650 m/sec.
The Diamond Jet spraying system presented in figure 4.2, uses oxygen, fuel gas and air to produce a high velocity flame, with uniform heating of the powder. The gas stream is accelerated through a converging/diverging De-Laval type nozzle to supersonic speed. The powder is introduced axially in the spray gun. The axial powder injection focuses the feedstock powder within the center of the flame, avoiding material buildup on the walls of the extended air cap and reduces wear. The Diamond Jet family offer efficient operation using less process gas in comparison with other HVOF spray systems. Material spray rates, depending on the system configuration and material applied, can be up to 150 g/min, reducing spray time. The gun works as well with hydrogen, methane, ethylene, propylene and propane [33]. In the present study propane, oxygen and air were used as process gases and nitrogen as carrier gas for the powder. The spraying parameters are presented in table 4.2, and they are typical parameters for cermet powders.

Table 4.2. HVOF spraying parameters

Propane [l/min]	68
Oxygen [l/min]	236
Air [l/min]	368
Powder feed rate [g/min]	60
Standoff distance [mm]	230
Traverse speed of gun [mm/s]	11

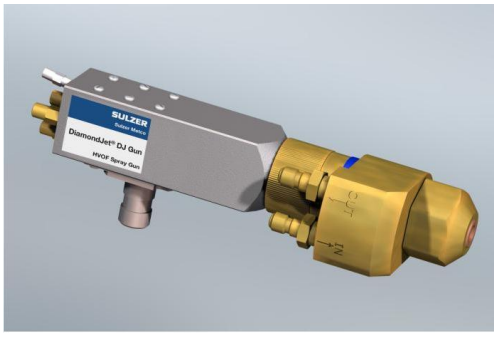

Figure 4.2 Diamond Jet Hybrid 2700 thermal spray gun

4.2.2 HVAF spray system

The M2 thermal spray gun (figure 4.3) operates at velocities in the range of 600-700 m/sec. It is suitable for carbides, metals and hard metal alloys. The gun is air cooled, with optimized combustion chamber developed for operation with natural gas, propane, propylene, MAPP gas which reduces operation costs. The gun is not susceptible to nozzle clogging and can operate many hours without interruptions. It is equipped with multiple nozzle configurations, for carbides and metals. It works with low operating cost while it uses compressed air instead of oxygen and it has a low consumption of spare parts [55].
In the present study air and propane were used as combustion fuels, and nitrogen as feedstock carrier gas. The spraying parameters are presented in table 4.3, and they are typical for carbides spraying.

Table 4.3. HVAF process parameters

Propane [MPa]	0.52
Air [MPa]	0.59
Standoff distance [mm]	150

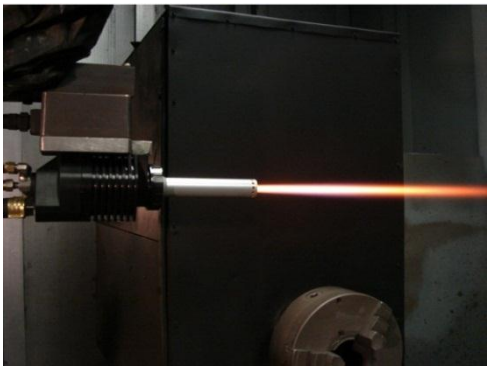

Figure 4.3 AC-HVAF M2 thermal spray gun

4.3 Characterization methods

Various characterization methods were used in order to characterize and analyze the used powders and the HVOF and HVAF deposited coatings.

4.3.1 Microscopic techniques

Optical/electron microscopes and a stereo microscope were used to characterize the micro and macro structures of deposited coatings. To study the morphology of the powder particles in cross section, powder particles were embedded in PolyFast resin then polished in order to prepare samples for microstructural characterization. The coated samples were cut using a Struers, Discotom 2 cut off machine using an abrasive disk with constant feed rate and constant pressure, afterwards the specimens were embedded in PolyFast resin, ground and polished according to Sulzer Metco's "Metallographic Preparation Data Sheet for Thermal Sprayed Samples" using an automated Pedemax 2 grinding/polishing apparatus.

Microscopes used in the research are described below.
Optical Microscope (OM)

The wear track of the samples after the sliding wear test were inspected by optical microscope system (Leica DM 2500).

Scanning Electron Microscope (SEM)

Morphology of the feedstock powders and structures of the deposited coatings were characterized using a scanning electron microscope (SEM, Philips XL-30). Secondary (SE) and back scattered (BSE) detectors were used. The structures of the coatings were analyzed from polished metallographic cross-sectional samples. The microscope was equipped with EDAX analyzer used for EDX chemical analysis.

Zoom Stereomicroscope (SM)

After abrasion rubber wheel tests the worn surface of the deposited coatings were analyzed with a stereomicroscope (SM, Leica MZ 7.5). Also worn cap of WC-Co ball after Ball on Disk tests was analyzed using the stereomicroscope. The abraded samples were ultrasonically cleaned in ethanol and the WC-Co balls with ethanol, prior to the surface respectively worn cap analysis.

Field Emission Scanning Electron Microscope (FESEM)

The morphology of the wear track of the coatings was investigated with a high resolution field-emission scanning electron microscope (FESEM, Zeiss ULTRAplus) in order to investigate the wear behavior.

4.3.2 XRD

XRD is perhaps the most common used tool for structural analysis of powders and deposited coatings. The accuracy of the XRD analysis is sufficient for general phase identification, texture and lattice parameter determination. The phase composition of the powders and coatings was investigated by Siemens Diffract 500 X-ray diffractometer using monochromatized Cu Kα radiation (1.5406 Å) using a 0.02° step size and 0.2 s step time. X-ray diffraction was performed at a tube voltage of 40 kV and a tube current of 30 mA. The X-ray intensity was measured over a 2θ diffraction angle from 10° to 100°.

4.3.3 Mechanical testing methods

Hardness

A Matsuzava MMT X7 Vickers tester was used to measure the microhardness ($HV_{0.3}$) as an average of ten measurements from the cross-section of coatings. The weight of the load was 300 g.

Roughness

The roughness measurements "Ra" and "Ry" of the as-deposited coatings were measured using a SJ-301 Mitutoyo surface roughness tester (8 measurements have been performed on each sample) in order to determine the main roughness values.

4.3.4 Wear tests

Abrasion wear test

Abrasion wear resistance of the coatings was evaluated by a rubber wheel abrasion wear testing device. Dry sand rubber wheel abrasion test is one of the most widely used testing method for abrasion wear. The tester allows performing tests on 5 samples in the same time. The dry sand is fed feed between the specimens and the rotating rubber wheel. Dry quartz sand was used as an abrasive with a grain size in the range of 0.1-0.6 mm, on ground samples. The diameter of the rubber wheel was 660 mm, the test load was 22 N, and the wear losses were measured after every 12 min. Duration of the test was 1h which equal to the total wear length of 5904 m. Before measurements the samples were cleaned with compressed air to remove the sand particles left on the samples.

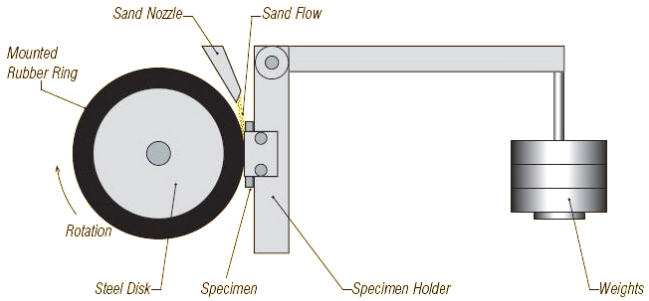

Figure 4.4 Schematics of rubber wheel abrasion test

Sliding wear test

The sliding wear tests were performed using a CETR UMT tribometer on polished surfaces with a 0.03 μm Ra final value. Three tests were carried out on each coating. A WC-Co ball with a diameter of 6.3 mm was used as a counter body. The applied normal force was 10 N and the diameter of the wear track was 22 mm. The test speed was 120 rev/min and it was performed on a 3000 m distance at room temperature.

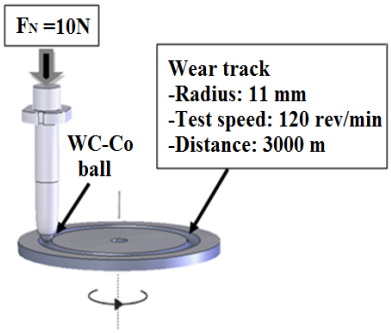

Figure 4.5 Pin-on-disk principle and parameters used for the tests

4.3.5 Corrosion tests

Open cell potential measurements

The denseness and the corrosion behavior of the coatings were evaluated with electrochemical open cell potential measurements. The electrochemical cell used in the open cell potential measurements was composed of a 20 mm diameter plastic tube and 12 ml volume glued on the surface of the coating specimen. A 3.5% NaCl solution was prepared and placed in the tube for 7/14/21/28 day measurements, taken with a Fluke 79 III multimeter. A silver/silver chloride (Ag/AgCl) was used as a reference electrode. The substrate, low carbon steel, was also tested as a reference. Between measurements the tubes were covered to prevent evaporation.

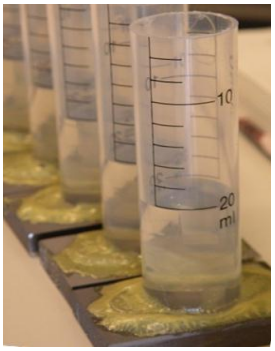

Figure 4.6 Samples subjected to open cell potential measurements

Salt spray test

The salt spray tests were performed according to standard ASTM B117 standard using a Liebisch S400 M-TR salt spray chamber. As-sprayed samples were masked with epoxy paint before test in order to allow only the coating surfaces to be in contact with the corroding salt spray fog. A 5-wt.% NaCl solution was used with an exposure of 96 h, a temperature of 35°C and a solution accumulation of 3 ml/h.

4.3.6 Other methods (image analysis, particle size measurements, optical profilometry)

In addition to the mentioned methods, particle size measurements, image analysis and optical profiling system were carried out.

Particle size measurements
Particle size distribution of the feedstock powders were measured with Sympatec Helos laser diffractometer in wet conditions.

Image analysis
The porosity of the coatings was quantified for each coating technique using Image Tool 3.00 software onto 7 BSE-SEM micrographs at 1000x magnification.

Optical profilometry
The topography of the surfaces after abrasion wear test were studied using a Veeco Wyko NT1100 optical profiler which provides three-dimensional surface images and more precise roughness measurements in comparison with the stylus type profilometer. The sliding wear tracks were also scanned with the optical profilometer and the volume loss was calculated with the Wyko Vison analytical software.

CHAPTER V. RESULTS AND DISCUSSIONS

5.1 Substrate material

The coatings were deposited onto low carbon steel substrates which contain up to 0.25 weigh percent of carbon with ferrite (the principal microstructural constituent) and perlite. Perlite is direct proportional with carbon content. From economical point of view this type of steel is cheap and possesses a good formability and weldability. It is used as sheet and strip steel, free cutting steel, case hardening steel, etc. [149,150].

5.2 Powder Materials

The most common and unavoidable problems of mechanical components of automobiles, powder generation units, aircraft, chemical processing equipment and so on are wear and corrosion. Wear and corrosion affect the lifetime of components and also considerably reduce their performances. Cermets composed of WC and Cr_xC_y grains embedded in Co, Cr, Ni based matrix are used nowadays for the protection against several forms of wear and corrosion in many type of industrial applications [151-154]. For industrial application cermet coatings, deposited by thermal spray techniques, are widely used for surface depositions to improve the wear and corrosion resistance of different components. Compared to WC-Co coatings, which are successfully applied for wear resistance, WC-CoCr coatings are suitable also for corrosive environments, due to Cr content [155]. These composites are blend of ceramic (cer) and metallic (met) materials (figure 5.1). The ceramic part has a good wear resistance while the metallic part, the matrix which tight together the carbide particles, has good corrosion resistance. Function of composition there are several types of cermets like oxide based cermets, carbide based cermets, boron nitride cermets, etc.

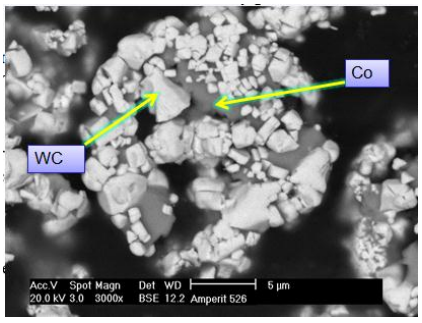

Figure 5.1 WC-15Co powder particle2

For comparison, standard carbide powders like WC-10Co-4Cr and Cr_3C_2-25NiCr as well as new developed powders recently introduced into the market, such as WOKA

7502, WOKA 7504 and Amperit 618074, were sprayed in this study by HVOF and HVAF methods. The powders are presented in table 5.1, as well their composition, grain size and producer. All powders are commercially available, excepting the XPT 520 powder which, at the moment, is an experimental powder manufactured by Sulzer Metco.

Table 5.1 Powders used in the HVOF and HVAF processes

	Trade name	Composition [%]	Grain Size [µm]	Producer
1	WOKA 3654FC	WC-10Co-4Cr	-30+10	Sulzer Metco
2	XPT 520	WC-10Co-4Cr	-38+10	Sulzer Metco
3	Durmat 135lo35	WC-10Co-4Cr	-15+5	Durum
4	Amperit 588	Cr_3C_2-NiCr	-25+10	HC. Starck
5	Durmat 251017	Cr_3C_2-NiCr	-35+5	Durum
6	WOKA 7502	CrC-37WC-18M	-45+15	Sulzer Metco
7	WOKA 7504	CrC-37WC-18M	-30+10	Sulzer Metco
8	Amperit 618074	WC-15FeCrAl	-45+15	HC. Starck

WOKA 3654FC (WC-10Co-4Cr)

The powder particles present typical agglomerated and sintered morphology prevailing rounded particles with certain degree of porosity. Due to the rounded powder particles it has a good flowability. The carbide grains were measured through SEM images and they are in the rage of 0.32-0.1 µm.

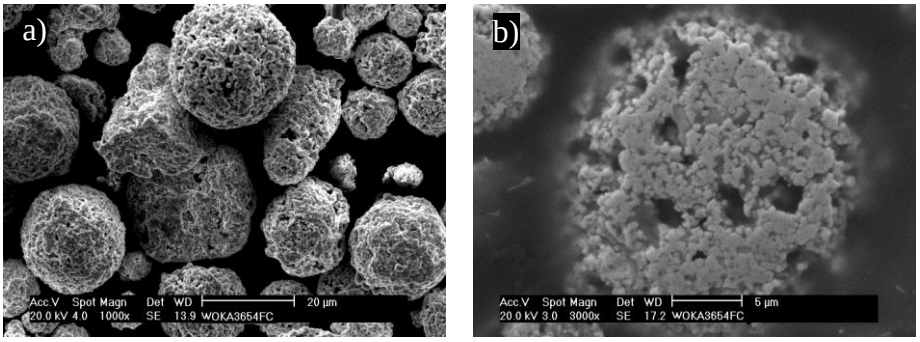

Figure 5.2 SEM images of WOKA 3654 FC powder: a) 1000x; b) particles cross-section at 3000X

The results of particle size measurements are summarized in table 5.2 and the results are similar with the nominal measurements given by the manufacturer.

Table 5.2 Results of particle size measurements

Powder	d_{10} [µm]	d_{50} [µm]	d_{90} [µm]
WOKA 3654 FC	10.92	19.93	30.90

The XRD pattern of the powder (figure 5.32) indicated the presence of WC as main phase in conjunction with Co_3W_3C and Cr as second phases.

XPT 520 (WC-10Co-4Cr)

The powder is an agglomerated and sintered WC-10Co-4Cr experimental powder designed to improve wear and corrosion resistance. The micrographs show spherical particles with pore entrances and low porosity content. The blocky shape under-micron carbides are in the range of 0.3 and 0.9 μm.

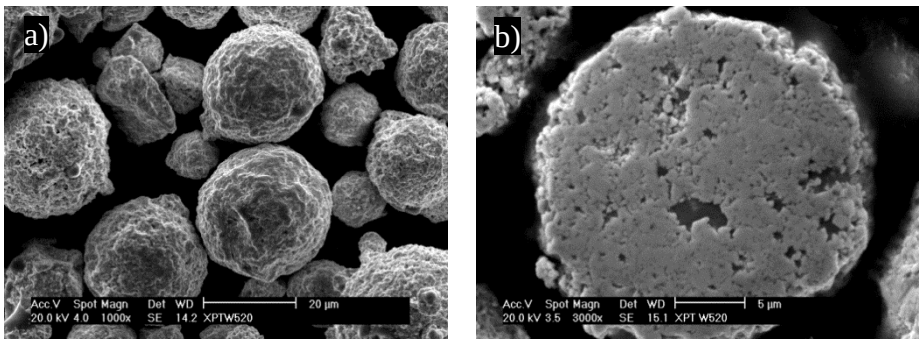

Figure 5.3 SEM images of XPT W520 powder: a) 1000x; b) particles cross-section at 3000x

The results of particle size measurements are presented in table 5.3 and it can be noticed that the powder particles are in the range of 13.71-38.76 μm, similar results with the nominal measurements given by the powder manufacturer.

Table 5.3 Results of particle size measurements

Powder	d_{10} [μm]	d_{50} [μm]	d_{90} [μm]
XPT W520	13.71	24.95	38.76

According to XRD spectra (figure 5.33), WC was identified as main phase in conjunction with Cr and Co_3W_3C as second phases.

Durmat 135lo35 (WC-10Co-4Cr)

The powder presents agglomerated and sintered microstructure with fine blocky carbide grains in the range of 0.15-0.75 μm. Particles are spherical mixed with particles with irregular form characterized by pore entrances and low degree of porosity.

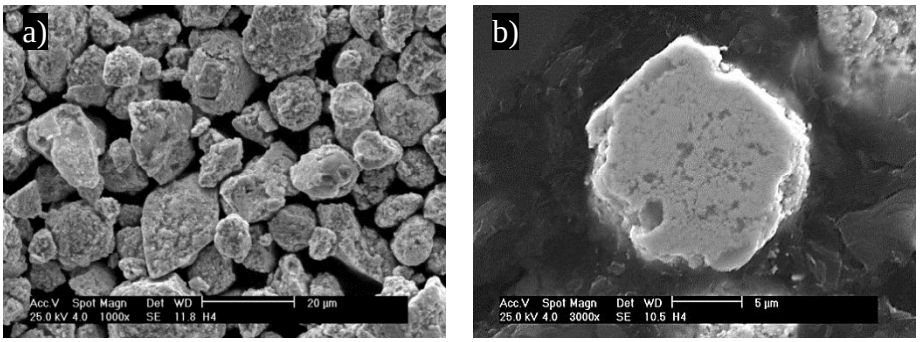

Figure 5.4 SEM images of Durmat 135lo35 powder: a) 1000x; b) particles cross-section at 3000x

The results of particle size distribution are presented in table 5.4, and the measured particles are somewhat above the nominal particle size.

Table 5.4 Results of particle size measurements

Powder	d_{10} [μm]	d_{50} [μm]	d_{90} [μm]
Durmat 135.LO35	9.16	13.90	20.81

According to the XRD spectrum, WC was found as main phase in the powder along with minor picks of Cr and Co_3W_3C. The powder is the finest one in the present study with fine carbide grains. It is expected that the sprayed coatings will have enhanced properties compared to coatings deposited with coarser powders and same chemical composition [156].

Amperit 588 (CrC-25NiCr)

The morphology of the powder is presented in figure 5.35. The powder is a mixture of rounded and irregular particles with small angular carbide grains aggregated by the metallic matrix. The internal microstructure of polished powder particle show the presence of two phases, carbide grains, which exhibit dark gray contrast and the metallic matrix, NiCr, which exhibits bright contrast.

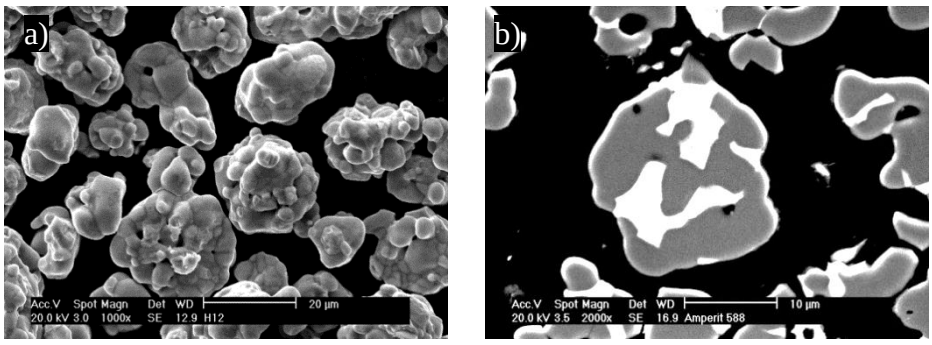

Figure 5.5 SEM images of Amperit 588 powder: a) 1000x; b) particles cross-section at 2000x

The powder particle size distribution is presented in table 5.5. It can be noticed that there are small differences between the obtained results compared to the nominal particle size.

Table 5.5 Results of particle size measurements

Powder	d_{10} [μm]	d_{50} [μm]	d_{90} [μm]
Amperit 588	13.99	20.85	29.50

The XRD spectrum of the powder (figure 5.34) showed Cr_3C_2 and NiCr major peaks.

Durmat 251017 (Cr_3C_2-25NiCr)

The morphology of the powder present agglomerated and sintered microstructure with spherical powder particles resulted from irregular carbide grains embedded into the metallic matrix. Within the cross-section of powder particles two phases can be

identified, carbide grains which exhibit dark gray areas and the metallic matrix which exhibits bright contrast.

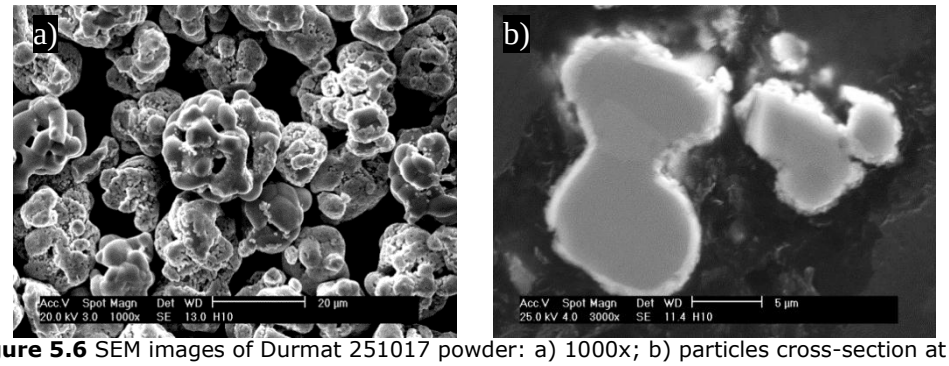

Figure 5.6 SEM images of Durmat 251017 powder: a) 1000x; b) particles cross-section at 3000x

The results of particle size measurements are presented in table 5.6. It can be noticed that the measurements are in the range of 15.54-34.41 μm, similar to values given by the powder manufacturer.

Table 5.6 Results of particle size measurements

Powder	d_{10} [μm]	d_{50} [μm]	d_{90} [μm]
Durmat 251 017	15.54	22.80	34.41

From the XRD spectrum of the powder Cr_3C_2 and NiCr were identified as main phases (figure 5.35).

WOKA 7502 (CrC-37WC-18M)

The CrC-37WC-18M powder has two stable carbide phases WC and Cr_3C_2 embedded into a Ni-Co-Fe metallic matrix which bind together the carbide phases. The powder particles show typical agglomerated and sintered rounded shapes. In cross section of some powder particles, pore entrances and reduced porosity can be noticed. The WC particles were measured by SEM and the grains were in the range of 0.25-1.7 μm.

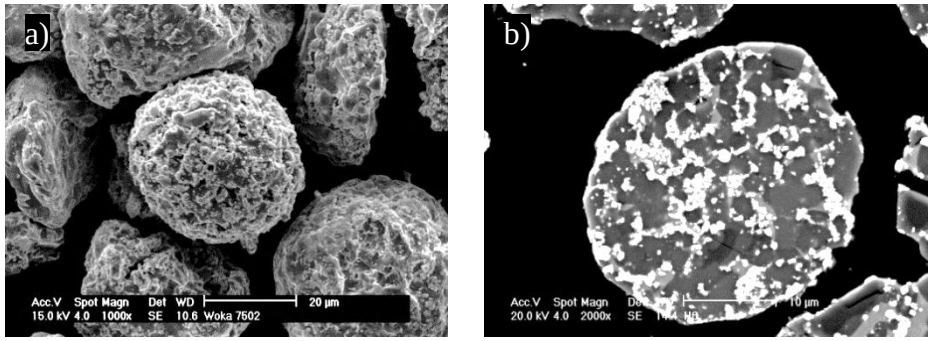

Figure 5.7 SEM images of WOKA 7502 powder: a) 1000x; b) particles cross-section at 2000x

Table 5.7 presents the size distribution measurements. According to the measurements the particles are distributed in the range of 22.17-50.9 μm, results above the nominal particle size which might be influenced by the different equipment used by the quality controlled measurements of the supplier.

Table 5.7 Results of particle size measurements

Powder	d_{10} [μm]	d_{50} [μm]	d_{90} [μm]
WOKA 7502	22,17	37,39	50,09

The XRD pattern of the feedstock powder (figure 5.36) indicated the presence of WC phases and Cr_3C_2 as main phases in conjunction with amounts of Ni.

WOKA 7504 (CrC-37WC-18M)

The CrC-37WC-18M powder has a finer grade than WOKA 7502 powder and similar morphology. As well the WOKA 7502 the powder is an agglomerated and sintered powder with rounded morphology and carbide grains in the range of 0.5-1.7 μm.

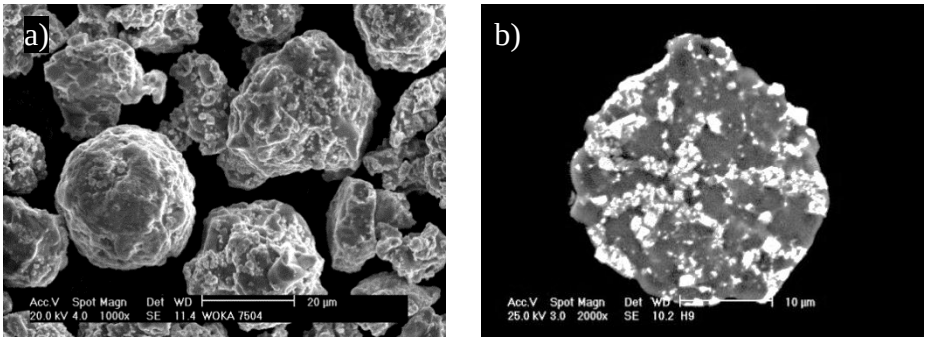

Figure 5.8. SEM images of WOKA 7504 powder: a) 1000x; b) particles cross-section at 2000x

The particle size distribution of the powder presented in table 5.8 is in the range of 15.77-34.77 μm and it is characterized by large amount of powder particles above the nominal size.

Table 5.8 Results of particle size measurements

Powder	d_{10} [μm]	d_{50} [μm]	d_{90} [μm]
WOKA 7504	15,77	25,22	34,77

Due to the fact that the powder has the same phase composition like WOKA 7502 powder the XRD pattern showed similar peaks ascribable to WC, Cr_3C_2 and Ni.

Amperit 618074 (WC-FeCrAl)

The WC-FeCrAl powder, exhibit a rounded morphology, characterized by pore entrances typical of agglomerated and sintered powders with pores, visible in cross section of powder particles. The powder presents sub-micron carbides, most of the grains in the rage of 0.29-0.49 μm. The powder contains WC rich regions, Cr rich regions which are embedded into a Fe-Al matrix.

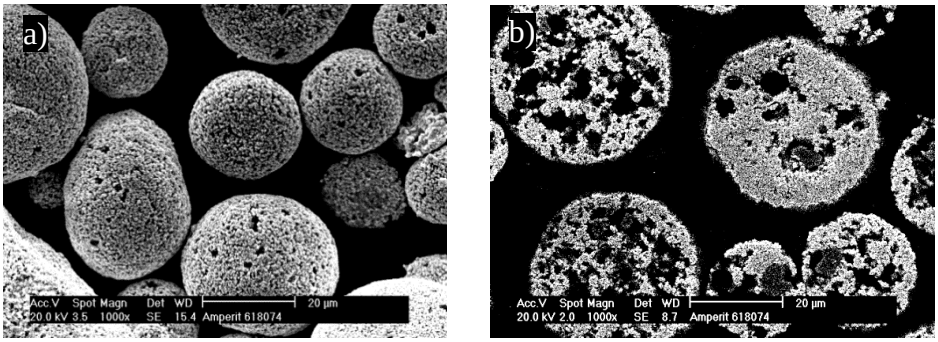

Figure 5.9 SEM images of Amperit 618074 powder: a) 1000x; b) particles cross-section at 1000x

The particle size distribution of the WC-FeCrAl powder is presented in table 5.9 and it is similar to the nominal size given by the manufacturer. It is a recently developed powder [157] and there are limited studies in the literature regarding this environmental friendly carbide.

Table 5.9 Results of particle size measurements

Powder	d_{10} [µm]	d_{50} [µm]	d_{90} [µm]
Amperit 618 074	23.26	40.33	59.28

The XRD pattern of the powder (figure 5.37) indicated the presence of WC phase along with Fe and $(Cr, Fe)_6C$ structure, similar to the literature [158].

5.3 Microscopic properties of HVOF and HVAF cermet coatings

Polished cross section of the coatings were investigated by SEM using BSE detector giving atomic number contrast and employed for microstructural observation at 100X, 1000X and 4000X magnification and local areas of semi quantitative assessments of chemical compositions were obtained by performing local EDX scans for each coating. Usually the sprayed coatings have a lamellar structure due to the impact of high speed of molten/unmolten particles on the substrate and they present pores due to generation of gas within the coatings or due to the solidification of molted particles and oxides generated during inflight by their reaction with atmosphere [159].

WOKA 3654 FC (WC-10Co-4Cr) HVOF coating

The cross sectional microstructures of the coating, presented in figure 5.10, show a dense coating with low porosity, ~0.73 vol.%, and uniformly dispersed angular WC grains. The sprayed coating has a thickness of ~300 µm and a hardness value 1054±151 HV_{300}. The mean surface roughness value of the as deposited coating was Ra=3.64 µm. The high magnification SEM micrograph and EDX local scans revealed three distinct areas within the coating. WC rich areas showed up very

bright while the metallic matrix has different shades of gray due to Cr and Co content, confirmed by EDX spectra in figure 5.11.

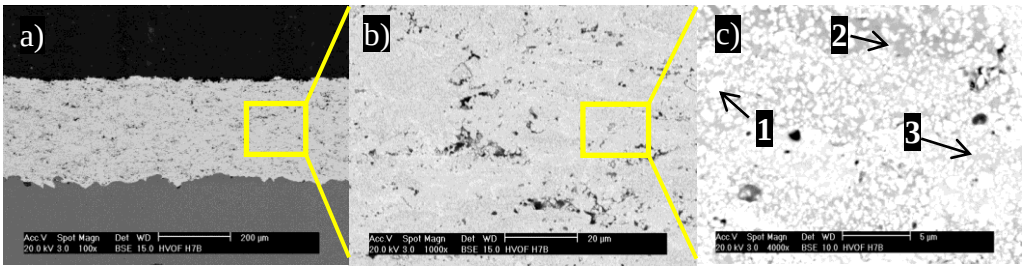

Figure 5.10 WOKA 3654 FC HVOF coating: a) 100X, b) 1000X and c) 4000 X BSE

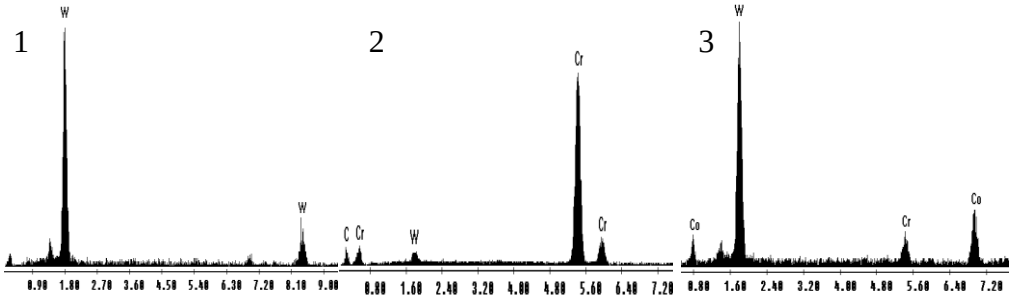

Figure 5.11 EDX spectra of WOKA 3654FC HVOF coating

WOKA 3654 FC (WC-10Co-4Cr) HVAF coating

The coating has a thickness of ~310 µm with low levels of porosity, ~0.93 vol.%, with mean roughness value of Ra=4.78 µm. An average hardness value of 1152±92 HV_{300} was measured for the deposited coating. The WC phase showed up very bright while the metallic matrix has different shades of gray depending on the amount of Cr and Co contained locally (figure 5.12). The coating presented angular WC grains embedded into a metallic matrix. The EDX spectra indicated that lighter areas correspond to WC areas, dark gray correspond to Cr rich areas and gray shades correspond to Co rich areas (figure 5.13).

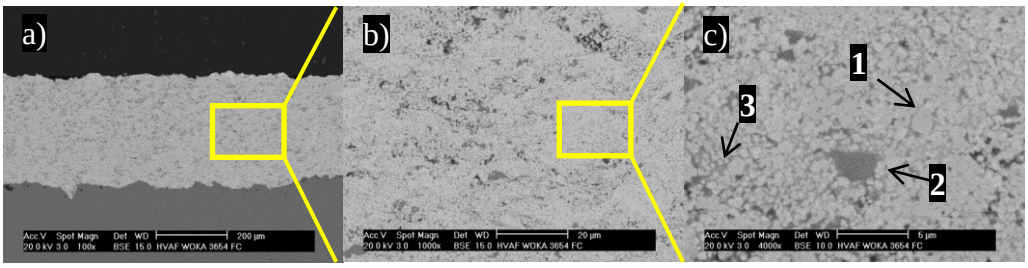

Figure 5.12 WOKA 3654 FC HVAF coating: a) 100X, b) 1000X and c) 4000 X BSE

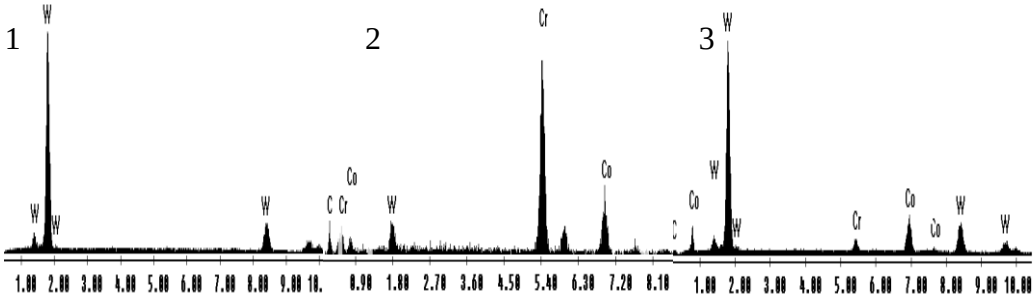

Figure 5.13 EDX spectra of WOKA 3654FC HVAF coating

XPT 520 (WC-10Co-4Cr) HVOF coating

The cross sectional microstructures of the coating, figure 5.14, show a dense coating with good adhesion to the substrate. The typical WC-CoCr coating presents quite low porosity, ~1.1 vol.%, and uniformly dispersed angular WC grains in the metal matrix. The sprayed coating has a thickness of ~300 μm and a hardness value of 1110±165 HV_{300}. The surface roughness of the as deposited coating was Ra=4.54 μm, similar to measurements found in the literature [160]. The high magnification SEM micrograph and EDX local scans (figure 5.15) revealed three typical areas within the WC-CoCr coating: bright areas which contain high amounts of WC and metallic matrix with different shades of gray due to locally contained Cr and Co. Dark gray shades correspond to Cr areas while gray shades correspond to Co rich areas.

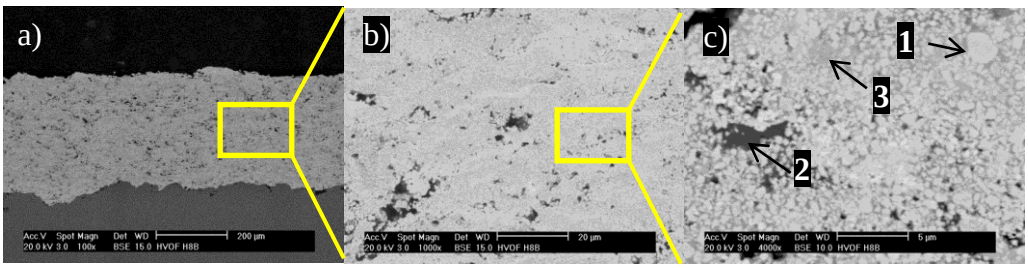

Figure 5.14 XPT 520 HVOF coating: a) 100X, b) 1000X and c) 4000 X BSE

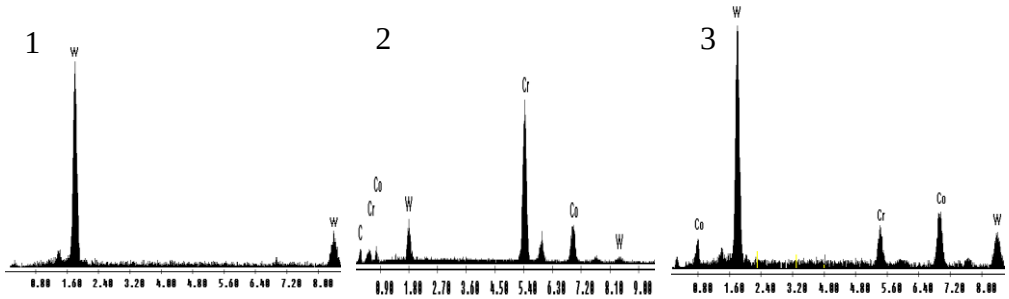

Figure 5.15 EDX spectra of XPT 520 HVOF coating

Durmat 135Lo35 (WC-10Co-4Cr) HVAF coating

The sprayed HVAF coating has a thickness of ~250 µm, presents low level of porosity (0.92 vol.%) and the mean roughness value of the as sprayed coating is Ra=3.06 µm. An average hardness value of 1148±84 HV_{300} was measured for the deposited coating. In the high magnification micrographs the WC phase showed up very bright while the metallic matrix has different shades of gray depending on the amount of Cr and Co contained locally (figure 5.16), which was confirmed by the EDX spectra (figure 5.17). Lighter areas correspond to WC areas, dark gray correspond to Cr rich areas and gray shades correspond to Co rich areas.

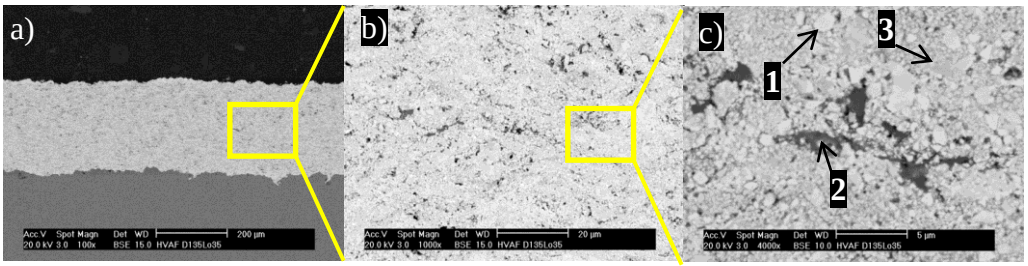

Figure 5.16 Durmat 135Lo 35 HVAF coating: a) 100X, b) 1000X and c) 4000 X BSE

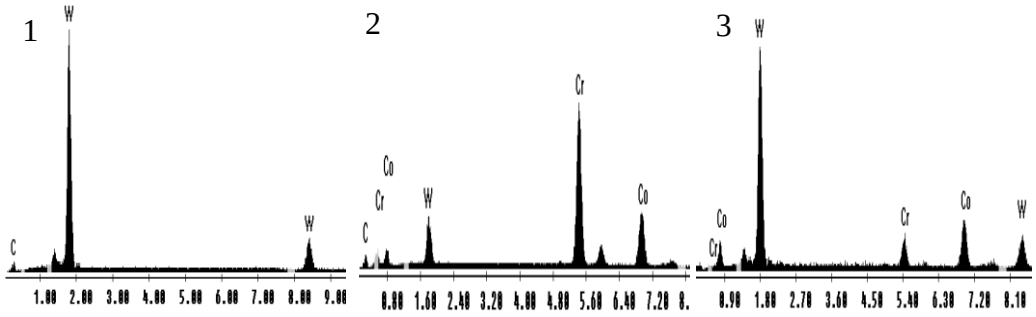

Figure 5.17 EDX spectra of Durmat 135lo35 HVAF coating

The WC-10Co-4Cr coatings deposited by HVOF respectively HVAF spraying processes have a good adherence to the substrate according to SEM micrographs. The presence of blocky WC grains within the coatings indicated that the spraying conditions did not affect the morphology of carbides which is similar after spraying with the morphology of carbides found in the feedstock powders this according to the high magnification micrographs. Differences might be noticed in the metallic matrix. In the HVAF coatings a higher retention of Cr rich areas might be noticed with varying compositions similar to the feedstock powder and there was no indication that the matrix changed during spraying. Comparing both coatings, HVOF and HVAF, deposited using as feedstock WOKA 3654 FC powder it might be noticed that there are differences regarding the hardness, roughness values and porosity levels of the coatings. The increased hardness of HVOF coating might be caused due to oxidation during well time. The lower hardness, slightly increased porosity level and higher roughness values of HVAF sprayed coatings might be due to insufficient

melting of powder particles. Using as feedstock finer powder an enhanced quality of HVAF coating might be noticed. The porosity within the coating decreased by decreasing the size of the powder particle due to higher impact speed of smaller particles compared to larger ones. If the particles are small enough they can easily fill the gaps between the larger particles [159]. This is also an important parameter which enhances the quality of the HVAF coating. With the HVAF process coatings with quite low level of porosity and high retention of WC as primary phase might be obtained. It might be concluded that the HVAF coatings deposited using fine powders with small carbide sizes have similar or even increased hardness, reduced roughness values and lower porosity levels compared to HVOF sprayed WC-CoCr coatings.

Amperit 588 (CrC-25NiCr) HVOF coating

According to the SEM images presented in figure 5.18, it appears that the coating is dense and homogenous distribution of the carbide in the metallic matrix can be noticed. The coating exhibits a lamellar structure manufactured by the deposition of elongated splats parallel to the surface of the substrate. The coating has a thickness of ~250 μm with 885±55 HV_{300} hardness value and a degree of porosity about 1.37 vol.%. The mean roughness value of the as-deposited coating is Ra = 5.12 μm. High magnification SEM and EDX spectra (figure 5.19) indicated the presence of Cr_3C_2 phase which show up in gray shades while the metallic matrix present different shades of light gray, depending on the amount of chromium contained locally. Most carbide particles in the as-sprayed coating are rounded and some of them present irregular shape and are embedded in the metallic matrix.

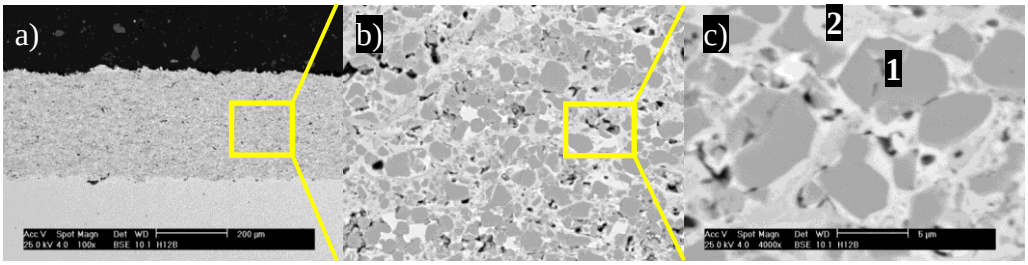

Figure 5.18 Amperit 588 HVOF coating: a) 100X, b) 1000X and c) 4000 X BSE

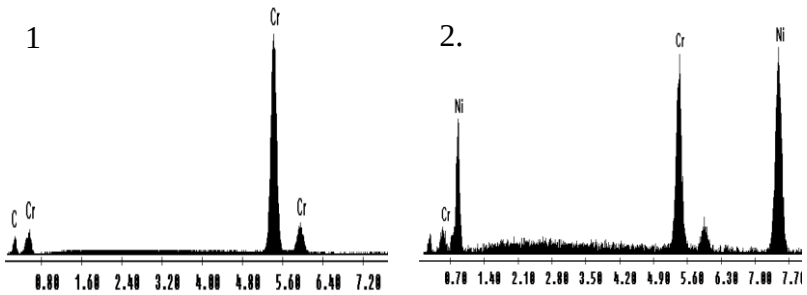

Figure 5.19 EDX spectra of Amperit 588 HVOF coating

Amperit 588 (CrC-25NiCr) HVAF coating

In figure 5.20 the microstructure of HVAF deposited Cr_3C_2-25NiCr coating is presented. The SEM images indicated a dense coating with good bonding with the substrate. The thickness of the coating is ~210 μm and the degree of porosity is about 2.82 vol.%. The surface roughness of the as-sprayed coating was Ra=3.92 μm and the hardness value was 779±36 HV_{300}. Cr_3C_2 and NiCr were the two phases detected by EDX (figure 5.21) and the carbide phase show up in gray shades while the metallic matrix has light gray shades. The carbide grains are rounded or have irregular shapes.

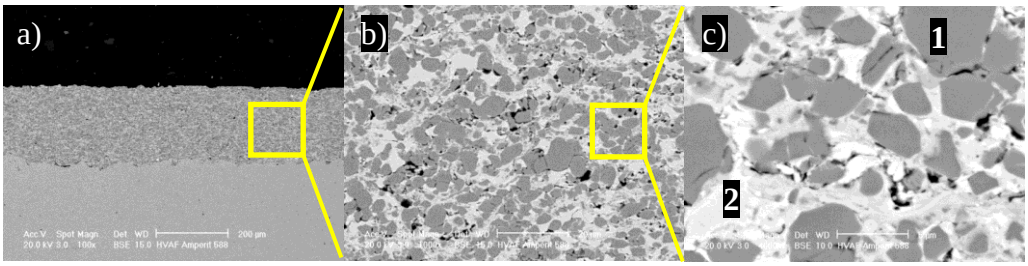

Figure 5.20 Amperit 588 HVAF coating: a) 100X, b) 1000X and c) 4000 X BSE

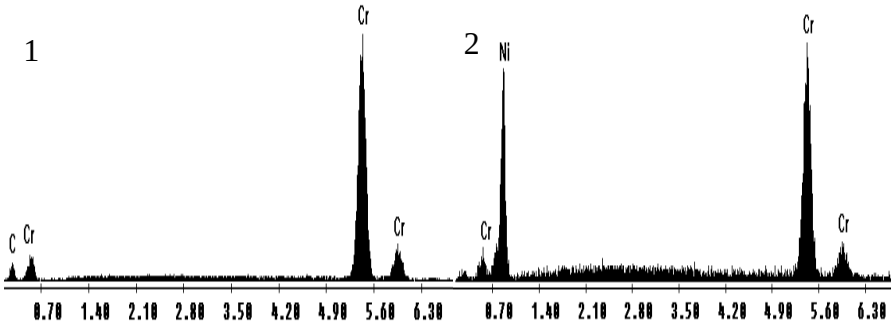

Figure 5.21 EDX spectra of Amperit 588 HVAF coating

Durmat 251017 (CrC-25NiCr) HVAF coating

The micrographs presented in figure 5.22, show the microstructure of the deposited coating. According to the micrographs the coating presents a good adhesion to the substrate and contains certain amount of pores. The coating has a thickness of ~220 μm with 873±74 HV_{300} hardness value and a degree of porosity about 1.93 vol%. The roughness value of the as-sprayed coating was Ra=4.83 μm. The high-magnification micrograph in figure 5.22c and EDX spectra (figure 5.23) revealed that the gray areas represent the Cr_3C_2 phase with high amount of Cr and the lighter shade represents the metallic matrix. The different shades in the metallic matrix are due to the different amount of Cr contained locally.

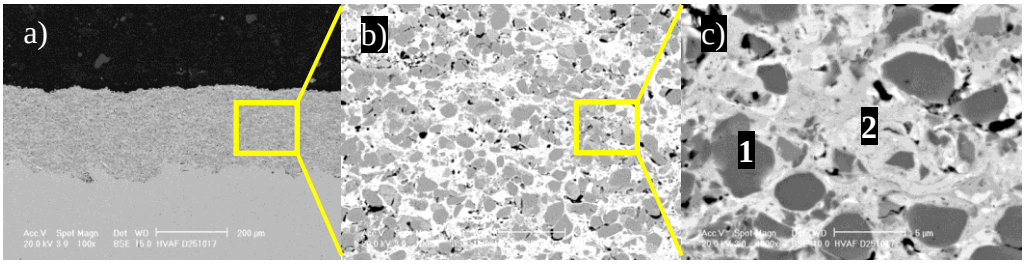

Figure 5.22 Durmat 257017 HVAF coating: a) 100X, b) 1000X and c) 4000 X BSE

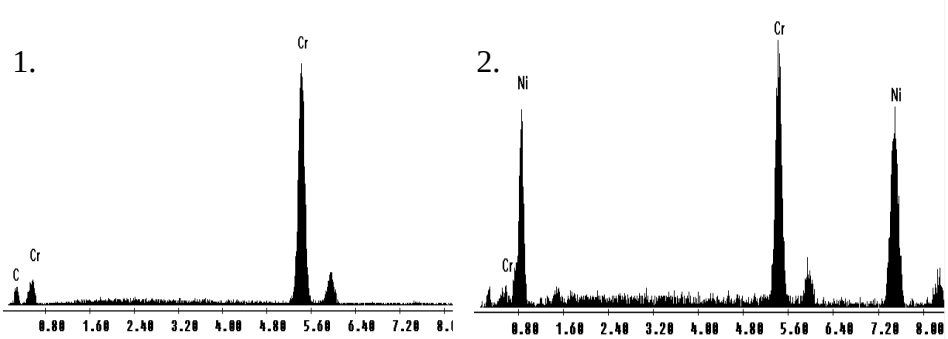

Figure 5.23. EDX spectra of Durmat 257017 HVAF coating

The HVAF coatings presented somehow higher degree of porosity due to "coldest" spraying conditions which kept the in-flight particle temperature at lower values. The lower temperature reduced the proportion of liquid phase and plastic behavior which affected the particle deformability. Some of the pores within the deposited coatings might result also from the pooling out of the poorly bounded particles during the sample preparation process. The roughness measurements indicated that the HVAF coatings have smoother surface compared to HVOF coating which on the other hand has an increased hardness which might be a result of an extensive carbide dissolution generated due to solid solution strengthening within the coating and oxidation during spraying.

WOKA 7502 (CrC-37WC-18M) HVOF coating

The SEM micrographs indicated that the WOKA 7502 HVOF coating has good adherence to the substrate according to SEM micrograph and low amounts of pores and impurities can be noticed. The degree of porosity was 1.63 vol.% and the coating has a thickness of ~270 µm with 1045±65 HV_{300} hardness value and Ra = 5.25 µm roughness values of as-deposited coating. The EDX spectra and high magnification SEM images, figure 5.24 and figure 5.24 indicated the presence of WC and Cr_3C_2 phases embedded in the metallic matrix. WC particles showed up very bright, while the Cr_3C_2 phase has different shades of gray, depending on the amount of chromium contained locally. The metallic matrix has a light gray shade.

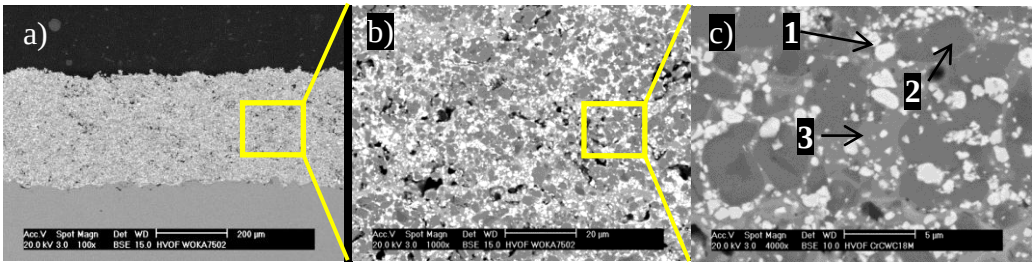

Figure 5.24 WOKA 7502 HVOF coating: a) 100X, b) 1000X and c) 4000 X BSE

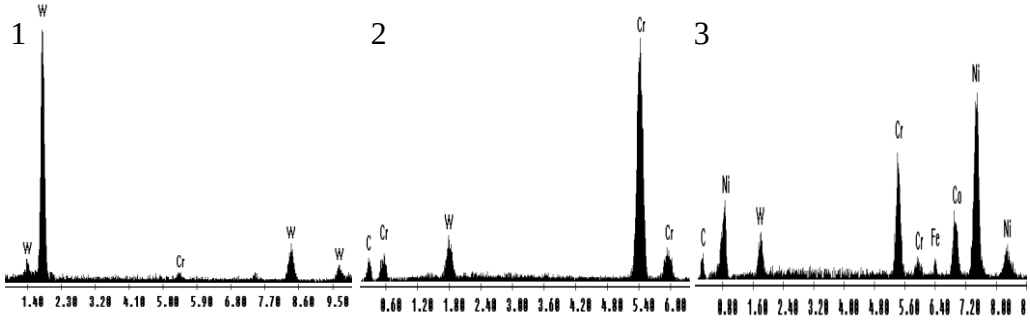

Figure 5.25 EDX spectra of WOKA 7502 HVOF coating

WOKA 7504 (CrC-37WC-18M) HVAF coating

Similar to HVOF coating, the HVAF sprayed coating indicated a good adherence to the substrate according to SEM micrograph with reduced impurities between coating and substrate (figure 5.26a). The deposited coating has a thickness of ~160 µm and presents a lower degree of porosity compared to HVOF coating. The degree of porosity was 0.96 %, and this might be due to an increased particle velocity and different particle size distribution of feedstock powder. The roughness value of the as-deposited coating was Ra=5.18 µm and the hardness value were about 932±47 HV_{300}. The EDX and high magnification SEM indicated the presence of WC (bright) and Cr_2C_3 (gray) phases and metallic matrix within the coating.

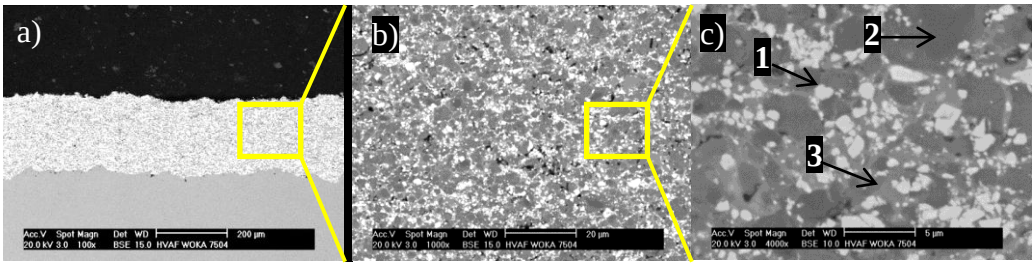

Figure 5.26 WOKA 7504 HVAF coating: a) 100X, b) 1000X and c) 4000 X BSE

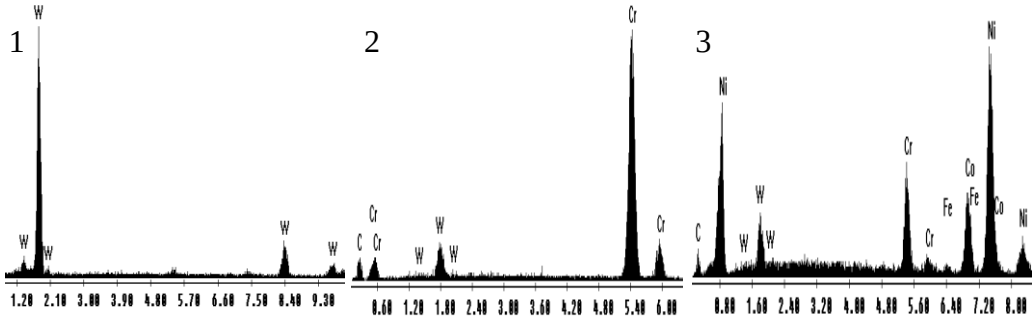

Figure 5.27 EDX spectra of WOKA 7504 HVAF coating

The presence of WC and Cr_2C_3 phases can be noticed in both coatings. EDX spectra (figure 5.27) of metallic matrix region in the HVOF coating indicates the presence of a much larger amount of Cr which is probably caused by some interdiffusion between the metallic matrix and the carbide phase. It is thought that the reason for the increased hardness within the HVOF coating is the presence of hard but brittle phases formed during spraying due to decarburization process.

Amperit 618074 (WC-FeCrAl) HVOF coating

Figure 5.28 presents a dense and homogenous coating with thickness about ~294 µm and reduced porosity. The WC carbide rich areas showed up very bright, Cr rich areas have dark gray shades while the metallic matrix contains Fe, Cr, Al and likely some dissolved W due to the higher process temperature of HVOF process (figure 5.29). The gray areas represent Cr rich areas, with different shades of gray depending on the amount of Cr contained locally. Within the metallic matrix the presence of W might be influenced also by the homogenous distribution of carbide phase in the metallic matrix and the reduced matrix between carbide grains which made more difficult the EDX quantification. It is thought that the metallic matrix was completely melted, during spraying; basically it was subjected to interdiffusion, homogenization and oxidation. When impacting the substrate and solidified due to high quenching rates amorphous phases might form [158]. After solidification the splats are subjected to re-heating for short periods of time while the gun successively passes the substrate which causes oxidation of the deposited lamellas. During in-flight Al is more liable to oxidation while it has a great affinity to oxygen. The degree of porosity within the coating was 0.72 vol.% and the surface roughness of coating was Ra=4.33 µm with hardness values about 1072±47 $HV_{300,}$ values influenced by dissolution and oxidation of the coating due to spraying parameters but somewhat lower compared to WC-CoCr deposited coatings studied in this work.

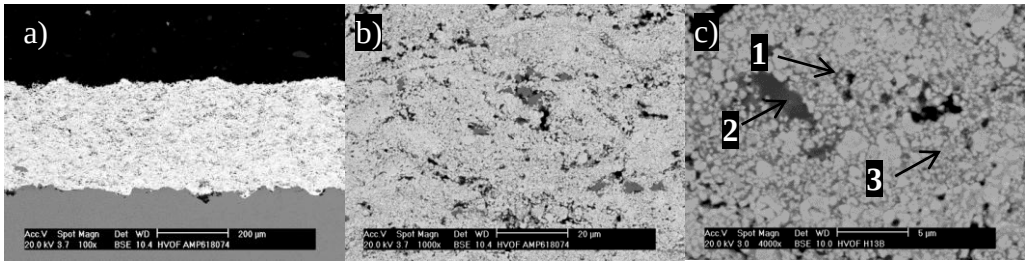

Figure 5.28 WC-FeCrAl HVOF coating: a) 100X, b) 1000X and c) 4000 X BSE

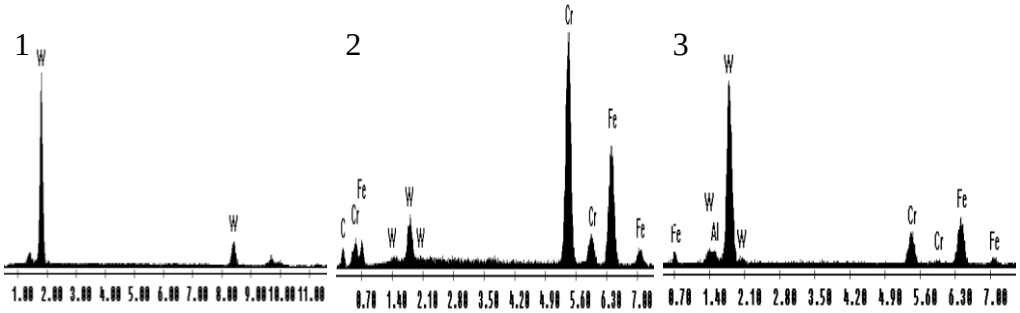

Figure 5.2 EDX spectra of Amperit 618074 HVOF coating

Amperit 618074 (WC-FeCrAl) HVAF coating

Figure 5.30 presents the morphology of the HVAF sprayed coating. There are some similarities between the HVAF coating and the previous mentioned HVOF coating. The coating presents a dense and homogenous structure with a thickness about ~230 µm. WC rich areas showed up very bright while the metallic matrix has gray shades due to Cr rich areas. The metallic matrix contains Fe, Cr, Al confirmed by EDX spectra (figure 5.31). The degree of porosity within the coating was 1.56% and surface roughness Ra=7.58 µm. The hardness of the coating was 756 HV_{300}, much lower than the hardness value of deposited coating using the HVOF system.

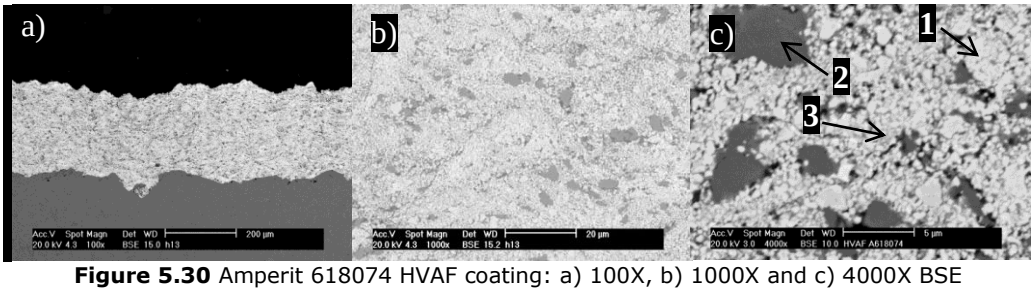

Figure 5.30 Amperit 618074 HVAF coating: a) 100X, b) 1000X and c) 4000X BSE

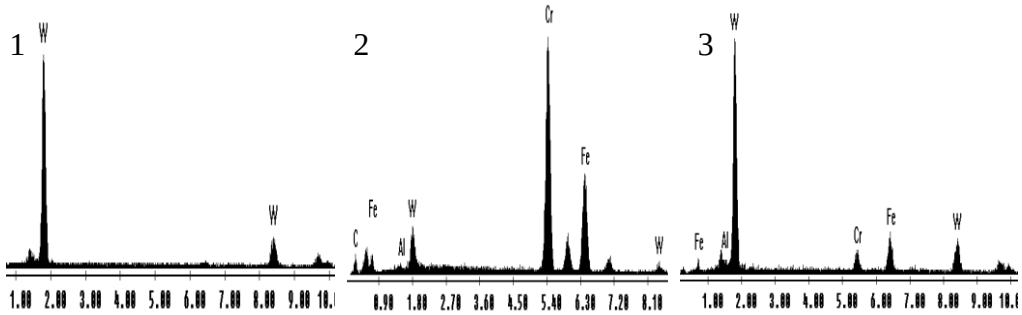

Figure 5.31 EDX spectra of Amperit 618074 HVAF coating

Even if the WC-FeCrAl HVAF deposited coating suffered less decarburization and presumably less oxidation during the spraying process the HVOF coating presented better properties. The reason might be the particle size distribution of feedstock powder which was a bit coarser for the HVAF deposition and also the spraying parameters played an important role in the spraying process. The presence of larger Cr rich areas in the HVAF coating indicated a lower dissolution within the coating compared to HVOF coating. The much lower hardness value of HVAF deposited coating might be due to spraying parameters which did not allowed a proper melting of powder particles. When impacting the substrate the powder particles did not form proper splats having as result increased porosity and increased roughness value of the as-sprayed surface. These factors as well the reduced oxidation might be the reasons for a lower hardness value of HVAF coating.

5.4 XRD pattern of HVOF and HVAF cermet coatings

An accurate phase analysis of powders and coatings was performed using the XRD (X-ray Diffraction) which has a significant importance when is about to characterize and compare thermally deposited powders and coatings.

WOKA 3654 FC (WC-10Co-4Cr) HVOF/HVAF coatings

The XRD patterns of WOKA 3654FC HVOF and HVAF powders are presented and compared in figure 5.32. The HVOF coating indicated that the coating contains a significant fraction of W_2C phase which results from the deposition process, similar to results reported in the literature [161, 162] and disappearance of Co_3W_3C phase. This indicates decarburization due to high temperature oxidation during the spraying process therefore the feedstock powder is subjected to significant phase transformation, as it was found in the literature [163-164, 172]. As opposed to, the HVAF coating presented no significant transformation compared to the diffraction pattern of the feedstock powder. This indicated that there is no significant decarburization during the HVAF process.

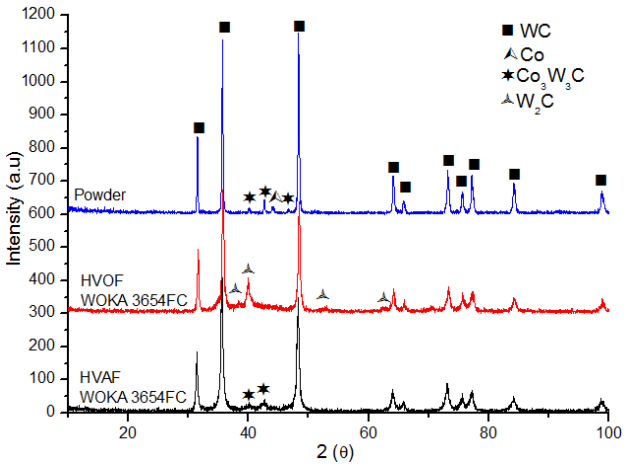

Figure 5.32 XRD pattern of WC-10Co-4Cr (WOKA 3654FC) feedstock powder, HVOF and HVAF coatings

XPT 520/Durmat 135Lo35 (WC-10Co-4Cr) HVOF/HVAF coatings

The XRD patterns of the WOKA 3654FC HVOF and HVAF powders are presented and compared in figure 5.33. As in the previous case, the HVOF coating indicated typical fraction of W_2C phase which results from the spraying process and disappearance of Co_3W_3C phase. This indicates decarburization due to high temperature oxidation during the spraying process therefore as in the previous case the feedstock powder is subjected to phase transformation during HVOF spraying. Similar behavior was found in the literature [166,167]. Unlike the HVOF sprayed coating, the HVAF sprayed one, presented no significant transformation compared to the diffraction pattern of the feedstock powder. This indicated that there is no significant decarburization during the HVAF process.

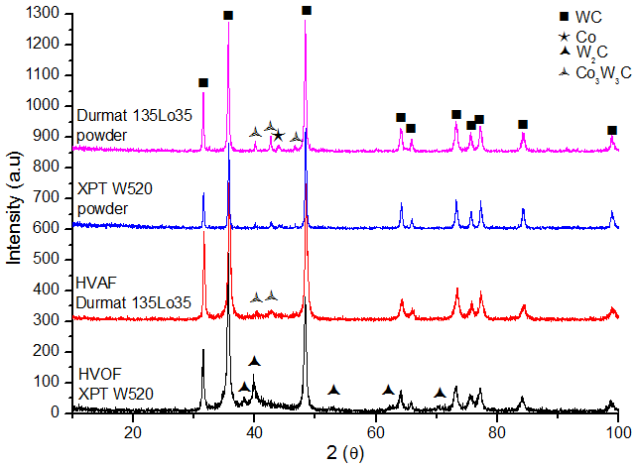

Figure 5.33 XRD pattern of WC-10Co-4Cr (XPT 520 and Durmat 15lo35) feedstock powders, HVOF and HVAF coatings

During HVOF spraying larger W_2C fractions in the deposited coatings are associated to fine powders, due to small momentum inertia of powder particles during inflight [168,169]. In the HVAF coatings this cannot be noticed due to the lower process temperatures. The Co phase in the HVAF coatings disappeared and the Co_3W_3C phase is a bit shifted, but it might be concluded that the coatings were not subjected to significant phase transformation.

Amperit 588 (CrC-25NiCr) HVOF/HVAF coatings

Figure 5.34 presents the XRD patterns of feedstock powder and as-sprayed HVAF and HVOF coatings.

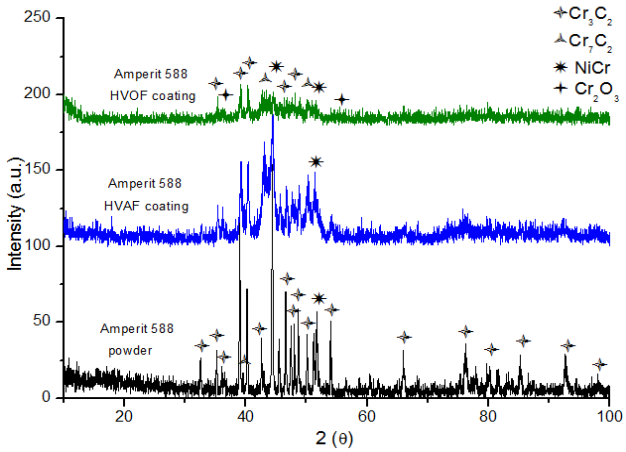

Figure 5.34. XRD pattern of CrC-NiCr (Amperit 588) feedstock powder, HVOF and HVAF coatings

The peaks are well define in the feedstock powder, but a significant peak broadening is noticed in both coatings due to the dissolution of carbides and the presence of amorphous phases. Into the feedstock powder Cr_3C_2 was detected representing the carbide phase and NiCr the metallic matrix. Phase constitution of boat coatings consisted of Cr_3C_2, Cr_7C_2 and NiCr solid solution while Cr_2O_3 was the only oxide phase hardly identify in XRD pattern of HVOF coating. This is attributed to oxidation occurred due to residence time of the particle in the hot flame and contact with oxygen during spraying.

Durmat 251017 (CrC-25NiCr) HVAF coating

The XRD patterns of feedstock powder Durmat 251017 and HVAF coating are presented in figure 5.35. Cr_3C_2 and NiCr were the only phases detected in the feedstock powder while the coating presented the same phases and in addition the presence of Cr_7C_2 phase was noticed according to JCPDS standard card. A broadening of the peaks might be noticed indicating reduced phase degradation during spraying.

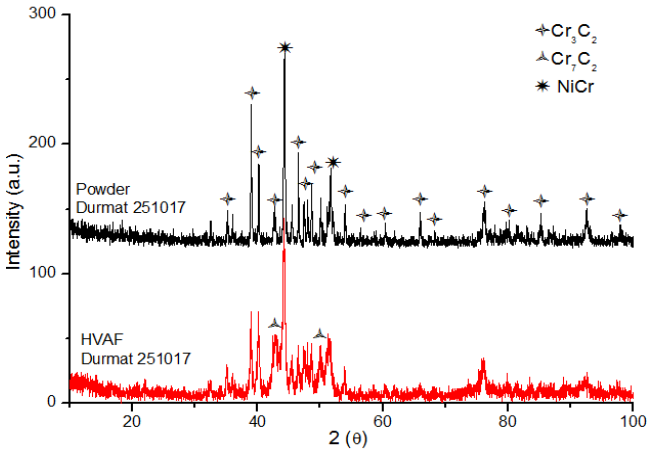

Figure 5.35 XRD pattern of CrC-25NiCr (Durmat 251017) feedstock powder and HVAF coating

In all thermally sprayed Cr_3C_2-25NiCr coatings the small amorphous peak is thought to result from the rapid solidification. All coatings presented phase degradation according to the XRD spectra. A difference between the powders and coatings is the presence of Cr_2O_3 in the HVOF coating and the Cr_7C_2 phase in both coatings. The reduced phase degradation in the HVAF coatings reflected mostly by the NiCr peak which were narrower and of higher intensity compared to HVOF coating indicated reduced phase degradation. The more intense degradation of metallic phase in the HVOF coatings might be due to residence time of the particle in the hot flame and contact of chromium carbide with oxygen during spraying; therefore the HVOF pattern indicated higher dissolution and lower peak intensity compared to HVAF coating.

WOKA 7502/WOKA 7504 (CrC-37WC-18M) HVOF/HVAF coatings

The XRD pattern indicated that the HVAF coating has an identical peak position with the feedstock powder but the diffraction peaks are somewhat brother. This might be caused to lower interdiffucion process compared to HVOF coating, between the chromium carbide phase and metallic matrix, which means that no significant transformation took place during spraying. The presence of WC, Cr_3C_2 and Ni phases can be noticed in both coatings and powder. As a difference between the coatings, the W_2C and Cr_2O_3 were also identified in the HVOF coating according to JCPDS standard card. Likewise, other small peaks were identified in the XRD pattern and it is thought that they might correspond to Cr_7C_3 or other phases which were hard to identify, as it was presented also in the literature [170].

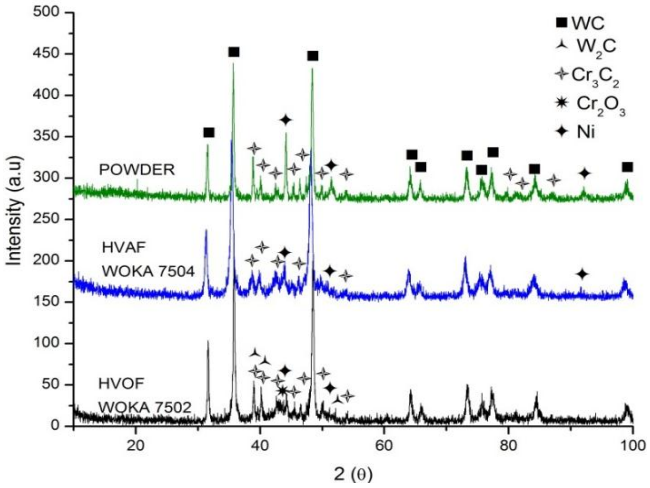

Figure 5.36. XRD spectra of CrC-37WC-18M feedstock powder, HVOF (WOKA 7502) and HVAF (WOKA 7504) coatings

WC-FeCrAl (Amperit 618074) HVOF/HVAF coatings

The XRD patterns of the powder and coatings are presented in figure 5.37. In the feedstock powder diffraction peaks of WC are detectable.

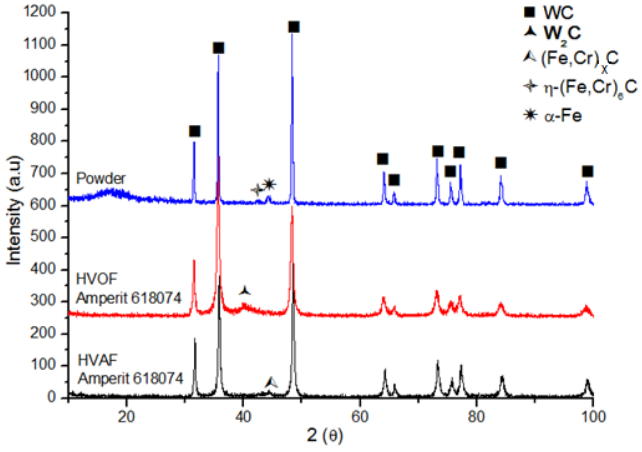

Figure 5.37 XRD spectra of WC-FeCrAl (Amperit 618074) feedstock powder, HVOF and HVAF coatings

Apart from WC peaks, α-Fe and (Fe, $Cr)_6C$ phases are detectable and they correspond to the Cr rich areas and Fe-Al metallic matrix. The HVOF coating exhibits a weak diffraction peak at 2θ=41° which might correspond to W_2C thereby is an evidence of decarburization. The position of the peak does not match exactly with the peak position reported in the JCPDF standard card but is thought it corresponds to W_2C while it forms during HVOF spraying of WC based carbide powders. The HVAF coating exhibits only a weak peak of (Fe, $Cr)_xC$ apart from WC peaks which are obvious, indicating a reduced phase degradation. The minimization of

decarburization process during HVAF spraying proves that the lower process temperatures have a significant influence on the W_2C brittle phase. The HVAF coating apart from WC peaks exhibits only a weak peak of $(Fe,Cr)_XC$ phase which is thought to correspond to the Cr rich regions and metallic matrix. Differences between the feedstock powder and HVOF coatings as a result of the deposition process are typical for WC based cermets as it was reported in literature [171].

5.5 Wear resistance of HVOF and HVAF cermet coatings

5.5.1 Abrasion wear resistance

Dry sand rubber wheel abrasion test is one of the most widely used testing methods for abrasive wear. The coatings sprayed by means of HVOF and HVAF techniques were tested and the results were compared in order to study their abrasive wear resistance.

WOKA 3654 FC HVOF/HVAF

Table 5.10 presents the abrasion wear results and it can be noticed that the coatings have a good wear resistance. Among them, the HVAF coating suffered less material removal during the test.

Table 5.10 Results of abrasion wear measurements

Coating	Process	m0	m1(12min)	12	m2(24min)	24	m5(60min)	60
W 3654fc	HVAF	136.264	136.249	15	136.237	27	136.212	52
W 3654fc	HVOF	162.139	162.103	36	162.085	54	162.059	80

Wear charts, presented in figure 5.38, showed that the HVAF sprayed coating has somewhat better wear resistance, compared to HVOF sprayed coating.

The topography of the coatings, figure 5.39 indicated that both WC-10Co-4Cr coatings experienced abrasive grooving and presented scars along the direction of abrasive flow. The influence of tough abrasive quartz on the HVAF coating might be noticed due to deeper grooves. This might be due to a better ductility which is caused by low oxide content. In both cases the softer matrix was preferentially removed while the carbide grains suffered pullouts. There is no evidence of carbide cracking during the test.

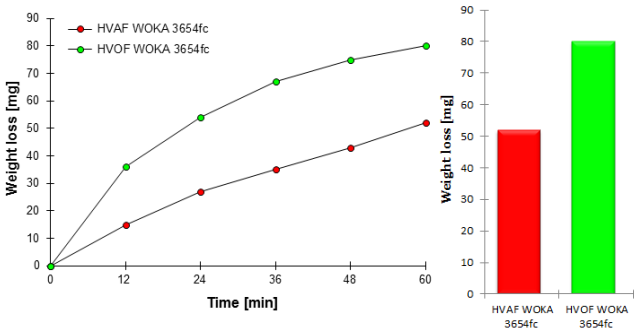

Figure 5.38 Abrasion wear results for WC-10Co-4Cr (WOKA 3654FC) HVOF and HVAF sprayed coatings

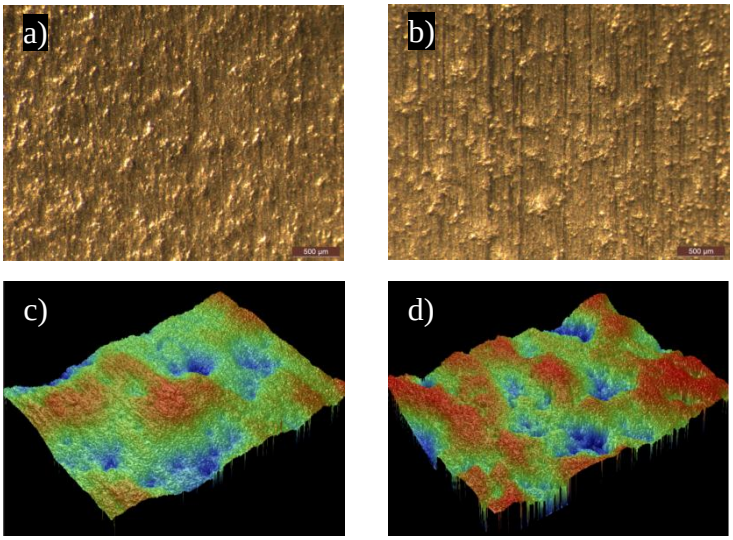

Figure 5.39 Topography of WC-10Co-4Cr (WOKA 3654FC) HVOF and HVAF sprayed coatings after abrasion test: a) HVOF surface, b) HVAF surface, c) HVOF 3D profile of the scanned area, and d) HVAF 3D profile of the scanned area

Even if the HVOF coating had somewhat lower hardness, the HVAF sprayed coating presented a better abrasion wear resistance. From the 3D profiles of the surfaces it might be noticed that the green and blue areas, representing increased material removal, were reduced on top of the HVAF sprayed coating. The blue areas represent deep pits which might correspond to carbide pullouts and pores. This also confirms that the HVAF sprayed coating suffered less material removal compared to HVOF sprayed coating. The abrasion wear resistance increase as the level of WC reaction during spraying decreases, according to the literature [172]. This might be also the reason why the HVAF coating experienced less material removal compared to HVOF sprayed coating which had higher hardness. The reduced decarburization during spraying due to lower spraying temperatures has a favorable effect on the abrasive wear resistance of the HVAF sprayed WC based coating.

XTP 520/Durmat 135Lo35 HVOF/HVAF

Table 5.11 presents the abrasion wear results and it might be noticed that the material loss is much lower when powders with finer grades are used for HVAF spraying.

Table 5.11 Results of abrasion wear measurements

Coating	Process	m0	m1(12min)	12	m2(24min)	24	m5(60min)	60
XPT520	HVOF	162.001	161.963	38	161.942	59	161.899	102
Durmat 135LO35	HVAF	152.374	152.363	11	152.354	20	152.332	42

From the chart presented in figure 5.40, it might be noticed that the HVAF sprayed coatings has a wear resistance that is about two times that of HVOF sprayed coating. It looks like the HVAF coating manufactured with finer powder has a reduced wear loss compared to the HVOF coating manufactured with conventional powder.

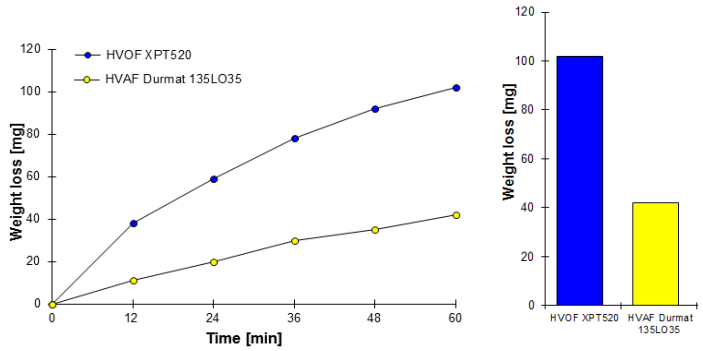

Figure 5.40 Abrasion wear results for WC-10Co-4Cr (XPT 520 HVOF and Durmat 135lo35 HVAF) sprayed coatings

The topography of the abraded surfaces presented grooves and scars along the direction of abrasive flow. It might be noticed that the HVAF coating presented much clearer grooves and scratches which might be due to better ductility of the coating. The ductility is also characterized by the lack of cracks after the abrasion test. It looks like the softer metallic matrix was removed preferentially during the test while the WC grains suffered pullouts. The 3D profile indicated the presence of extended green and blue area on top of the HVOF coating which means that the coating experienced increased material loss during the test compared to HVAF coating. The reason for a reduced material removal in the HVAF sprayed coating might be the lower reaction of carbide phase during spraying due to a reduced process temperature.

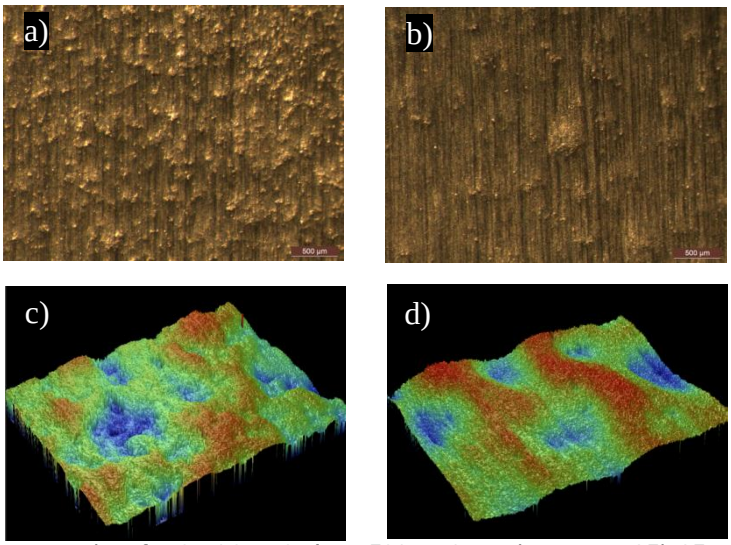

Figure 5.41 Topography of WC-10Co-4Cr (XPT 520 HVOF and Durmat 135lo35 HVAF) HVOF and HVAF coatings after abrasion test: a) HVOF surface, b) HVAF surface, c) HVOF 3D profile of the scanned area, d) HVAF 3D profile of the scanned area

It might be concluded that the finer powders have a favorable influence on the abrasive wear resistance of HVAF sprayed coatings. A feedstock powder containing fine powder particles is heated easier and projected towards a substrate at high speed which allows the manufacturing of coatings with enhanced properties. The HVAF sprayed coating using finer feedstock powder experienced more than twice lower material removal during abrasion wear test compared to HVOF sprayed coating.

Amperit 588 HVOF/HVAF

The abrasion test results and material removal of CrC based coatings are presented in table 5.12. In the present study, among the Amperit 588 coatings deposited using the same feedstock powder; the HVOF sprayed coating showed better wear resistance.

Table 5.12 Results of abrasion wear measurements

Coating	Process	m0	m1(12min)	12	m2(24min)	24	m5(60min)	60
Amperit 588	HVAF	161.089	161.055	34	161.009	80	160.863	226
Amperit 588	HVOF	137.715	137.675	40	137.651	64	137.615	100
Durmat 251017	HVAF	149.808	149.786	22	149.77	38	149.733	75

The influence of the dry quartz sand on the grinded coatings is presented in figure 5.42. It can be noticed that the coatings presented a good wear resistance for Cr_3C_2 based coatings and a linear wear loss during time. Using the same feedstock powder, Amperit 588, for HVOF and HVAF coatings lead to the manufacturing of coatings with different properties. The HVOF coating presented higher hardness

therefore less material loss occurred in this case during the abrasive test. On the other hand, the HVAF sprayed coating, using as feedstock powder the conventional Durmat 251017, presented the best wear resistance among the Cr_xC_y based cermet coatings studied in the present work.

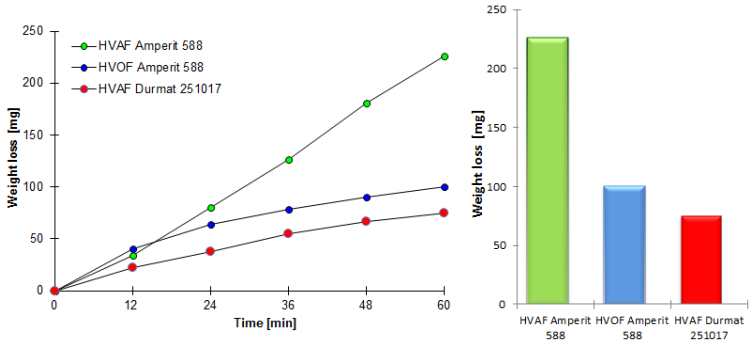

Figure 5.42 Abrasion wear results for CrC-25NiCr (Amperit 588 HVOF/HVAF and Durmat 251017 HVAF) sprayed coatings

The material removal occurred due to the hard quartz particles forced against the surface of the sample and moving along the direction of abrasive flow. The low stress abrasion caused surface damage by material removal, ploughing (on HVOF sprayed coating) splat flaking and plastic deformation as it can be seen in figure 5.43. The 3D profiles indicated also that the HVOF coating had a better wear resistance compared to HVAF sprayed coating, manufactured using the same feedstock powder, Amperit 588.

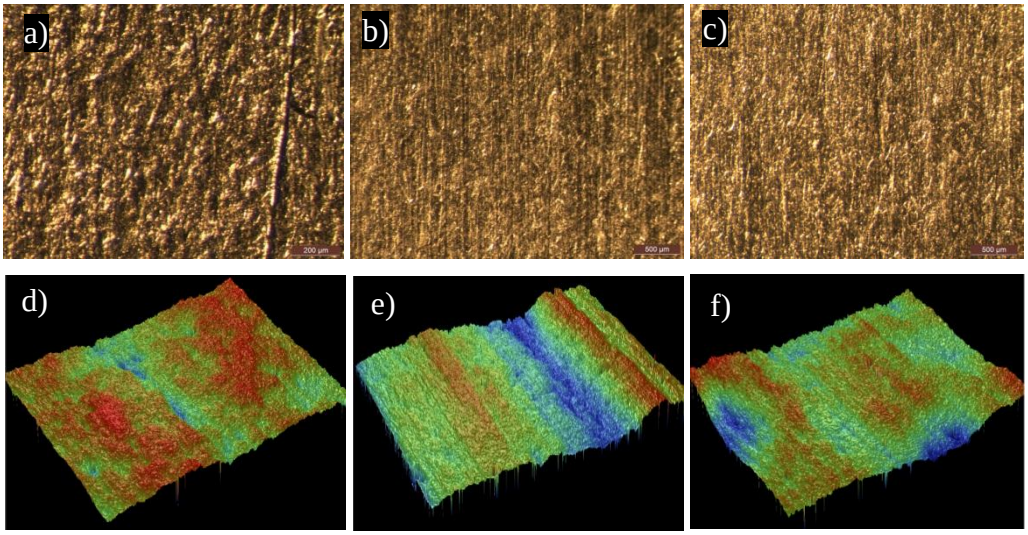

Figure 5.43 Topography of CrC-NiCr (Amperit 588 HVOF/HVAF and Durmat 251017 HVAF) coatings after abrasion test: a) HVOF Amperit 588 surface, b) HVAF Amperit 588 surface, c) HVAF Durmat 251017, d) HVOF Amperit 588 3D profile of the scanned area, e) HVAF Amperit 588 3D profile of the scanned area, and f) HVAF Durmat 251017 3D profile of the scanned area

The erosive wear resistance of the coatings depends predominantly on the mechanism of splat flaking controlled by the cohesion between splats. Among the coatings sprayed using as feedstock Amperit 588 powder, the HVOF coating presented lower mass loss during the test due to a harder coating with less porosity compared to HVAF coating. Unlike the previous case, using as feedstock Durmat 251017 powder for HVAF coating, the highest hardness value among the Cr_3C_2-25NiCr sprayed coatings was obtained. According to the results, when is about spraying Cr_3C_2-25NiCr coatings with good abrasive wear resistance important factors are the hardness of the coating and fine feedstock powders.

WOKA 7502/WOKA 7504 HVOF/HVAF

The results of the abrasion wear test are presented in table 5.13. After one hour it can be noticed that both coatings have suffered reduced material loss.

Table 5.13 Results of abrasion wear measurements

Coating	Process	m0	m1(12min)	12	m2(24min)	24	m5(60min)	60
WOKA 7502	HVOF	160.529	160.499	30	160.484	45	160.454	75
WOKA 7504	HVAF	151.249	151.234	15	151.224	25	151.192	57

Based on abrasion wear measurements the abrasion charts were built for a better material loss comparison of both coatings. It can be noticed that both coatings have a good wear resistance but still the HVAF coating suffered lower material removal during the test.

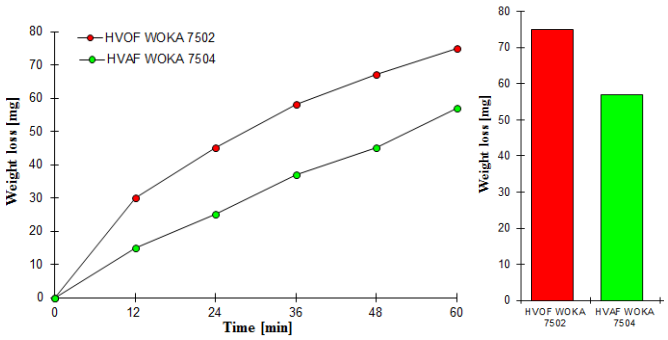

Figure 5.44 Abrasion wear results for CrC-37WC-18M (WOKA 7502 HVOF and WOKA 7504 HVAF) sprayed coatings

The topography of the worn surfaces and 3D scans of the surfaces are presented in figure 5.45. It might be noticed that the matrix and Cr_3C_2 phases were preferentially removed due to a softer structure, whilst the WC grains remain intact, due to an increased hardness, and suffered pullouts during the friction with the dry abrasive media. The 3D scans present blue areas representing deeper abrasive grooves and pits which correspond to carbide pullouts. It might be noticed that the HVAF coating presents reduced blue areas compared to HVOF coating. This might be due to a dense coating, with increased hardness value, smoother surface and lower level of porosity. The lack of oxides, reduced decarburization and lower process temperature

might be also a reason for a better abrasive wear resistance and reduced material loss.

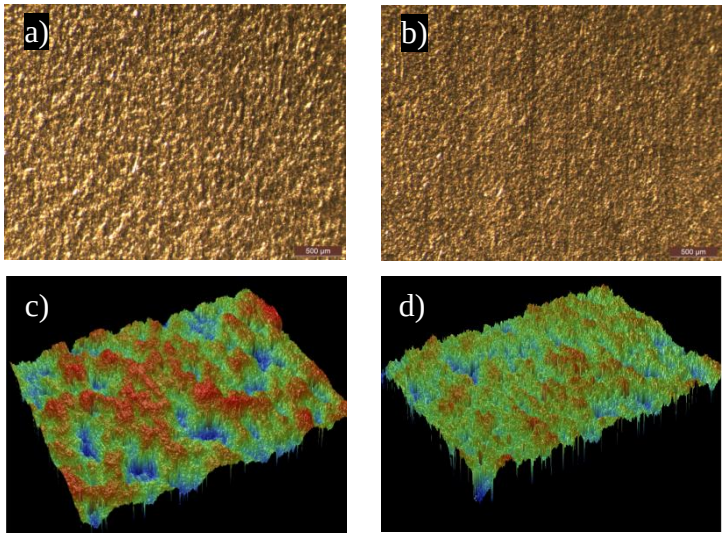

Figure 5.45 Topography of CrC-37WC-18M (WOKA 7502 HVOF and WOKA 7504 HVAF) coatings after abrasion test: a) HVOF surface, b) HVAF surface, c) HVOF 3D profile of the scanned area, d) HVAF 3D profile of the scanned area

The influence of the dry quartz abrasive media on the grinded coatings proved that both coatings have a good wear resistance with similar mass losses, but the HVAF coating suffered somewhat lower wear loss. The topography of the coatings indicated that both Cr_3C_2 phase and metallic matrix suffered scratches which in time lead to material removal while the WC carbide grains suffered pullouts. Comparing the 3D scanned profiles it can be noticed that the HVAF sprayed coating suffered less material removal. Therefore, it can be concluded that the HVAF coating possess a better abrasive wear resistance compared to HVOF coating.

Amperit 618074 HVOF/HVAF

The results of abrasive wear measurements and material loss of the sprayed coatings are presented in table 5.14. It might be noticed that the coatings have similar wear resistance according to the material loss during the test.

Table 5.14 Results of abrasion wear measurements

Coating	Process	m0	m1(12min)	12	m2(24min)	24	m5(60min)	60
Amperit 618074	HVOF	161.543	161.51	33	161.492	51	161.44	103
Amperit 618074	HVAF	161.254	161.226	28	161.21	44	161.154	100

From the abrasive wear chart presented in figure 5.46 it might be noticed that the coatings have similar wear resistance. Even if the HVOF sprayed coating quality is superior to HVAF sprayed coating the results are almost the same. It is thought that powder particles were not melted properly during the HVAF spraying which

contributed to a coating with lower hardness, increased porosity and rough surface compared to HVOF sprayed coating.

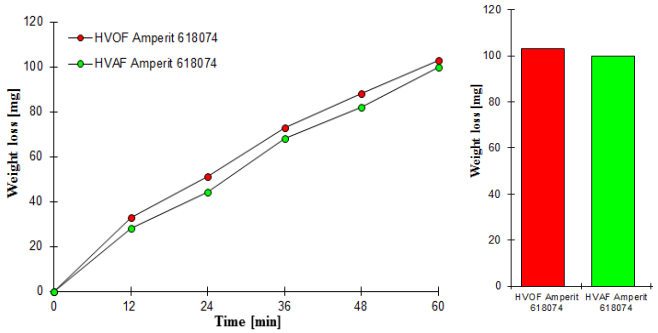

Figure 5.46 Abrasion wear results for WC-FeCrAl (Amperit 618074) HVOF and HVAF sprayed coatings

The topography of the worn surfaces and also 3D scans of the surfaces are presented in figure 5.47. It might be noticed that the matrix was preferentially removed due to a softer structure, while the WC grains remain intact, due to an increased hardness, and suffered pullouts during the test.

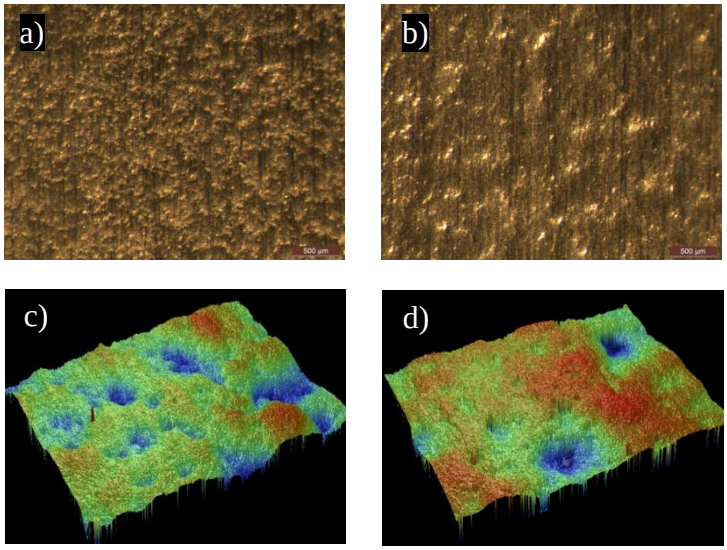

Figure 5.47 Topography of WC-FeCrAl (Amperit 618074) HVOF and HVAF coatings after abrasion test: a) HVOF surface, b) HVAF surface, c) HVOF 3D profile of the scanned area, d) HVAF 3D profile of the scanned area

The 3D scans present larger green and blue areas representing deeper abrasive grooving and pits, on top of HVOF sprayed coating, indicating somewhat lower abrasive wear resistance compared to HVAF sprayed coating, but still the difference is insignificant. The wear results showed that both WC-FeCrAl based coatings have similar wear behavior. Even if the HVOF coating presented higher hardness and lower porosity level and is thought that the dissolution of WC carbide during

spraying affects negatively the abrasion wear resistance of the sprayed coatings, the results revealed that the coating have comparable wear resistance. It is presumed that an increase in the HVAF spray temperature or a finer feedstock powder will considerably increase the abrasive wear performance of HVAF coating.

5.5.2 Sliding wear resistance

Wear represent the displacement of material from a solid surface caused by rolling or sliding of another solid, which in case of homogenous materials is explained by adhesion, delamination, deformation, depending on their physical properties [159]. The main factors influencing the wear behavior are carbide size, hardness, toughness, porosity, phase distribution and the content of binder phase and powder microstructure [173]. In the case of carbide coatings besides the general wear mechanism carbides pullout take place and material removal is caused by delamination of splats.

Woka 3654FC HVOF/HVAF

The CoF (coefficient of friction) was monitored during the test and both coatings display good frictional behavior. The CoF as a function of sliding time is presented in figure 5.48. Among the coatings the HVAF coating displays somewhat lower CoF. During the test the CoF of HVOF coating increased slightly while the CoF of HVAF coating was most of the time constant. Both CoF fluctuated which might be attributed to fine particle debris entrapped between the wear scar and counter body.

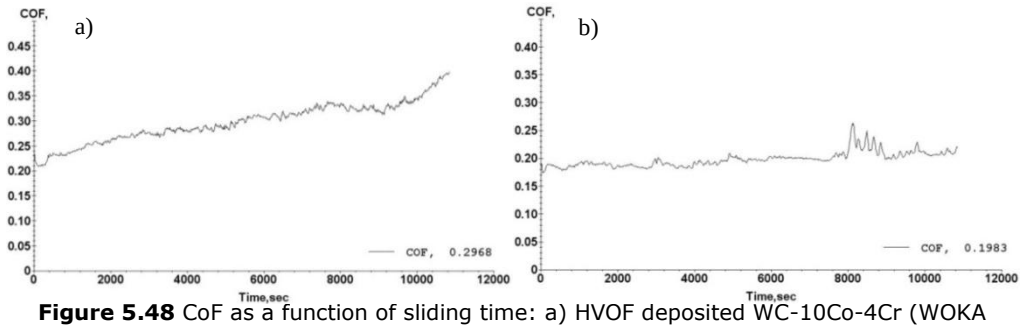

Figure 5.48 CoF as a function of sliding time: a) HVOF deposited WC-10Co-4Cr (WOKA 3654FC) coating and b) HVAF WC-10Co-4Cr (WOKA 3654FC) deposited coating

The sliding test results are presented in table 5.15. It can be noticed that the coatings have similar mass loss. The ball worn caps have similar diameters and also the ball wear rate is similar. This indicated that the coatings suffered reduced mass loss. It might be concluded that in this study the HVAF coating have similar sliding wear behavior comparable to HVOF coating.

Table 5.15 Results of pin on disk wear test

Measurements/coating	HVOF	HVAF
Ball worn cap diameter [μm]	0.466	0.462
Sample wear rate [$mm^3/N/m$]	$1.21*10^{-5}$	$1.38*10^{-5}$
Ball wear rate [$mm^3/N/m$]	$3.89*10^{-4}$	$3.86*10^{-4}$

Figure 5.49 shows the wear tracks of the two coatings. The HVOF coating presented somewhat pronounced wear track which might be attributed to the formation of new phases within the coatings during spraying.

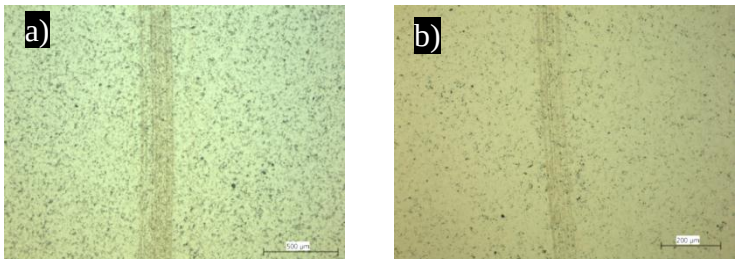

Figure 5.49 Wear tracks on: a) HVOF deposited WC-10Co-4Cr (WOKA 3654FC), and b) HVAF deposited WC-10Co-4Cr (WOKA 3654FC) specimens

Due to the testing speed and the applied load without lubricant the sliding wear is considered to be mainly adhesive wear. Detachments of the coatings also formed on both worn tracks (figure 5.50). The grooves are caused by oxidized debris or carbides which suffered pullouts during the test. The removed material acts as an abrasive media entrapped between the coatings and the counter body. Due to the lack of tribolayer the HVAF coating presents somewhat increased amount of debris attached to the worn track compared to HVOF coating.

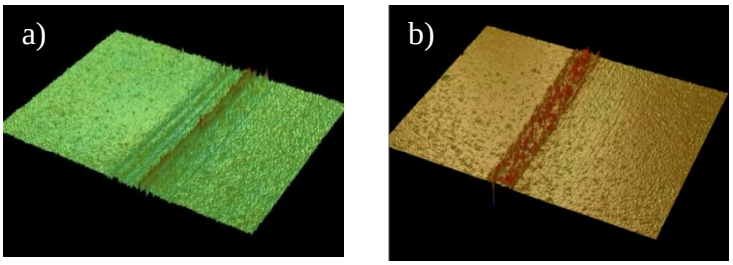

Figure 5.50 Wear tracks 3D profile: a) HVOF deposited WC-10Co-4Cr (WOKA 3654FC), and b) HVAF deposited WC-10Co-4Cr (WOKA 3654FC)

The morphology of the wear tracks of both coatings is presented in figure 5.51 and confirms that the wear arose trough material removal and carbide pullouts. The wear track of HVOF sprayed coating showed particle debris and cracks. On the other coating a more clean wear track can be noticed which presents scars and carbide pull outs.

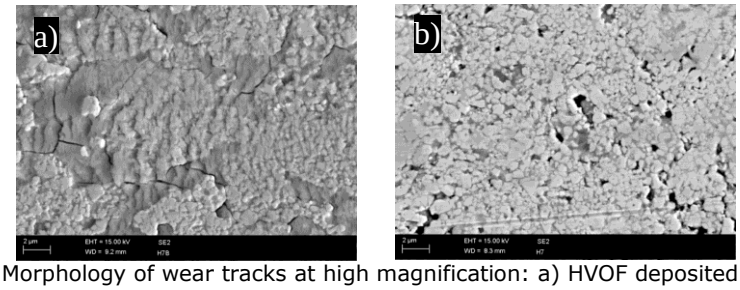

Figure 5.51 Morphology of wear tracks at high magnification: a) HVOF deposited WC-10Co-4Cr (WOKA 3654FC) coating and b) HVAF deposited WC-10Co-4Cr (WOKA 3654FC) coating

The CoF and sliding wear results indicated similar sliding wear behavior of HVOF and HVAF sprayed coatings. Due to increased hardness of HVOF coating a slightly reduced material loss was noticed. In both cases the material removal was caused by matrix removal and carbide pullout which acted as an abrasive media between the coating and the counter body. It might be noticed from figure 5.51 that the wear track of HVOF coating is covered almost entirely with particle debris while the HVOF wear track is clean. Using the same feedstock powder WOKA 3654FC, it was noticed that HVAF spraying is suitable to manufacture coatings with similar sliding wear properties comparable with HVOF coatings.

XPT 520 HVOF/Durmat 135lo35 HVAF

The CoF as a function of sliding time is presented in figure 5.52. It can be noticed that the coatings have almost the same CoF, but the HVOF coating presented a smaller and constant value due to the lubrication. At the beginning of the test the value of CoF increased for both coatings which might be caused by adhesive micro-contacts between the surface and counter body. For the HVOF coating a slightly and constant increase might be noticed which might be due the tribolayer formed during the test. The unstable CoF in case of HVAF spraying might be influenced by the brittle oxides, which acts as an abrasive media entrapped between the surface and counter body.

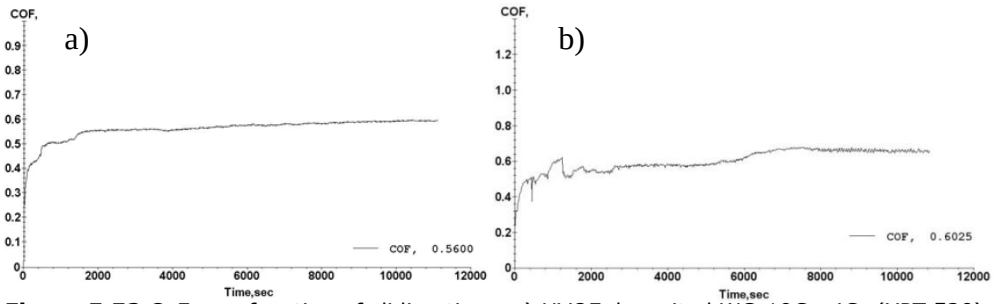

Figure 5.52 CoF as a function of sliding time: a) HVOF deposited WC-10Co-4Cr (XPT 520) coating, and b) HVAF WC-10Co-4Cr (Durmat 135lo35) deposited coating

The sliding test results are presented in table 5.16. Due to the formation of tribolayer on the HVOF sprayed coating, the friction was somewhat reduced. The ball worn cap diameter was almost twice smaller and the ball mass loss was reduced

compared to the HVAF coating. The lack of tribolayer on the surface of HVAF sprayed coating contributed to an increased wear loss of counter body which worn considerably during the test and also the mass loss of the sample was slightly increased.

Table 5.16 Results of pin on disk wear test

Measurements/coating	HVOF	HVAF
Ball worn cap diameter [µm]	0.648	1.024
Sample wear rate [mm^3/N/m]	$7.05*10^{-6}$	$7.72*10^{-6}$
Ball wear rate [mm^3/N/m]	$3.01*10^{-7}$	$4.81*10^{-8}$

Figure 5.53 shows the wear tracks of the two coatings. On the coating produced using the HVOF spraying technique a pronounced tribolayer can be noticed which is attributed to the presence of oxidized debris. During friction the oxidized particles play a lubricant role, as it was found also in the literature [174]. During HVAF spraying the decarburization of WC is reduced, thus the lack of tribolayer can be noticed.

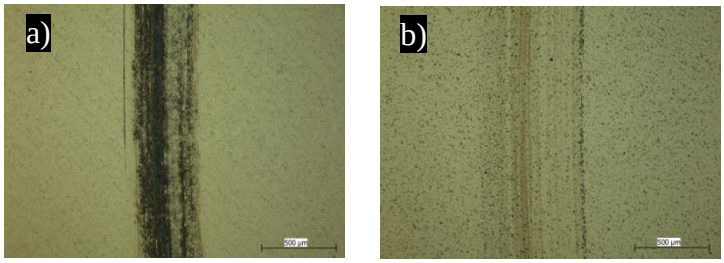

Figure 5.53 Wear tracks on: a) HVOF deposited WC-10Co-4Cr (XPT 520), and b) HVAF deposited WC-10Co-4Cr (Durmat 135lo35) specimens

In figure 5.54 particle debris might be noticed on both worn tracks. The grooves are caused by oxidized debris or WC grains which suffered pullouts during the test. The particle debris acts as an abrasive media between the coatings and the counter body. Due to the presence of tribolayer on the HVOF surface, the reduced amount of grooves can be noticed compared to HVAF coating where due to dry and tough testing conditions the mechanism of wear is more severe. The HVOF coating shows also a reduction of the wear track depth.

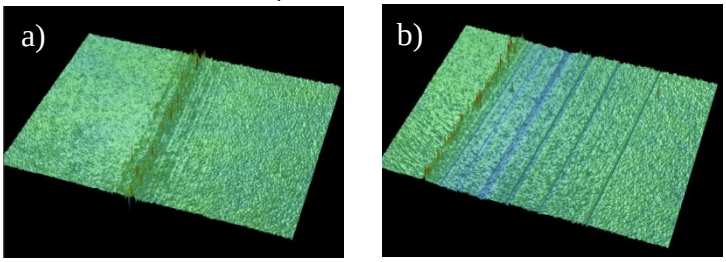

Figure 5.54 Wear tracks 3D profile: a) HVOF deposited WC-10Co-4Cr (XPT 520), and b) HVAF deposited WC-10Co-4Cr (Durmat 135lo35)

The morphology of the wear tracks is presented in figure 5.55. The wear caused due to the friction between the coating surface and counter body is characterized by matrix removal and carbide pullouts. The wear track of HVOF sprayed coating

presents cracks within the tribolayer and carbide pullouts while the HVAF sprayed coating experienced the lack of tribolayer and presents a clean surface.

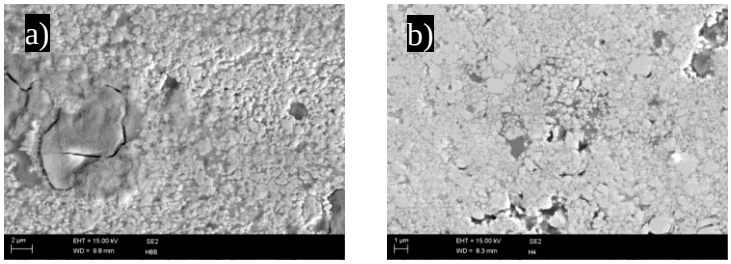

Figure 5.55 Morphology of wear tracks at high magnification: a) HVOF deposited WC-10Co-4Cr (XPT 520) coating, and b) HVAF deposited WC-10Co-4Cr (Durmat 135lo35) coating

Using different powders with different particle distribution it was found out that the HVOF coating presented a much stable CoF with a smaller value due to the formation of tribolayer which consists of oxidized particle debris formed during the sliding wear test. In both cases the material removal was caused due to matrix removal and carbide pullout which acted as an abrasive media between the surface of the coating and the counter body.

Amperit 588 HVOF/HVAF and Durmat 251017 HVAF

The variation of CoF as a function of sliding time for the Cr_3C_2-25NiCr sprayed coatings are presented in figure 5.56. During the test the CoF for each coating slightly increased.

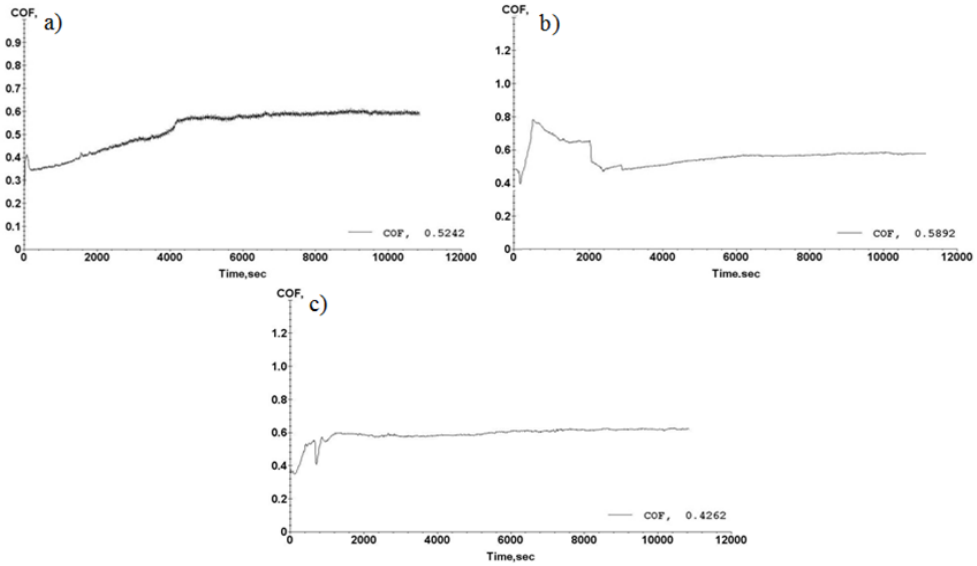

Figure 5.56 CoF as a function of sliding time: a) HVOF deposited Cr_3C_2-25NiCr (Amperit 588) coating, b) HVAF deposited Cr_3C_2-25NiCr (Amperit 588) coating, and c) HVAF deposited Cr_3C_2-25NiCr (Durmat 251017) coating

The adhesive micro-contacts are thought to be the reason for the increase of CoF of coatings because they lead to the formation of abrasive material entrapped between

the WC-Co ball and coating. The HVAF deposited coatings manufactured using Durmat feedstock powder showed the lowest CoF. This might be due to the reduced porosity within the coating and higher hardness value, among the Cr_3C_2-25NiCr deposited coatings. The sliding test results are presented in table 5.17. The HVOF and HVAF coatings manufactured using the same feedstock powder, Amperit 588, have different sliding wear behavior. The HVAF coating presents somewhat better wear properties due to lower wear rate. Also, it look like the hardness of the coating plays an important role when is about sliding wear resistance. Among the Cr_3C_2-25NiCr sprayed coatings the HVAF coating manufactured using as feedstock material Durmat 251017 powder has the best sliding wear resistance which is attributed to the higher hardness value.

Table 5.17. Results of pin on disk wear test

Measurements/coating	HVOF A588	HVAF A588	HVAF Durmat
Ball worn cap diameter [μm]	0.833	0.937	0.816
Sample wear rate [mm^3/N/m]	$1.32*10^{-7}$	$2.11*10^{-7}$	$1.21*10^{-7}$
Ball wear rate [mm^3/N/m]	$2.13*10^{-6}$	$4.18*10^{-9}$	$2.17*10^{-6}$

Figure 5.57 shows the wear tracks of the Cr_3C_2-25NiCr coatings. The wear track of HVOF sprayed coating presents a pronounced tribolayer which is attributed to the decomposition of carbide phase during spraying and oxidized debris. The HVOF and HVAF coatings manufactured from Amperit 588 feedstock powder present particle pullouts and accumulation of removed material. The removed material is transferred into the grooves and pores evolved during the test. During HVAF spraying the decarburization is reduced and a reduced tribolayer can be noticed on both HVAF sprayed coating, this being more visible on the wear track of coating deposited using Durmat powder. The black areas on the HVAF deposited coating are thought to be oxidized particle debris due to high temperature during the sliding test.

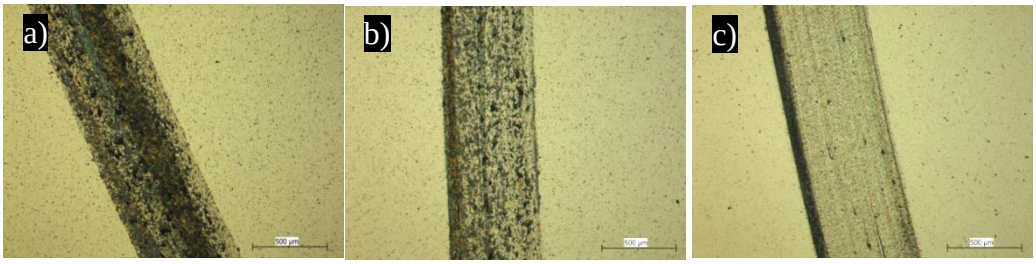

Figure 5.57 Wear tracks on: a) HVOF deposited Cr_3C_2-25NiCr (Amperit 588), b) HVAF deposited Cr_3C_2-25NiCr (Amperit 588), and c) HVAF deposited Cr_3C_2-25NiCr (Durmat 251017) specimens

Figure 5.58 presents 3D scanned areas of the deposited Cr_3C_2-25NiCr coatings. Particle debris adhered to the wear track might be noticed. The mechanism of abrasive wear shows up very clear in the images.

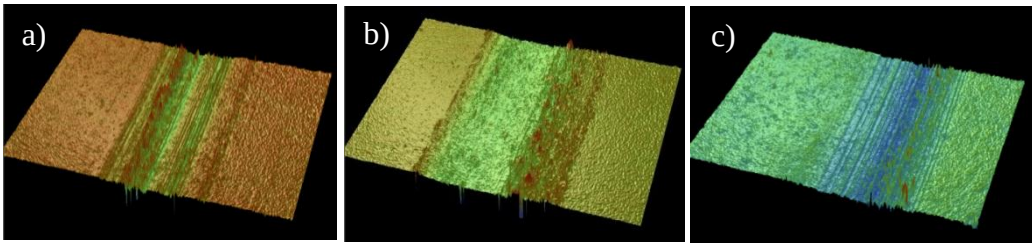

Figure5.58 Wear tracks 3D profile: a) HVOF deposited Cr_3C_2-25NiCr (Amperit 588), b) HVAF deposited Cr_3C_2-25NiCr (Amperit 588), and c) HVAF deposited Cr_3C_2-25NiCr (Durmat 251017)

The grooves are caused by oxidized debris which were entrapped between the two sliding surfaces. The HVAF coating manufactured by Amperit 588 powder shows the widest wear track profile and deepest wear track, which confirms the highest mass loss. The HVAF coating manufactured by Durmat powder shows a reduction in the wear track depth due to an increased hardness value.

The morphology of the wear tracks is presented in figure 5.59. When Cr_3C_2-25NiCr based coatings are taking into sliding contact with the counter body, at the beginning of the test, the NiCr matrix undergoes severe deformation due to the compression produced by the tough counter body [175]. The HVOF worn track is characterized by material removal which adhered to the surface of the sample and also to the wear track as particle debris. The presence of a tribolayer might be noticed which is caused due to oxidation at high temperature of particle debris entrapped between the WC-Co ball and coating. Material removal, formation and propagation of cracks at grain boundaries and deeper groves can be noticed in the Amperit 588 HVAF sprayed coating, which might be attributed to a lower hardness and softer coating. The HVAF coatings are characterized by cleaner surface with no significant particle debris on the surface of worn track.

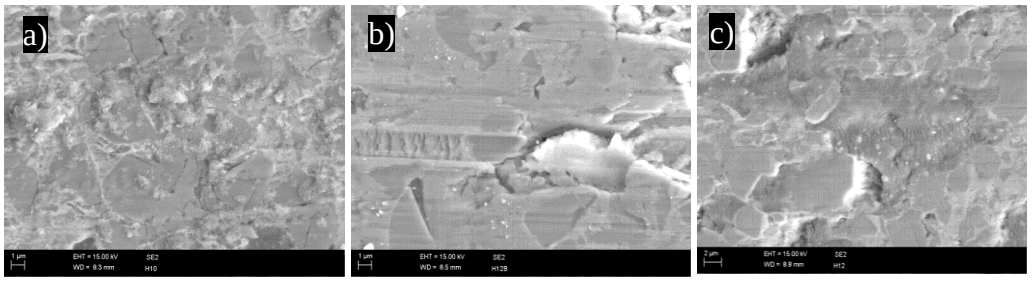

Figure 5.59 Morphology of wear tracks at high magnification: a) HVOF deposited Cr_3C_2-25NiCr (Amperit 588) coating, b) HVAF deposited Cr_3C_2-25NiCr (Amperit 588) coating, and c) HVAF deposited Cr_3C_2-25NiCr (Durmat 251017)

All coatings present plastic deformation and material removal with debris particles trapped between the two surfaces brought in contact during the test. Unlike the coatings manufactured using Amperit 588 feedstock powder, the Durmat HVAF coating presented the lowest CoF and best sliding wear behavior due to an increased hardness value. In the present study it was observed that the wear resistance of the Cr_3C_2-25NiCr coatings increased with the hardness of the coatings and the use of fine feedstock powder.

WOKA 7502 HVOF/ WOKA 7504 HVAF

The CoF as a function of sliding time is presented in figure 5.60. It might be noticed that the coatings have almost the same CoF, but still the HVAF coating presented a much stable one. At the beginning of the test the CoF increased for both coatings. For the HVOF coating a sharply increased might be noticed which might be due to highly adhesive micro-contacts between the surface and counter body.

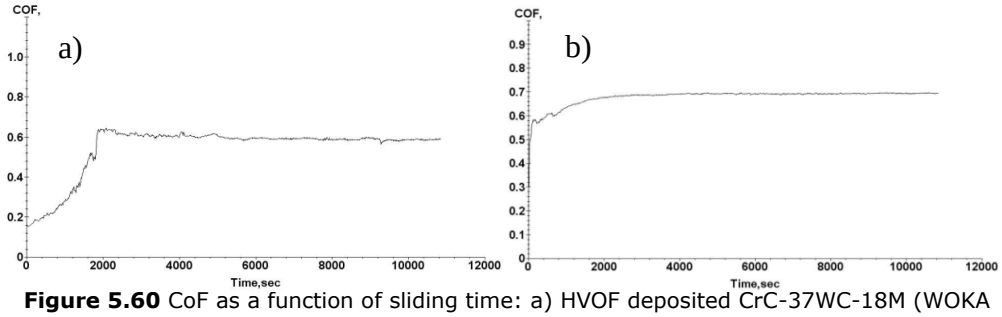

Figure 5.60 CoF as a function of sliding time: a) HVOF deposited CrC-37WC-18M (WOKA 7502) coating, and b) HVAF CrC-37WC-18M (WOKA 7504) deposited coating

The sliding test results are presented in table 5.18 and it can be noticed that the coatings have similar wear loss. The difference between the ball worn caps diameters indicated that the HVOF coating has increased hardness compared to the HVAF coating. This might be due hard but brittle phases formed during spraying.

Table 5.18 Results of pin on disk wear test

Measurements/coating	HVOF	HVAF
Ball worn cap diameter [µm]	0.760	0.384
Sample wear rate [mm^3/N/m]	$2.62*10^{-5}$	$2.66*10^{-5}$
Ball wear rate [mm^3/N/m]	$1.74*10^{-7}$	$1.13*10^{-8}$

Figure 5.61 shows the wear tracks of the two coatings. On the coating produced using the HVOF spraying technique deep pits might be noticed which might be caused due to pore enlargements.

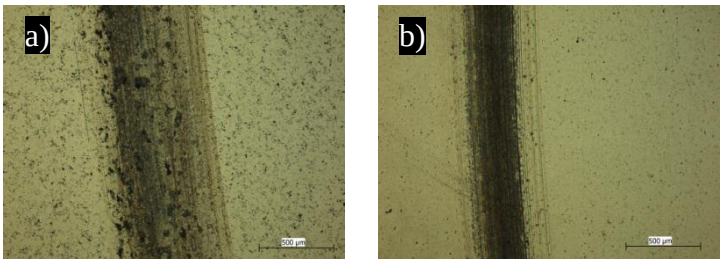

Figure 5.61 Wear tracks on: a) HVOF deposited CrC-37WC-18M (WOKA 7502), and b) HVAF deposited CrC-37WC-18M (WOKA 7504) specimens

The larger wear track on the HVOF coating indicated a hard coating while the HVAF coating looks more ductile. The tribolayer formed during the test at elevated temperature contains oxides.

Due to high rotation speed and the applied load without lubricant the sliding wear is considered to be mainly adhesive wear. Detachments of the coatings also formed on both worn tracks (figure 5.62). The grooves are caused by the detachments of coatings and debris particle which act as an abrasive third body between the coatings and counter body. The HVOF coating shows also a reduction of the wear track depth.

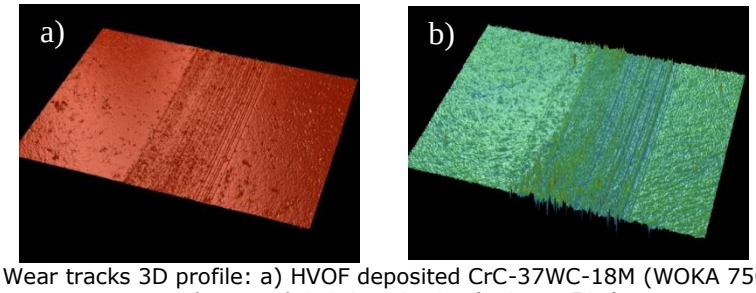

Figure 5.62 Wear tracks 3D profile: a) HVOF deposited CrC-37WC-18M (WOKA 7502), and b) HVAF deposited CrC-37WC-18M (WOKA 7504)

Material removal, formation and propagation of cracks and deeper groves in the C_3C_2 matrix and metallic matrix can be noticed in the HVOF coating while the HVAF coating presents deeper grooves (figure 5.63), which might be due to a lower hardness. Also in both coatings WC carbide pull outs can be noticed.

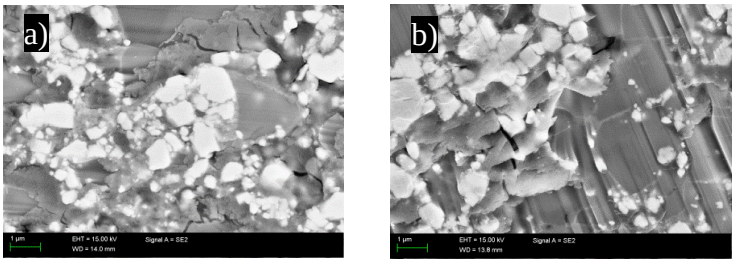

Figure 5.63 Morphology of wear tracks at high magnification: a) HVOF deposited CrC-37WC-18M (WOKA 7052) coating, and b) HVAF deposited CrC-37WC-18M (WOKA 7054) coating

The CoF of both coatings have similar values, and both coating were subjected to material removal and cracks. Due to a hard coating the ball used to test the HVOF coating shows somewhat higher mass loss. The HVOF coating is characterized by the presence of brittle phases which contribute to increased particle pullout during the test. Even the HVAF coating has a lower micro-hardness and the non-oxidized coating can effectively retain mechanical strength having a lower wear rate.

Amperit 618074 HVOF/HVAF

The CoF was continuously monitored during the wear test (figure 5.64). It can be noticed that the HVAF presented a lower value of CoF, but after 2.2h of testing time a significant increase of CoF can be noticed. The HVOF coating presented an unstable CoF during the first hour of test afterwards it became constant with very small deviations. This behavior might be related to the pores found in the upper layer of the coating and particle debris.

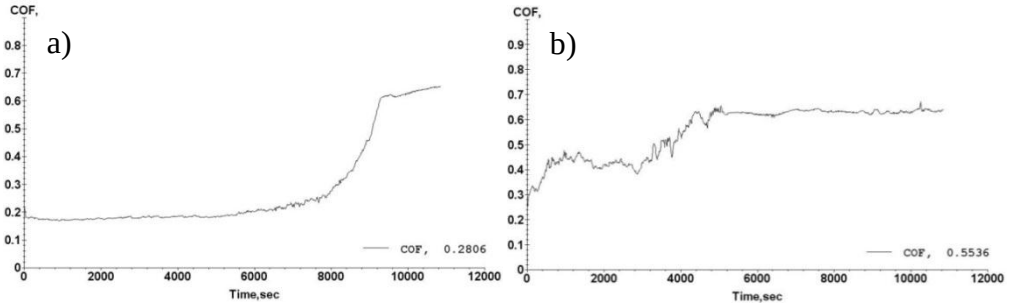

Figure 5.64 CoF as a function of sliding time: a) HVOF deposited WC-FeCrAl (Amperit 618074) coating, and b) HVAF WC-FeCrAl (Amperit 618074) deposited coating

The sliding test results are presented in table 5.19. The worn cap diameter of counter body was twice that large in case of HVAF coating. The increased wear loss of ball and coating is caused due to an increased friction between the HVAF coating and counter body, which is also confirmed by the CoF.

Table 5.19 Results of pin on disk wear test

Measurements/coating	HVOF	HVAF
Ball worn cap diameter [μm]	0.485	0.826
Sample wear rate [mm^3/N/m]	$4.13*10^{-6}$	$7.21*10^{-7}$
Ball wear rate [mm^3/N/m]	$1.51*10^{-8}$	$1.27*10^{-7}$

Figure 5.65 presents representative wear track profiles of each coating.

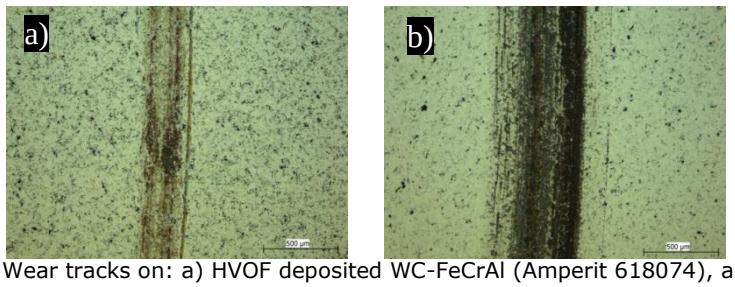

Figure 5.65 Wear tracks on: a) HVOF deposited WC-FeCrAl (Amperit 618074), and b) HVAF deposited WC-FeCrAl (Amperit 618074) specimens

The HVOF coating has a narrow wear track compared to HVAF coating due to increased hardness. According to the results presented in table 5.19, the worn track of HVAF coating confirms that the friction between the coating and counter body

increased. The dark region indicated oxidation during the test, which was caused due to the high temperatures occurred during the friction of debris and surface.

The wear track profiles are presented in figure 5.66. Detachments of the coatings also formed on both worn tracks. The grooves are caused by the detachments of coatings and debris particle which act as an abrasive third body between the coatings and counter body. The HVAF coating has the deepest wear track profile while the HVOF coating shows a narrow wear track and also a considerable reduction of the wear track depth.

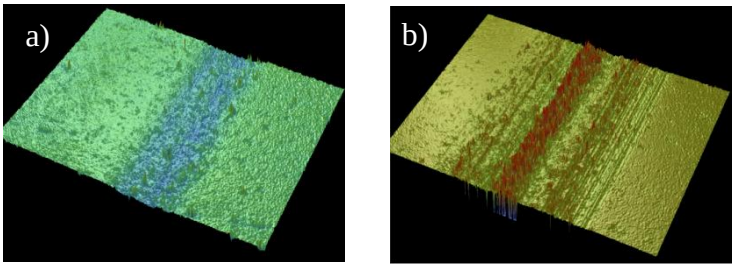

Figure 5.66 Wear tracks 3D profile: a) HVOF deposited WC-FeCrAl (Amperit 618074), and b) HVAF deposited WC-FeCrAl (Amperit 618074)

The morphology of the wear tracks of both coatings confirms that the wear arose trough carbide pullouts and matrix removal. Particle debris stay in the contact area and led to abrasive wear, which is the main wear type (figure 5.67). Accumulation of removed material might be noticed which are transferred into the grooves and pores resulted during the test.

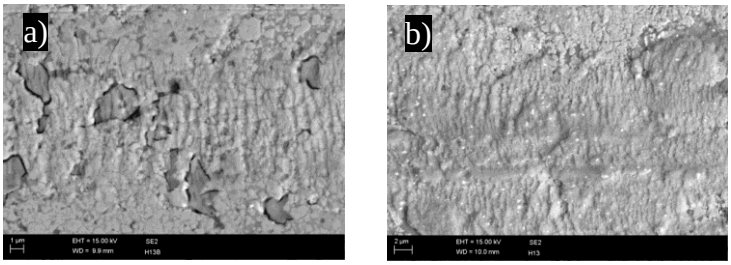

Figure 5.67 Morphology of wear tracks at high magnification: a) HVOF deposited WC-FeCrAl (Amperit 618074) coating, and b) HVAF deposited WC-FeCrAl (Amperit 618074) coating

The HVAF coating displayed unstable CoF during the first hour of test but afterwards the frictional behavior became stable compared to the HVOF coating which presented a reduced CoF which increased significantly after 2.2h of test. Due to an increased friction the counter body wore twice as much as the HVOF counter body. The HVOF coating is characterized by increased hardness and lower porosity, compared to HVAF sprayed coating, which in the present study showed a better sliding wear behavior.

5.6 Corrosion resistance of HVOF and HVAF cermet coatings

Corrosion resistance of coatings is controlled by denseness which indicated impermeability and structures without through porosity. The denseness of the deposited coating is evaluated by means of corrosion test. In this study open cell potential measurements and salt spray test were performed in order to evaluate the denseness.

5.6.1 Open cell potential measurements

The open cell potential measurement is a simple and useful method to reveal connection between the electrolyte and substrate through interconnected pores, micro-cracks and splat boundaries. This test was performed in order to study the long time impermeable behavior of the coatings. The open cell potentials of the coating were compared to the values of the low carbon steel substrate. If the potential values of the coatings are close to the potential of the substrate this indicates through porosity which means that there is an open path for the electrolyte to penetrate the coating surface to the interface between the coating and substrate, which causes coating failure [176].

Woka 3654FC HVOF/HVAF

In figure 5.68 the open cell potential value of the HVAF coating stabilized under the low carbon steel value.

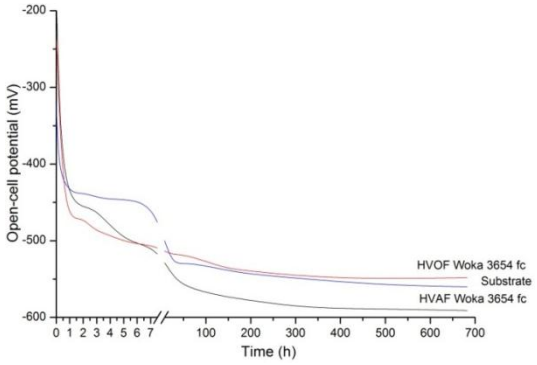

Figure 5.68 Open cell potentials of HVOF and HVAF WC-CoCr (WOKA 3654FC) deposited coatings and low carbon steel substrate as a function of exposure time in 3.5% NaCl solution

The open cell potential of HVAF coatings stabilized at the level of -560 mV, which indicated that the coating has a lower potential then the substrate. Unlike, the HVOF coating indicated a more noble caracter than the substrate and better corrosion resistance.
At the beginning of the tests, after couple of hours, corrosion products appeared on both exposed coatings. After 8 days of immersion the difference between the amounts of corrosion products appeared on top of the coatings was noticeable. After 28 days it can be noticed that the HVOF coating showed less corrosion products compared to HVAF coating which had the entire exposed surface covered with corrosion products (figure 5.69).

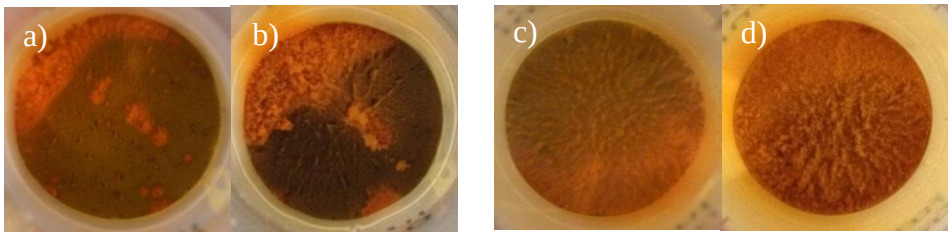

Figure 5.69 WC-10Co-4Cr corrosion behaviour: a) HVOF (WOKA 3654FC) coating after 8 days; b) HVOF (WOKA 3654FC) coating after 28 days; c) HVAF (WOKA 3654FC) coating after 8 days; d) HVAF (WOKA 3654FC) coating after 28 days

At the end of the test the HVOF coating exhibited improved corrosion behaviour indicating a better structural durability. The open cell potential indicated a lower potential value for the HVOF coating and lower amount of corrosion products developed on top of the coating was noticed. The increased corrosion resistance is atributed to lower level of porosity within the HVOF coating and a smoother surface of the as sprayed coating. Also a better bounding between splats during HVOF spraying due to higher process temperatures which softened the powder particles might contribute to the better corrosion behavior.

XPT 520/Durmat 135Lo35 HVOF/HVAF

The open cell potential results are presented in figure 5.70. Both coatings have potential values stabilized under the potential of low carbon steel, indicating a nobler character. The unstable potential values at the beginning of the test indicated corrosion activity. Among the coatings, the HVAF sprayed coating presents the more noble caracter than the substrate and HVOF coating and thus better corrosion resistance.

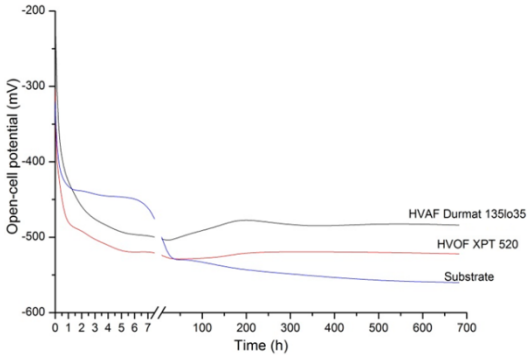

Figure 5.70 Open cell potentials of HVOF and HVAF WC-10Co-4Cr (XPT 520 and Durmat 150lo35) deposited coatings and low carbon steel substrate as a function of exposure time in 3.5% NaCl solution

After 8 days of immersion, a visual analysis was carried out and the images are presented in figure 5.71. It might be noticed that the HVOF coating exhibited

corrosion products indicating corrosion activity which evolved during the time and at the end of the test, the corroded areas grown larger. This behavior was presented also in [177]. The HVAF coating due to a denser coating, manufactured using finer powder, is characterized by low porosity level, smoother surface and increased hardness, indicated high impermeability and a good corrosion protection.

Figure 5.71 WC-10Co-4Cr corrosion behaviour: a) HVOF (XPT 520) coating after 8 days; b) HVOF (XPT 520) coating after 28 days; c) HVAF (Durmat 135lo35) coating after 8 days; d) HVAF (Durmat 135lo35) coating after 28 days

Sprayed by HVAF process, the Durmat WC-10Co-4Cr fine powder, led to a dense coating with higher harness, reduced porosity and smoother surface compared to HVOF coating. This might be due to the finer powder particles which were properly melted during spraying and during impact a better bounding between splats occurred.

Amperit 588 HVOF/HVAF and Durmat 251017 HVAF

In figure 5.72, open cell potentials of the coatings were compared to the value corresponding to the low carbon substrate. During the first 100h of test, all coatings present an unstable open cell potential which indicates corrosion behavior. Afterwards, the potential values started to stabilize indicating a nobler character compared to the substrate, giving an anodic protection. Among them, the HVOF coating showed a better corrosion behavior.

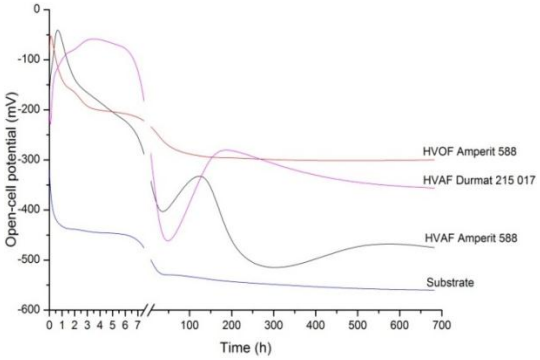

Figure 5.72 Open cell potentials of HVOF, HVAF Cr_3C_2-NiCr (Amperit 588 and Durmat 215017) deposited coatings and low carbon steel substrate as a function of exposure time in 3.5% NaCl solution

After 8 days corrosion products might be noticed on the surfaces of exposed as-sprayed coatings. The HVOF coating, presents the best structural durability (figure 5.73).

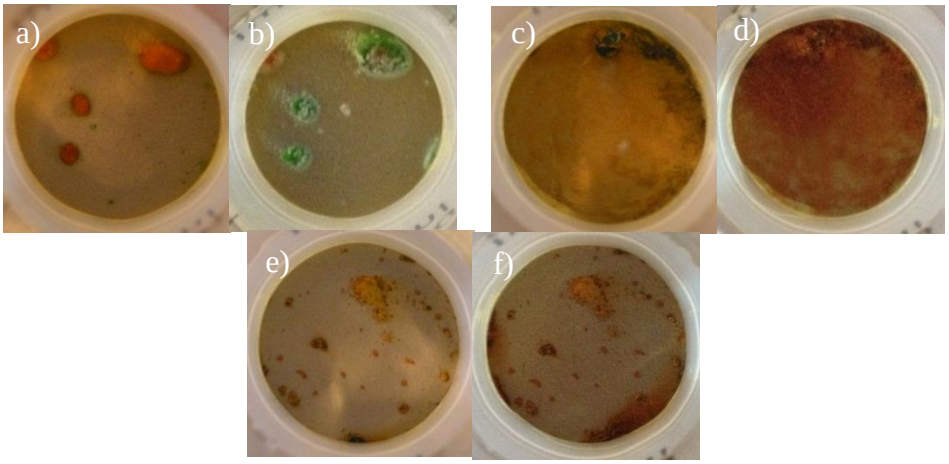

Figure 5.73 CrC-NiCr corrosion behaviour a) HVOF (Amperit 588) coating after 8 days; b) HVOF (Amperit 588) coating after 28 days; c) HVAF (Amperit 588) coating after 8 days; d) HVAF (Amperit 588) coating after 28 days, e) HVAF (Durmat 251017) coating after 8 days; f) HVAF (Durmat 251017) coatings after 28 days

After 28 days the HVOF coating proved to be nobler than the substrate giving anodic protection. Compared to the HVOF coating, the HVAF one sprayed with the same feedstock powder, Amperit 588, showed lower corrosion behavior being noticed that the surface exposed to the electrolyte was covered entirely with corrosion products after the first days. Thus, indicating through porosity. Unlike the HVAF Amperit 588 coating, the HVAF Durmat coating presented nobler character, indicating a better corrosion protection.
Compared to WC-10Co-4Cr, Cr_3C_2-NiCr coatings indicated higher impermeability, according to open cell potential values, due to Ni and higher Cr content. The HVOF sprayed coating with Cr_3C_2-NiCr feedstock powder showed better corrosion properties due to lower porosity level, high hardness and better splat adhesion induced by the bonding force generated between the splats attributed to higher process temperature which heated the powder particles.

WOKA 7502 HVOF/WOKA 7504 HVAF

Figure 5.74 presents the open cell potentials of CrC-37WC-18M coatings. Looks like the values of both coatings are lower than the substrate reflecting the presence of through porosity, thereby, an open path for the electrolyte to reach the substrate through the coating was formed.

After 8 days the exposed surfaces to the electrolyte started to corrode. Large areas were covered with corrosion products which entirely covered the exposed surfaces after 28 days (figure 5.75). It is thought that the corrosion products developed also due to the increased surface roughness which plays an important role on general corrosion rate.

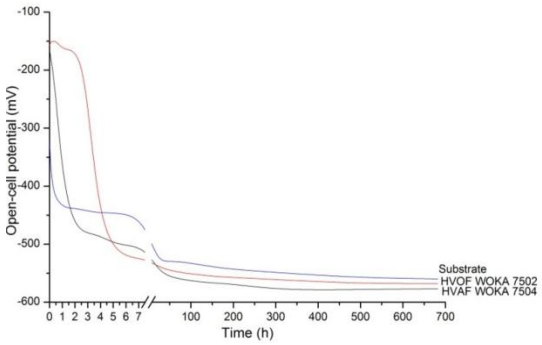

Figure 5.74 Open cell potentials of HVOF, HVAF CrC-37WC-18M (WOKA 7502 and WOKA 7504) deposited coatings and low carbon steel substrate as a function of exposure time in 3.5% NaCl solution

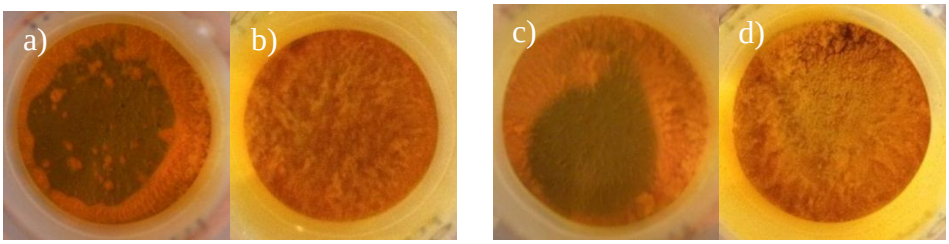

Figure 5.75 CrC-37WC-18M corrosion behavior: a) HVOF (WOKA 7502) coating after 8 days; b) HVOF (WOKA 7502) coatings after 28 days; c) HVAF (WOKA 7504) coatings after 8 days; d) HVAF (WOKA 7504) coating after 28 day

The CrC-37WC-18M sprayed coatings by HVOF respectively HVAF thermal spraying techniques, proved a cathodic behavior during the corrosion test. Even if both coatings present low porosity levels, the open cell potential values and the corroded surfaces exposed to the electrolyte indicated an enhanced corrosion behavior which is thought to be caused by the rough surfaces of the as deposited coatings and in both cases lower bounding between splats during spraying.

Amperit 618074 HVOF/HVAF

In figure 5.76, open cell potentials values of the HVOF, respectively HVAF coatings were compared to the value corresponding to the substrate. All coatings present an unstable open cell potential value, at the beginning of the test, which indicates corrosion behavior. Afterwards, the potential values started to stabilize. The open cell potential values of coatings indicate a nobler character compared to the substrate, giving an anodic protection. Among them, the HVOF coating showed a better corrosion behavior due to a denser coating and smoother as sprayed surface.
After 8 days of immersion, a visual analysis was carried out and it might be noticed that the HVOF coating exhibited corrosion products indicating corrosion activity, compared to HVAF coating which had no corrosion product on the exposed surface. During the time, the corrosion products have become somewhat larger on top of

HVOF coating and on the HVAF exposed surface corrosion product appeared (figure 5.77).

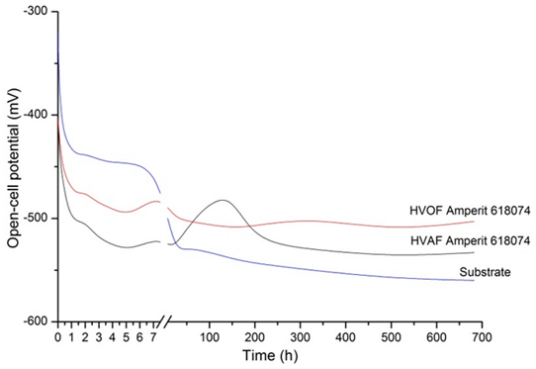

Figure 5.76 Open cell potentials of HVOF, HVAF WC-FeCrAl (Amperit 618074) deposited coatings and low carbon steel substrate as a function of exposure time in 3.5% NaCl solution

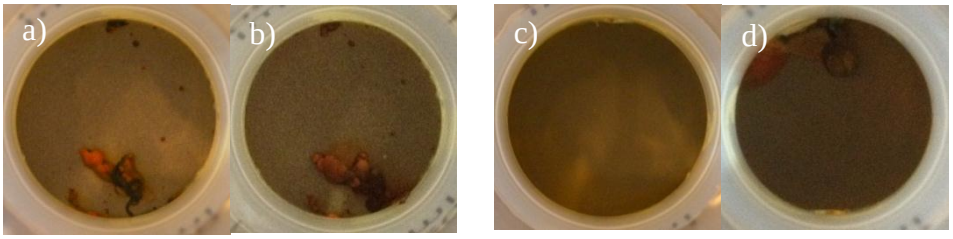

Figure 5.77 WC-FeCrAl corrosion behaviour a) HVOF (Amperit 618074) coating after 8 days; b) HVOF (Amperit 618074) coatings after 28 days; c) HVAF (Amperit 618074) coatings after 8 days; d) HVAF (Amperit 618074) coating after 28 days

The open cell potential measurements indicated that the coatings have similar potential values and are nobler than the substrate. Among the coatings, the HVOF sprayed coating showed better structural durability due to higher hardness and lower porosity rate.

5.6.2 Salt spray test

Salt spray test is a complementary test to evaluate the existence of porosity within the deposited coatings. The results of salt spray test are presented in table 5.20.
Salt spray tests of the as-deposited coatings have been done according to ASTM B117 standard for a long duration, up to 96h, using a Liebisch S400 M-TR salt spray chamber. Substrates were masked with epoxy paint before test in order to allow the coating surfaces only to be contact with the corroding salt spray fog. A 5-wt. % NaCl solution was used with an exposure of 96 h, a temperature of 35ºC, and a solution accumulation of 3 ml/h.
The corrosion resistance of WC-CoCr HVOF deposited coatings depends upon oxides, pores and the phase transformation occurred during spraying. The higher oxide level in HVOF coatings is the main reason of rust formation during the salt spray tests [153].

Table 5.20 Results of salt spray test

Sample	After 6h	After 24h	After 48h	After 96h
WOKA 3654 FC HVOF	-	Small spots	Large spots	Large corroded area
WOKA 3654 FC HVAF	Small spots	Small spots	Small spots	Large spots
XPT 520 HVOF	-	Small spots	Large spots	Almost fully corroded
Durmat 520 HVAF	-	-	Small spots	Large corroded areas
Amperit 588 HVOF	-	-	Small spots	Small and large spots
Amperit 588 HVAF	-	-	-	-
Durmat 251017 HVAF	-	-	-	-
WOKA 7502 HVOF	Small spots	Many spots	Fully corroded	Fully corroded
WOKA 7504 HVAF	Small spots	Large spots	Large spots	Large corroded areas
Amperit 618074 HVOF	Small spots	Many spots	Fully corroded	Fully corroded
Amperit 618074 HVAF	Many spots	Fully corroded	Fully corroded	Fully corroded

The surface aspect after salt spray testing indicated that the visual corrosion increased due to decarburization and probably oxidation during HVOF spraying (figure 5.78). Both coatings indicated through-porosity. It is thought that due to the higher testing temperature, 35°C, and higher concentration of the electrolyte the HVOF coatings an increased visual corrosion was noticed.

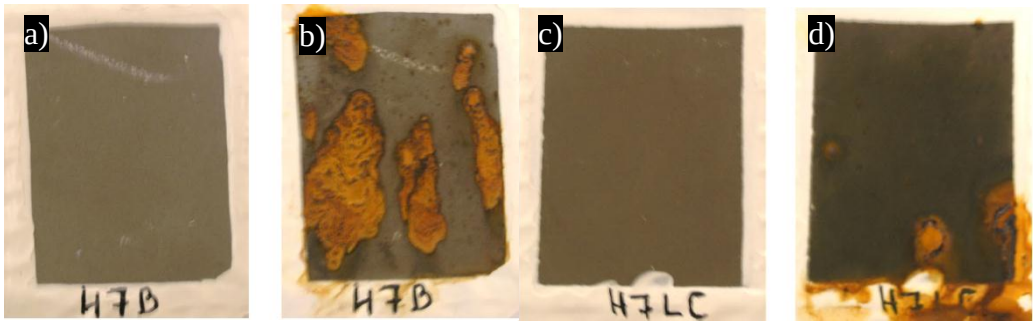

Figure 5.78 Coating surface of WC-10Co-4Cr: a) HVOF WOKA 3654FC as-sprayed coating; b) HVOF WOKA 3654FC coating after 96h salt spray test, c) HVAF WOKA 3654FC as-sprayed coating; d) HVAF WOKA 3654FC coating after 96h salt spray test.

Likewise, the previous case, the HVOF coating presents larger rusted areas compared to HVAF coating (Figure 5.79). This might be attributed to phase

degradation during HVOF spraying and the severe reaction of the new phases with the salt spray at higher testing temperature. Both coatings indicated through-porosity.

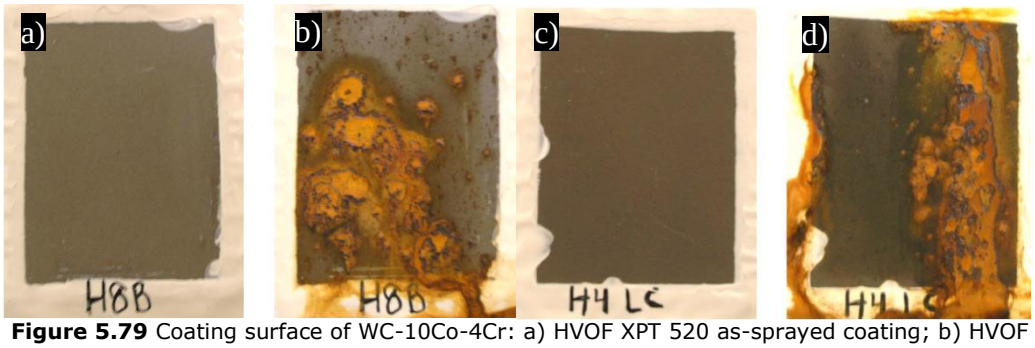

Figure 5.79 Coating surface of WC-10Co-4Cr: a) HVOF XPT 520 as-sprayed coating; b) HVOF XPT 520 coating after 96h salt spray test, c) HVAF Durmat 135lo35 as-sprayed coating; d) HVAF Durmat 135lo35 coating after 96h salt spray test

Due to higher Cr and Ni content all Cr_3C_2-25NiCr indicated good corrosion behavior under salt spray conditions (figure 5.80). Even if the HVOF sprayed coating had low porosity according to porosity quantification results, still visual corrosion can be noticed on top of the coating. This might be due to the reaction of salt spray with the oxides or new phases formed during HVOF spraying, found at the surface of the coating. The rougher surface compare to HVAF coating might be a reason for this behaviour. No corrosion products were observed on HVAF sprayed coatings.

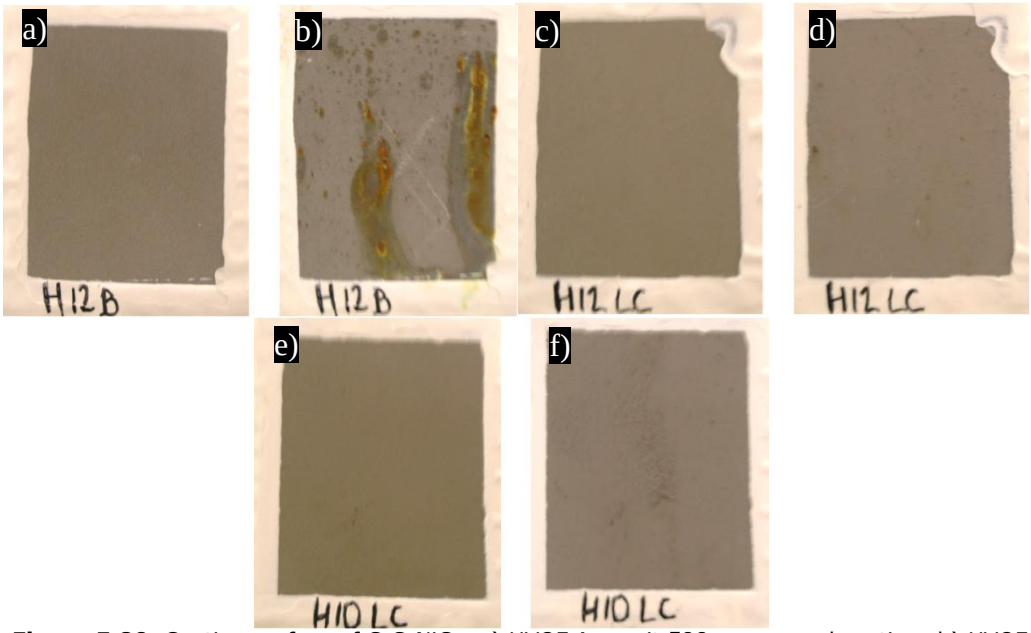

Figure 5.80. Coating surface of CrC-NiCr: a) HVOF Amperit 588 as-sprayed coating; b) HVOF Amperit 588 coating after 96h salt spray test, c) HVAF Amperit 588 as-sprayed coating; d) HVAF Amperit 588 coating after 96h salt spray test, d) HVAF Durmat 251017 as-sprayed coating, d) HVAF Durmat 251017 coating after 96h salt spray test

The surface aspect after salt spray test indicated that the visual corrosion covered the entire exposed HVOF CrC-37WC-18M surface (figure 5.81). Thereby, the decarburization, higher testing temperature and concentrated salt solution and probably oxidation contributed to formation of rust, and also the porosity level which is somewhat higher compared to HVAF coating. Both coatings indicated through-porosity. Unlike, the HVAF coating showed better corrosion protection during salt spray test and presented reduced rusted area.

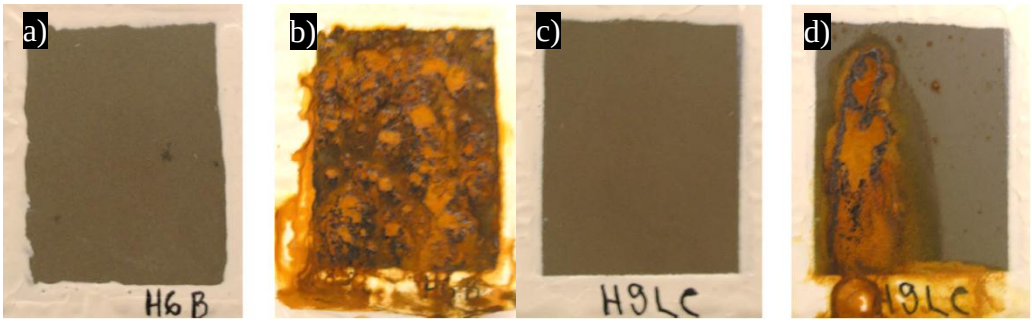

Figure 5.81 Coating surface of CrC-37WC-18M: a) HVOF WOKA 7502 as-sprayed coating; b) HVOF WOKA 7502 coating after 96h salt spray test, c) HVAF WOKA 7504 as-sprayed coating; d) HVAF WOKA 7504 coating after 96h salt spray test

Both WC-FeCrAl coatings were fully corroded after 96h, this indicates that 100% visual corrosion occurred (figure 5.82) which signify through porosity in the coating structure. In both cases the reason is the high porosity levels and rough surface. Also, the rust on top of HVOF coating was enhanced due to oxides and new phases formed during spraying.

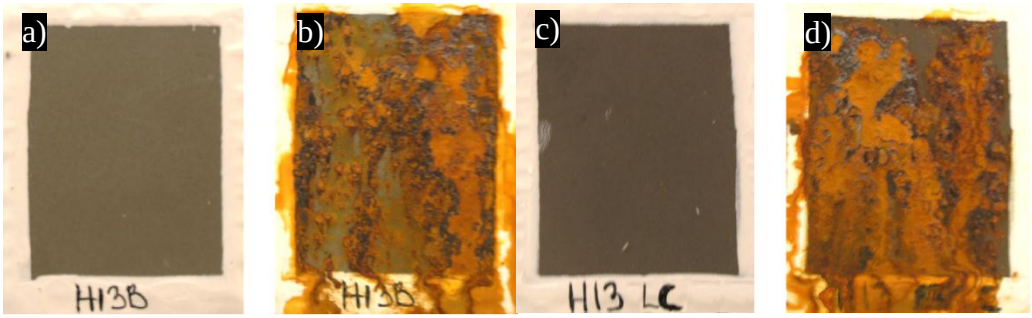

Figure 5.82 Coating surface of WC-FeCrAl: a) HVOF Amperit 618074 as-sprayed coating; b) HVOF Amperit 618074 coating after 96h salt spray test, c) HVAF Amperit 618074 as-sprayed coating; d) HVAF Amperit 618074 coating after 96h salt spray test

Normally the corrosion resistance of thermally sprayed coatings is associated also to the surface roughness, thus the higher surface area the corrosion covered areas are larger [178, 179]. Unlike Bodger and Mcgram [179], in this study visual corrosion is noticed even after 24h on WC based coating. In this study, even if most of the HVOF as sprayed coating have a smoother surface according to roughness measurements, still the HVAF coatings had better corrosion behavior. This might be due to an enhance corrosion reaction between the salt spray and the decarburized HVOF coatings which probably contains also oxides. Also the higher testing temperature

and higher concentration of NaCl might lower the corrosion resistance of HVOF deposited coatings. From this study it can be concluded that the visual corrosion decreases with reduction of decarburization and probably oxides. HVAF coatings have a better corrosion behavior due to lower process temperature and reduced phase degradation.

CHAPTER VI. CONCLUDING REMARKS AND SUGGESTIONS FOR FUTURE WORK

6.1 Conclusions

This study is highlighted in theoretical and experimental plan with possible industrial applications. The literature review aimed to study in detail new spraying techniques and materials which deposited with the right technique are able to improve wear and corrosion resistance of different parts. Also it contributed to the selection of HVAF and HVOF techniques respectively cermet materials. The mentioned spraying techniques were analyzed and the morphology, mechanical characteristics, wear and corrosion behavior of cermet coatings were compared in order to observe if HVAF spraying technique might be an alternative to HVOF spraying. It was found out that the HVAF process is suitable to manufacture cermet based coatings and it is a cheaper way to obtain the coatings while the process runs with air instead of oxygen, lowering the spraying costs.
The aim of the study was to find a new and cheaper alternative to HVOF spraying technique which allows the deposition of cermet coatings. WC and Cr_3C_2 coatings, deposited by HVOF and HVAF processes were studied and the obtained results are discussed below.

- High velocity air fuel spraying enables the production of dense coatings with low level of porosity. From microstructural point of view HVAF and HVOF coatings presented similar morphology.
- Using fine WC-10Co-4Cr denser HVAF coatings might be obtained with reduced porosity levels and higher hardness compared to HVOF coatings. HVAF sprayed CrC-37WC18M coating showed lower porosity level, smoother surface and similar hardness value compared to HVOF coating.
- The main characteristic of the HVAF spraying is the reduced decarburization and degradation during spraying, indicated by XRD patterns, due to lower process temperature and high velocity spraying. In the HVAF WC based coating the lack of W_2C was noticed.
- The abrasion wear resistance increases as the level of carbide reaction during spraying decreases. Thereby, the HVAF coating experienced less material removal compared to HVOF sprayed coating which had higher hardness and lower porosity level. The HVAF coatings were subjected to lower process temperature which in the present study significantly lowered decarburization having a favorable effect on the abrasive wear resistance of the HVAF sprayed cermet coatings.
- Due to the testing speed and the applied load without lubricant the sliding wear is considered to be mainly abrasive wear. Detachments of the coatings, wear debris, adhered on worn tracks contributing to the formation of grooves. A part of these wear debris were entrapped between the surface of the coating and the counter body and act as an abrasive material which cause further damage to the surface. The

removed material is mainly constituted by material from the metallic matrix which at high temperature oxidized during friction and carbide pullouts. It was noticed the presence of tribolayer on HVOF wear tracks which is caused due to oxidized particle debris.

- The HVAF coatings showed in many cases similar sliding wear behavior with constant CoF. It might be concluded that WC-10Co-4Cr HVAF coatings have similar sliding wear behavior compared to HVOF deposited coatings. HVAF deposited CrC-37WC-4Cr coatings have better sliding wear behavior compared to the HVOF deposited coating.
- HVAF WC-10Co-4Cr deposited coatings a better corrosion resistance and a denser coating is obtained for HVAF coatings if fine powders are used as feedstock material. Finer WC-10Co-4Cr powders deposited by HVAF spraying passivize being more noble than the substrate and the HVOF deposited coating. Using as feedstock Durmat Cr_3C_2-NiCr powder for HVAF spaying comparable open cell potential values and corrosion behavior to Cr_3C_2-NiCr HVOF coating was noticed. Compared to HVOF deposited coating, HVAF deposited WC-FeCrAl coating had similar corrosion behavior and potential values. The open cell potential measurements were influenced by the coating porosity, the roughness of the as sprayed coatings and also by the higher bounding force between splats.
- The corrosion resistance of thermally sprayed coatings is also associated to the surface roughness, the higher the surface area contact with the electrolyte the larger the rusted area. In this study visual corrosion is noticed after 96h on cermet coatings. Even if most of the HVOF as sprayed coating have a smoother surface according to roughness measurements, still the HVAF coatings had reduced corroded areas or even no symptoms of corrosion were observed in top of Cr_3C_2-25NiCr based coatings. This might be due to a reduced corrosion reaction between the salt spray and the HVAF coatings which contain reduced phase degradation.
- From this study it can be concluded that the visual corrosion decreases with reduction of decarburization and probably oxides, thus HVAF coating have a better corrosion behavior due to lower process temperature and reduced phase degradation.
- The WC-FeCrAl sprayed HVOF and HVAF coatings showed reduced salt spray corrosion resistance.

Using HVAF spraying process, WC and Cr_3C_2 based cermet coatings with similar characteristics and properties comparable to HVOF deposited coatings might be obtained at lower costs due to the use of air instead of oxygen which significantly lower the operational costs.

6.2 Author's contribution

Regarding the proposed objectives of the study as well the results the main personal contributions of the author might be mentioned as follows:

- Literature research regarding the state of the art in thermal spraying including new processes and technical equipment.
- Studied cermet coating deposited by HVAF thermal spraying and compared the results with HVOF coating manufactured from the same feedstock material.

- Powders selection, planned and organized all the experiments, performed most of the tests and characterizations, analyzed the results, at Tampere University of Technology, Materials Science Department, Finland under the guidance of Petri Vuoristo and Kari Niemi.
- Prepared the manuscript.
- Used feedstock powders like WC-10Co-4Cr and Cr_3C_2-25NiCr as well new type of powders like Cr_3C_2-37WC-18M and WC-FeCrAl powders.
- Powder particle size distribution measurements for all the powders using a Sympatec Helos laser diffractometer.
- Sample preparation for: microscopic techniques, material characterization, XRD, hardness and roughness measurements, wear and corrosion tests.
- Microscopic techniques: Optical Microscope to investigate the deposited coatings after sliding wear tests using a Leica DM 2500 light microscope, SEM+EDAX to investigate the microstructure of all powders and coatings, Stereomicroscope to investigate the abraded surfaces after abrasion tests of all coatings and ball worn cap measurements after sliding wear tests using a Leica MZ 7.5 stereomicroscope.
- XRD to determine the phases into all powders and coatings using a Siemens Diffract 500 diffractometer.
- Mechanical testing to determine the micro-harness using a Matsuzava MMT X7 Vickers tester and SJ-301 Mitutoyo surface roughness tester to measure the surface roughness of all coatings.
- Abrasion wear resistance using the rubber wheel abrasion test method and sliding wear resistance using the pin-on-disk method and a CETR UMT tribometer for all coatings (sliding exception for CrC-37WC-18M coatings)
- Open cell potential measurements using a 3.5%NaCl electrolyte in a plastic tube glued to the coatings surfaces using a Fluke 79 III multimeter.
- Porosity quantification using SEM micrographs and Image Tool 3.00 software
- Optical profilometry to scan all coatings surfaces after abrasion tests and wear track after pin-on-disk tests to determine the material loss using a Veeco Wyko NT1100 optical profiler.

According to the results it might be concluded that the HVAF spraying process offers similar properties to coatings deposited by different thermal spraying techniques at lower operational costs.

6.3 Future work

More detailed studies might be carried out in order to enhance the quality of HVAF coatings by:

- using fine powder, nanostructured powders, as feedstock
- using different materials as substrate
- optimizing the spraying parameters for HVAF spraying
- wear tests under increased loads
- corrosion studies and tests in more aggressive environments
- use of environmentally friendly WC based coatings free of Co to improve wear and corrosion resistance.

REFERENCES:

[1] Lech Pawlowski, *The science and engineering of thermal spray coatings*, John Wiley and Sons, Ltd. 2008, ISBN: 978-0-471-49049-4;
[2] K. E. Schneider, V. Belashchenko, M. Dratwinski, S. Siegmann, A. Zagorski, *Thermal spraying for Power Generation Components*, WILEY-VCH Verlag GmbH & Co. KGaA, 2006, Weinheim, p. 47-48;
[3] Stan Grainger, Jane Blunt, *Engineering coatings: Design and Application*, William Andrew Publishing, 1998, England, ISBN 1-884207-68-5;
[4] International Thermal Spray Association, information on: www.thermalspray.org;
[5] C. Robert, Jr. Tucker, *Thermal Spray Coatings*, ASM Handbook, Vol. 5, Surface Engineering, USA, 1994, ISBN: 0-87170-384-X;
[6] M.U. Schoop, H. Guenther, *Das Schoopsche Metallspritz-Verfahren*, Franckh Verlag, Stuttgard, Germany, 1917;
[7] Robert B. Heimann, *Plasma Spray Coating – Principles and Applications*, VCH Verlagsgesellschaft mbH, Weinheim, Germany, 1996, ISBN: 3-527-29430-9;
[8] Christopher C. Berndt*, The origins of Thermal Spray Literature, Thermal Spray 2001: New Surfaces for a New Millennium*, Proceedings of the International Thermal Spray Conference, 2001, p. 1351-1360;
[9] J. R. Davis, Davis and Associates, *Handbook of Thermal Spray Technology*, ASM International, 2004, ISBN 0-87170-795-0;
[10] Petri Vuoristo, *Development trends in thermal spray technologies*, Thermal Spray Coatings in Paper Processing and Printing Industries, ETSA Summer School, 13-14 June, 2012, TUT, Finland;
[11] C. Verdon, A. Karimi, J.L. Martin, *A study of high velocity oxy-fuel thermally sprayed tungsten carbide based coatings. Part 1: Microstructures*, Materials Science and Engineering A246, 1998, p. 11-24;
[12] J. Tuominen, P. Vuoristo, T. Mäntylä, S. Ahmaniemi, J. Vihinen, P.H. Andersson, *Corrosion Behavior of HVOF Sprayed and Nd-YAG Laser-Remelted High-Chromium, Nickel-Chromium Coatings*, Journal of Thermal Spray Technology, Vol. 11 (2) June, 2002, p. 233-243;
[13] J. Dubsky, J. Matějiček, *Residual and applied stresses in thermally sprayed metallic and ceramic coatings,* Thermal Spray 2002. Proceedings, International Thermal Spray Conference, Essen, March, 2002, p. 606-609;
[14] A. Kulkarni, J. Gutleber, S. Sampath, A. Goland,W. B. Lindquist, H. Herman, A. J. Allen, B.Dowd, *Studies of the microstructure and properties of dense ceramic coatings produced by high-velocity oxygen-fuel combustion spraying*, Materials Science and Engineering A369, 2004, p. 124-137;
[15] D. A. J. Ramm, T. W. Clyne, A. J. Sturgeon, S. Dunkerton, *Correlations between spraying conditions and microstructure for alumina coatings produced by HVOF and VPS*, Proceedings of the 7th National Thermal Spray Conference, June Boston, USA, 1994, p. 239-244;
[16] K. Li, D. Shi, P.D. Christofides, *Model-based estimation and control of particle velocity and melting in HVOF thermal spray*, Chemical Engineering Science Vol. 59, 2004, p. 5647-5656;
[17] Erja Turunen, *Diagnostic tools for HVOF process optimization*, Dissertation for the degree of Doctor of Science in Technology, VTT Industrial Systems, December 2005, Helsinki, ISBN 951.38.6678.5;
[18] K. Honda, I. Chida, M. Saito, Y. Ito, S. Sugiyama, F. Kobayashi, *Effect of preheating on the coating process in the low-pressure plasma spraying*, Welding International, Vol. 9, Issue 4, 1995, p. 271-277;

[19] H. Yang, *Physical Bonding of Spray Particles to the Substrate for High Impact Velocity Droplet*, Proceedings of the 2006 International Spray Conference, May 15-18, 2006, Seattle, USA;
[20] Cordon England, website: www.gordonengland.co.uk;
[21] M. Seeger, E. D. Reese, D. P. Jonke, M. Englhart, K. Drechsler, *Cost effective manufacturing of molds for CFRP component production*, Thermal Spray 2011: Proceedings of the International Thermal Spray Conference, Sep 2011;
[22] S. Kuroda, T.W. Clyne, *The Quenching Stress in Thermally Sprayed Coatings*, Thin Solid Films Vol. 200, 1991, Issue 1, p. 49-66;
[23] Rayment, T. et al.: *Phase Transformations and Control of Residual Stresses in Thick Spray - Formed Steel Shells*. Metallurgical and Materials Transactions B 35, 2004, Issue 6, p. 1113-1122;
[24] A. Natomi, N. Sakakibara, T. Torigoe, *Recent Application of Thermal Spray to Thermal power plants*, ITSC 2009, Expanding Thermal Spray Performances to new Markets and Applications, Proceedings of the 2009 International Spray Conference, Las Vegas, USA, 2009, p. 1106-1111;
[25] M. Arai, X. H. Wu, K. Fujimoto, *Inelastic Deformation of Freestanding Plasma Sprayed Thermal Barrier Coatings*, Thermal Spray 2009: Expending Thermal Spray Performance to New Markets and Applications, May 2009, p. 7-11;
[26] R. P. Krepski, *Thermal Spray Coating Applications in the Chemical Process Industries*, NACE Intl, Houston, USA, 1993, ISBN: 1877914592;
[27] Saint Gobain, website: www. coatingsolution.saint-gobain.com
[28] A. Allimant, D. Billieres, *New conventional plasma gun with high performance: ProPlasma HP*, International Thermal Spray Conference and Exposition 2010, Thermal Spray: Global Solutions for Future Applications, May 2010, p. 28-32;
[29] Northwest Mettech Corp., website: www.mettech.com;
[30] M. Dzulko, G. Forster, K.D. Landes, J. Zierhut, K. Nassenstein, *Plasma torch developments*, Thermal Spray 2005: Thermal Spray connects: Explore its surfacing potential, 2005, p. 431-434;
[31] D. Hawley, C. Dambra, R. Molz, *Triplexpro-200 Gun Platform: Impacting all Operational Aspects of Thermal Spraying*, International Thermal Spray Conference & Exposition 2010, Thermal Spray: Global Solutions for Future Application, May 2010, p. 33-37;
[32] D. Chen, J. Colmenares-Angulo, R. Molz, C. Dambra, D. Hawley, *Helium-free parameter development for TriplexPro-210 plasma gun*, Thermal Spray 2011: Proceedings of the International Thermal Spray Conference, Sep 2011, p. 627-632;
[33] Sulzer Metco, information available on: www.sulzer.com/products-and-service/coating equipment;
[34] Jianping Li, Lei Li, Zhong Yang, Yongchun Guo, Peihu Gao, *Preparation of Al/SiC Composite Coating on the Surface of Aluminum Alloy through Atmospheric Plasma Spraying,* Thermal Spray 2012: Proceedings from the International Thermal Spray Conference and Exposition, May 21-24, 2012, Houston, USA, p. 34-39;
[35] Chang Jiu Li, Guan Jun Yang, Cheng Xin Li, *Recent Developments of Porous Materials and Structured Surface Fabrication by Spray Deposition of Surface Molten Particles*, Thermal Spray 2012: Proceedings from the International Thermal Spray Conference and Exposition, May 21-24, 2012, Houston, USA, p. 40-46;
[36] K. Bobzin, T. Schlafer, T. Warda, M. Bruhl, *Thermally Sprayed Oxidation Protection Coatings for Y-TiAl Substrate*, International Thermal Spray Conference and Exposition 2010, Thermal Spray: Global Solutions for Future Applications, May 2010;

[37] M.O. Jarligo, D.E. Mack, G. Mauer, R. Vaßen, D. Stöver, *Atmospheric Plasma Spraying of High Melting Temperature Complex Perovskites for TBC Application*, Thermal Spray 2009: Expending Thermal Spray Performance to New Markets and Applications, May 2009, p. 65-70;
[38] Vladimir L. Solozhenko, Oleksandr O. Kurakevych, *Equation of State of Aluminum Silicon Carbide α-Al4SiC4*, Solid State Communications, 135(1-2), 2005, p. 87-89;
[39] J. Rams, A. Ureña, M. Campo, *Dual Layer Silica Coatings of SiC Particle Reinforcements in Aluminium Matrix Composites*, Surface and Coatings Technology, 200(12-13), 2006, p. 4017-4026;
[40] Chang-Jiu Li, Guan-Jun Yang, Cheng-Xin Li, *Recent Development of Porous Materials and Structured Surface Fabrication by Spray Deposition of Surface-Molten Particles*, Thermal Spray 2012: Proceedings from the International Thermal Spray Conference and Exposition, May 2012, Houston, USA, p. 40-46;
[41] A. Liu, M. Guo, J. Gao, M. Zhao, *Influence of Bond Coat on Shear Adhesion Strength of Erosion and Thermal Resistant Coating for Carbon Fiber Reinforce Thermosetting Polyimide*, Surface and Coattings Technology, 201(6), 2006, p. 2696-2700;
[42] V. Lins, J. Branco, F. Diniz, J. Brogan, C. Berndt, *Erosion Behavior of Thermal Sprayed,* Recycled Polymer and Ethylene-Methacrylic Acid Composite Coatings, Wear, 262 (3), 2007, p. 274-281
[43] M. Ivosevic, R. Knight, S.Kalidindi, G.Palmese, J. Sutter, *Solid Particle Erosion Resistance of Thermally Sprayed Functionally Graded Coatings for Polymer Matrix Composites*, Surface and Coatings Technology, 200(16), 2006, p. 5145-5151;
[44] D. Therrien, A. McDonald, P. Mertiny, *Temperature Measurements of Polymer Composite Flat Plates Coated with Aluminum-12Silicon*, Thermal Spray 2012: Proceedings from the International Thermal Spray Conference and Exposition, May 2012, Houston, USA, p. 1-6;
[45] J.A. Picas, M. Punset, M.T. Baile, E. Martin, A. Forn, *Effect of oxygen/fuel ratio on the in- flight particles parameters and properties of HVOF WC-CoCr coatings*, Surface and Coatings Technology 205, 2011, p. 5364-5368;
[46] Rober J.K. Wood, *Tribology of thermal sprayed WC-Co coatings*, Int. Journal of Refractory Materials and Hard Materials 28, 2010, p. 82-94;
[47] Praxair Surface Technology, website: www.praxair.com;
[48] S. Sampath, X. Jiang, A. Kulkarni, J. Matejicek, D.L Gilmore, R.A. Neiser, *Development of process maps for plasma spray: case study for molybdenum*, Materials Science and Engineering A348 (2003), p. 54-66;
[49] Carlos P. Bergmann, Juliane Vicenzi, *Protection against erosive wear using thermal sprayed cermet,* Springer-Verlag Berlin Heidelberg, 2011, ISBN 978-3-642-21986-3;
[50] I. Hulka, D. Uțu, V. A. Șerban, *Comparison between the wear resistance behaviour of WC-Co coatings deposited by different HVOF torches*, Proceedings of The 4th International Conference - Innovative technologies for joining advanced materials, 10-11 iunie, Timisoara, Romania, p. 318-321;
[51] R. A. Roşu, V. A. Şerban, V. Tsakiris, D. Uțu, B. Ibolyka, I. Hulka, *Caracterization of Titanium nitride layers obtained by HVOF thermal spraying method*, ModTech International Conference - New face of TMCR Modern Technologies, Quality and Innovation - New face of TMCR, 25-27 May, Vadul lui Voda-Chisinau, Republic of Moldova, vol. II, 2011, p. 925-928;
[52] Sudhangshu Bose, *High Temperature Coatings*, Elsevier, 2007, ISBN: 0-7605-8252-3;

[53] Z. Zeng, N. Sakoda, T. Tajiri, S. Kuroda, *Structure and corrosion behavior of 316L stainless steel coatings formed by HVAF spraying*, ITSC 2008: Thermal Spray Crossing Borders, Maastricht, The Netherlands, 2008, p. 284-290;
[54] C. M. Deng, K. S. Zhou, M. Liu, C. G. Deng, R. J. Hong, *Wear behaviors of HVAF sprayed nano WC-Co coating against Al-Ni-Bronze alloy*, ITSC 2008: Thermal Spray Crossing Borders, Maastricht, The Netherlands, 2008, p. 1333-1337;
[55] Uniquecoat Technologies Inc., website: www.uniquecoat.com;
[56] G. Kusinski, A. Verstak, *High Velocity Air-Fuel Spraying and its Applications in Oil and Gas Industry*, Thermal Spray 2012: Proceedings from the International Thermal Spray Conference and Exposition, May 2012, Houston, USA, p.529-534;
[57] A. Pukasiewicz, A. Capra, R. Paredes, *Influence of process parameters in the microstructure and cavitation resistance of the Fe-Mn-Cr-Si metal cored wire developed for arc thermal spraying*, ITSC 2008: Thermal Spray Crossing Borders, Maastricht, The Netherlands, 2008, p. 1176-1182;
[58] A. D. Gerdemann, N. L. Hecht, *Arc Plasma Technology in Materials Science*, New York, Springer, 1972;
[59] O. Cevher, A. Gulec, A. Turk, F. Ustel, F. Yilmaz, *Study on corrosion resistance behaviors of Zn, Al, Zn/Al 85/15 coatings produced by twin arc spray technique on steel*, ITSC 2008: Thermal Spray Crossing Borders, Maastricht, The Netherlands, 2008, p. 1156-1158;
[60] W. Tillmann, E. Vogli, M. Abdulgader, M. Gurris, D. Kuzmin, S. Turek, *Particle trajectories by arc spraying with cored wires*, ITSC 2008: Thermal Spray Crossing Borders, Maastricht, The Netherlands, 2008, p. 1150-1155;
[61] L. Latka, S. B. Goryachen, S. Kozerski, L. Pawlowski, T. Lampke, *Buildup mechanism of suspension plasma sprayed ZrO_2+8wt.% Y_2O_3 coatings,* Thermal Spray 2011: Proceedings of the International Thermal Spray Conference, Sep 2011, p. 104-108;
[62] L. Łatka, L. Pawłowski, S. Valette, B. Pateyron, J.P. Lecompte, A. Denoirjean, A. Cattini, R. Kumar, *Thermal Diffusivity and Conductivity of Yttria Stabilized Zirconia Coatings Obtained by Suspension Plasma Spraying*, Thermal Spray 2012: Proceedings from the International Thermal Spray Conference and Exposition, May 2012, Houston, USA, p. 800-804;
[63] M. Erne, D. Kolar, K. Möhwald, Fr.-W. Bach, *Tribological behavior of suspension plasma sprayed coatings for hot extrusion tools*, Thermal Spray 2011: Proceedings of the International Thermal Spray Conference, Sep 2011, p. 20-24;
[64] D. Soysal, A. Ansar, *Novel Insights into Liquid Behavior in Atmospheric Plasma Jets*, Thermal Spray 2012: Proceedings from the International Thermal Spray Conference and Exposition, May 2012, Houston, USA, p. 816-821;
[65] L. Łatka, L. Pawłowski, A. Cattini, A. Denoirjean, D. Chicot, S. Kozerski, F. Petit*, Mechanical Properties of Yttria and Ceria Stabilized Zirconia Coatings Obtained by Suspension Plasma Spraying*, Thermal Spray 2012: Proceedings from the International Thermal Spray Conference and Exposition, May 2012, Houston, USA, p. 805-809;
[66] J. Puranen, J. Laakso, L. Hyvärinen, M. Kylmälahti, P. Vuoristo, *Influence of Spray Parameters and Characteristics of Solutions on Microstructure and Phase Composition of Solution Precursor Atmospheric Plasma Sprayed (SPPS) Mn-Co Spinel Coating*, Thermal Spray 2012: Proceedings from the International Thermal Spray Conference and Exposition, May 2012, Houston, USA, p. 810-815
[67] A. Killinger, P. Müller, R. Gadow, *High Velocity suspension flame spraying of nano oxide containing suspensions*, Thermal Spray 2011: Proceedings of the International Thermal Spray Conference, Sep 2011, p. 44-48;

[68] K. Wittmann Teneze, J. M. Pereira, P. Brelivet, L. Bianchi, *Development of composite coatings composed of stainless steel matrix and tungsten carbide nano-inclusions by plasma praying*, Thermal Spray 2011: Proceedings of the International Thermal Spray Conference, Sep 2011, p. 152-156;
[69] M. Golozar, K. Chien, T.W. Coyle, *Porous Ultra Capacitor Electrodes Fabricated by Solution Precursor Plasma Spray: Molybdenum Oxide vs. Molybdenum Nitride*, Thermal Spray 2012: Proceedings from the International Thermal Spray Conference and Exposition, May 2012, Houston, USA, p. 822-827;
[70] A. Papyrin, V. Kosarev, S. Klinkov, A. Alkimov, V. Fomin, *Cold Spray Technology*, Elsevier, The Netherlands, 2007, ISBN: 0-08-045155-1;
[71] Kevin Hodder, Adrian Gerlich, Julio Villafuerte, *Fabrication of Aluminum-Alumina Metal Matrix Composite via Cold gas Dynamic Spraying at Low Pressure followed by Friction Stir Processing*, Thermal Spray 2012: Proceedings from the International Thermal Spray Conference and Exposition, May 21-24, 2012, Houston, Texas, USA;
[72] S.G. Klinkov, V. F. Kosarev, M. Rein, *Cold spray deposition: Significance of particle impact phenomena*, Aerospace Science and Technology, Vol. 9 (7), October 2005, p. 582-591;
[73] A. McDonald, A. Ryabinin, E. Irissou, J.K. Legoux, *Gas Substrate heat exchange during Cold Gas Dynamic Spraying*, Thermal Spray 2012: Proceedings from the International Thermal Spray Conference and Exposition, May 21-24, 2012, Houston, Texas, USA;
[74] Heli Koivuluoto, *Microstructural Characteristics and Corrosion Properties of Cold Spray Coatings*, Thesis for the degree of Doctor of Technology, Tampere University of Technology Publication, 2010;
[75] P. Richter, H. Hoell, *Latest Technology for Commercially Available Cold Spray System*, Thermal Spray 2006: Science, Innovation and Application, ASM International, 2006, p. 1447-1449;
[76] Thermal Spray Technologies, Inc., website: www.tstcoatings.com;
[77] W. Wong, E. Irissou, J.G. Legoux, F. Bernier, P. Vo, S. Yue, S. Michiyoshi, H. Fukanuma, *Cold Spray Forming Inconel 718*, Thermal Spray 2012: Proceedings from the International Thermal Spray Conference and Exposition, May 21-24, 2012, Houston, Texas, USA, p. 243-248;
[78] P.K. Koh, P. Cheang, K. Loke, S.C.M. Yu, S.M. Ang, *Deposition of Amorphous Aluminum Powder Using Cold spray*, Thermal Spray 2012: Proceedings from the International Thermal Spray Conference and Exposition, May 21-24, 2012, Houston, Texas, USA, p. 249-253;
[79] A. Kashirin, O. Klyuev, T. Buzdygar, A. Shkodkin, *DYMET Technology Evolution and Application*, Thermal spray 2007: Global Coating Solutions, ASM International, 2007, p. 141-145;
[80] A. Sova, A. Papyrin, I. Smurov, *Influence of Ceramic Powder Size on Process of Cermet Coatings Formation by Cold Spray*, Journal of Thermal Spray Technology. Vol. 18 (4), 2009, p. 633-641;
[81] S. Hartmann, Bad Krozingen/D, *New industrial applications for cold spraying, Thermal Spray 2010: Global Solutions for Future Applications*, International Thermal Spray Conference and Exposition, Singapore, 3-5 May, 2010;
[82] J. Wilden, S. Jahn, S. Reich, G. Fischer and V. E. Drescher, *FeNiW-coatings for casting molds in the aluminium industry*, Thermal Spray 2008: Crossing Borders, ASM, 2008, p. 1523-1528;
[83] Thermal Spray Depot, website: www. thermalspraydepot.com;
[84] Hayden Corporation, website: www.haydencorp.com;

[85] U. Bardi, C. Giolli, A. Scrivani, G. Rizzi, F. Borgioli, A. Fossati, K. Partes, T. Seefeld, D. Sporer, A. Refke, *Development and investigation on new composite and ceramic coatings as possible abradable seals*, ITSC 2008: Thermal Spray Crossing Borders, Maastricht, The Netherlands, 2008, p. 805-811;
[86] C. Zhenda, L. L. Chew, Qian Ming, *Laser Cladding of WC-Ni composite*, Journal of Materials Processing Technology, Vol. 62, Issue 4, December 1996, p. 321-323;
[87] P. M. Martin, *Handbook of deposition technologies for films and coatings – Science, Application and technology-Science*, Applications and Technology, Elsevier Inc., USA, 2010, ISBN 987-0-8155-2031-3;
[88] EN 13507 – Thermal Spraying: Pretreatment of surfaces of metallic parts and components for thermal spraying;
[89] M. G. Nicholas and K.T. Scott, *Characterization of grit blasting surfaces*, Surfacing Journal, 1981, Vol 12, p. 5;
[90] H. Yang, H.G. Wang, X. P. Cao, L. Wang, *Influence of substrate surface roughness on adhesive strength*, Thermal Spray 2006: Science, Innovation, and Application (ASM International), 2006, p. 1277-1281;
[91] C. H. Hare, *Painting of steel bridges and other structures*, Van Nostrand Reinhold, New York, 1990, ISBN 978-0442234997;
[92] ASM Handbook Vol. 5, *Surface Engineering*, ASM International, 1994, ISBN: 978-0-87170-384-2;
[93] S. M. DeHayes, D. Stark, *Petrography of cementitious materials*, American Society for testing and Materials, Philadelphia, 1994, ISBN: 978-0-8031-1878-2
[94] A. W. Momber, Blast Cleaning Technology, Springer, Hamburg, Germany, 2008, ISBN: 978-3-540-73644-8;
[95] J. R. Gould, B. Wilson, *Glass research report by Pera Knowledge*, The Waste and Resources Action Programme – The Old Academy, Banbury, 2003;
[96] B. Appleman, *Lead-based Paint Removal for Steel Highway Bridges*, Transportation Research Board, USA, 1997;
[97] Substech – Substances and Technologies, website: www.subtech.com;
[98] Saint-Gobain, website: www.saint-gobain.com;
[99] J. Pereira, *Which abrasive: sand, slag or garnet?* Protective Coatings Europe 1998, Vol. 3, no. 5, 26-27, 1998;
[100] Saint Gobain, Grains & Powders Brochure, Saint-Gobain Ceramic Materials Canada, 2004;
[101] Günter Schürholt, *Developments in surface preparation techniques for thermal sprayed coatings,* Saint Gobain Coatings Solution, ASE, 2011, Tampere Finland
[102] Kermetico, website: www.kermetico.com;
[103] J. A. Ellor, W. T. Young, J. Repp, *NCHRP – Report 528, Thermally Sprayed Metal Coatings to Protect Steel Pilings: Final Report and Guide*, Transportation Research Board, 2004, ISBN: 0-309-08801-1;
[104] ASM-TSS Committee, *Thermal Spray Booth Guidelines*, Thermal Spray Society ASM, 2007;
[105] L. L. Sheir, R. A. Jarman, G. T. Burstein, *Corrosion Vol. 2 – Corrosion Control*, Butterworth Heinemann, Great Britain, 1998, ISBN: 0-7506-1077-8;
[106] Bharat Bhushan, *Introduction to tribology*, John Wiley and Sons, New York, 2002, ISBN: 0-471-15893-3;
[107] Standard Terminology Relating the Wear and Erosion, G 40, Annual Book of Standards, Vol. 03.02, ASTM, 1987;
[108] J. T. Burwell, *Survey of Possible Wear Mechanisms*, Wear, Vol. 1, 1957, 119-141;

[109] ASM Handbook – Vol. 18*, Friction, Lubrication and Wear Technology*, ASM, USA, 1992, ISBN: 0-87170-380-7;
[110] J. R. Davis, Davis and Associated, *Surface Engineering for Corrosion and Wear Resistance*, ASM International, USA, 2001, ISBN: 0-87170-700-4;
[111] C. P. Bergmann, J. Vicenzi, *Protection against Erosive Wear Using Thermal Sprayed Cermet – A review*, Springer Verlag Berlin Heidelberg, 2011, ISBN: 978-3-642-21987-0;
[112] J. R. Davis, *Corrosion of Aluminum and Aluminum Alloys*, ASM International 1999, USA, ISBN: 0-87170-629-6;
[113] Luca d'Agostino, M. Vittoria Salveti, *Fluid Dynamics of Cavitation and Cavitating Turbopumps*, CISM Course and Lectures, CISM, Vol. 496, ISBN: 978-3-211-76668-2;
[114] William D. Callister Jr., *Fundamental of Materials Science and Engineering*, Fifth Edition, John Wiley and Sons Inc., 2001, ISBN: 0-471-39551-X;
[115] Shizhu Wen, Ping Huang, *Principles of tribology*, John Wiley and Sons Asia, 2012, ISBN: 978-1-118-06290-6;
[116] Prasanta Sahoo, *Engineering Tribology*, Prentice-Hall of India, New Delphi, 2005, ISBN: 81-203-2724-1;
[117] M. G. Fontana, N. D. Greene, *Corrosion Engineering*, McGraw Hill, 1967;
[118] ASM Committee, *Handbook of Corrosion*, *Vol. 13*, ASM International, USA, 1987, ISBN: 0-87170-007-7;
[119] Philip A. Schweitzer, *Fundamentals of Corrosion, Mechanisms, Causes and Preventing Methods*, CRC Press, USA, 2010, ISBN: 978-1-4200-6770-5;
[120] Philippe Marcus, *Corrosion Mechanism in Theory and Practice*, Second Edition, Marcel Dekker Inc., New York, 2002, ISBN: 0-8247-0666-8;
[121] Linga Garverick, *Corrosion in the Petrochemical Industry*, ASM International, 1994, ISBN: 0-87170-505-2;
[122] V.S. Sastri, E. Ghali, M. Elboujdaini, *Corrosion Prevention and Protection – Practical Solutions*, John Wiley and Sons, England, 2007, ISBN: 978-0-470-02402-7;
[123] ASM Committee, *Corrosion: Fundamentals, Testing, and Protection*, Vol. 13A, ASM International, USA, 2003, ISBN: 0-87170-705-5;
[124] Browning J.A. *US patent*, 4416421, 1983;
[125] R. W. Cahn, P. Haasen, *Physical Metallurgy*, Elsevier Science B.V., Amsterdam, The Netherlands, 1996, ISBN: 0-444-89875-1;
[126] A. Verstak, V. Baranovski, *Activated Combustion HVAF Coatings for Protection against Wear and High Temperature Corrosion*, Thermal Spray 2003: Advancing the Science and Applying the Technology, ASM International, 2003, p. 535-541;
[127] A. Verstak, V. Baranovski, *Deposition of Carbides by Activated Combustion HVAF spraying, Thermal Spray Solution: Advances in Technology and Applications*, May 10-14, Osaka, Japan, DVS-German Welding Society, 2004, p. 551-555;
[128] A. Verstak, V. Baranovski, *AC-HVAF Sprayed Tungsten Carbide: Properties and Applications*, Thermal Spray 2006: Science, Innovation, and Application, ASM International, 2006, p. 643-648;
[129] I.A. Gorlach, *The Application of High Velocity Air Fuel Process for the Deposition Coatings*, R&D Journal, 23 (30) South African Institute of Mechanical Engineering, 2008;
[130] H. Genliang, X. Kewei, S. Xunjia, Y. Xiaojing, *Flame Flow Analysis for HVOF/HVAF System by Two-Dimension Computational Fluid Dynamics Method*, Thermal Spray 2007: Global Coating Solutions, ASM International®, Materials Park, Ohio, USA, p. 163-166;

[131] M. L. Thorpe, H.J. Richter, *A Pragmatic Analysis and Comparison of HVOF Processes*, Journal of Thermal Spray Technology, Vol. 1(2) June, 1992, p. 161-170;
[132] Hobart Tafa Technologies, Inc., Technical Bulletin, 1.3.1.2, 1992;
[134] L. Jacobs, M. M. Hyland, M. De Bonte, *Comparative study of WC-Cermet Coatings Sprayed via the HVOF and HVAF Process*, Journal of Thermal Spray Technology, Vol. 7 (2), 1998, 213-219;
[133] C. Q. Wu, K. S. Zhou, C. G. Deng, C. M. Deng, *HVAF Sprayed Composite Coating with Ni based Self Fluxing Alloy and WC on a Copper Substrate*, Thermal Spray 2006: Science, Innovation, and Application (ASM International), 2006, p. 689-691;
[134] C. Dang, K. Zhou, M. Liu, J. Song, C. Wu, *Impingement Resistance of HVAF WC based Coatings*, Thermal spray 2007: Global Coating Solutions, ASM International, 2007, p. 912-915;
[135] H. Cui, K. Tao, X. Zhou, J. Zhang, *Thermal stability of nanostructured NiCrC coating prepared by HVAF spraying of cryomilled powders*, Rare Metals, Vol. 27 (4), August 2008, p. 418-424;
[136] R. Q. Guo, C. Zhang, Q. Chen, Y. Yang, N. Li, L. Liu, *Study of structure and corrosion resistance of Fe based amorphous coatings prepared by HVAF and HVOF*, Corrosion Science, Vol. 53 (2), July 2011, p. 2351-2356;
[137] S. Matthews, B. James, M. Hyland, *The role of microstructure in the mechanism of high velocity erosion if Cr3C2-NiCr thermal spray coatings*, *Part 1-As sprayed coatings*, Surface and Coatings Technology, Vol. 203 (8) January 2009, p. 1086-1093;
[138] K. Akimoto, Y. Horie, *Study of HVAF WC-Cermet Coatings*, Thermal Spray: Current status and Future Trends, High Temperature Society of Japan, Osaka, 1995, p. 313-316;
[139] L. Jacobs, M. M. Hyland, M. De Bonte, *Study of the Influence of Microstructural Properties on the sliding wear behavior of HVOF and HVAF sprayed WC Cermet Coatings*, Journal of Thermal Spray Technology, Vol. 8 (1), 1999, p. 125-132;
[140] P. Heinrich, Ch. Penszior, H. Meinaß, *Gases for HVOF flame sprazing*, Proceedings of the 4th Conference for HVOF Spraying, 13-14 November, 1997, Erding, Germany;
[141] W. Kroemmer, P. Heinrich, *Development of Coatings and the Influence of Industrial Gases on the Thermal Spray Process*, Thermal Spray 2007: Global Coating Solution, ASM International, 2007, Materials Park, Ohio, USA;
[142] A. Voronetski, V. Belashchenko, *Analysis of Potential Improvements of HVOF Based Processes*, Thermal Spray 2006: Science, Innovation, and Application (ASM International), 2006, 637-642;
[143] T. Talako, A. Ilyuschenko, A. Letsko, *SHS Powders for Thermal Spray Coating*, KONA Powder and Particle Journal, No. 27, 2009, p. 55-72;
[144] L. Thakur, N. Arora, R. Jayaganthan, R. Sood, *An investigation on erosion behavior of HVOF sprayed WC-CoCr coatings*, Applied surface Science 258 (2011) 1225-1234;
[145] Amperit Thermal Spray Powders Brochure, H.C. Starck, information on: www.tecnospray.net;
[146] P. Fauchais, G. Montavon, G. Bertrand, *From powders to thermally sprayed coatings*, Journal of Thermal Spray Technology, Vol. 19 (1-2), January 2012, p. 56-70;
[147] MBI Coatings, information on: www.mbicoatings.com;

[148] J. E. Kogel, N. C. Trivedi, J. M. Barker, S. T. Krukowski, *Indutrial Mineral and Rocks, 7th edition, Commodities, Markets and Uses*, Society of Mining, Metallurgy and Exploration, Inc. (SME), USA, 2006, ISBN: 978-0-87335-233-8;
[149] T. V. Rajan, C. P. Sharma, A. Sharma, *Heat Treatment – Principles and Techniques*, Revised Edition, Pretince-Hall of India Private Limited, New Delhi, 1992, ISBN: 81-203-0716-X;
[150] George Krauss, *Steels – Processing, Structure and Performance*, ASM International, 2005, ISBN: 0-87170-817-5;
[151] B. S. Mann, V. Arya, P. Joshi, *Advanced high-velocity oxygen-fuel coating and candidate materials for protecting LP steam turbine blades against droplet erosion*, Journal of Materials Engineering and Performance, Vol. 14(4), 2005, p. 487-494;
[152] S.J. Matthews, B.J. James, M.M. Hyland, *Microstructural influence on erosion behavior of thermal spray coatings*, Materials Characterization, Vol. 58, 2007, p. 59-64;
[153] B.S. Mann, Vivek Arya, A.K. Maiti, M.U.B. Rao, Pankaj Joshi, *Corrosion and erosion performance of HVOF/TiAlN PVD coatings and candidate materials for high pressure gate valve application*, Wear, Vol. 260, 2006, p. 75-82;
[154] X.C. Zhang, B.S. Xu, F.Z. Xuan, S.T. Tu, H.D. Wang, Y.X. Wu, *Rolling contact fatigue behavior of plasma-sprayed CrC–NiCr cermet coatings*, Wear, Vol. 265, (11–12, 26) 2008, p. 1875-1883;
[155] K. Kumari, K. Anand, M. Bellacci, M. Giannozzi, Effect of microstructure on abrasive wear behavior of thermally sprayed WC–10Co–4Cr coatings, Wear, Vol. 268, 2010, p. 1309-1319
[156] D. A. Stewart, P. H. Shipway, D. G. McCartney, *Abrasive wear behavior of conventional and nanocomposite HVOF-sprayed WC-Co Coatings*, Wear 225-229, 1999, p. 789-798;
[157] S. Zimmermann, Laufenburg and B. Brüning, *New cermet powders for HVOF spraying with improved corrosion and oxidation resistance for offshore, mining and power generation applications*, Thermal Spray 2011, Proceedings of the international Thermal Spray Conference (DVS-AMS), Sep 2011, p. 177-181;
[158] Giovanni Bolelli, Tim Börner, Francesco Bozza, Valeria Cannillo, Gennaro Cirillo, Luca Lusvarghi, *Cermet coatings with Fe-based matrix as alternative to WC-CoCr: mechanical and tribological behaviors*, Surface and Coatings Technology, 206 (19-20), 25May 2012, Pages 4079-4094;
[159] C.W. Lee, H. Han, J. Yoon, M.C. Shin, S.I. Kwun, *A study of powder mixing for high fracture toughness and wear resistance of WC-Co-Cr coatings sprayed by HVOF*, Surface and Coatings Technology, Vol. 204, 2010, p. 2223-2229
[160] I. Hulka, V. A. Şerban, K. Niemi, P. Vuoristo, J. Wolf, *Comparison of Structure and Wear Properties of Fine-Structured WC-CoCr Coatings Deposited by HVOF and HVAF Spraying Processes* , Solid State Phenomena, vol. 188, 2012, p. 422-427;
[161] A. K. Maiti, N. Mukhopadhyay, R. Raman, *Improuving the wear behaviour of WC-CoCr based HVOF Coatings by Surface Grinding*, Journal of Materials Engineering and Performance, Vol. 18(8), 2009, p. 1060-1066;
[162] G. Bolelli, L. Lusvarghi, M. Barletta, *HVOF-sprayed WC–CoCr coatings on Al alloy: Effect of the coating thickness on the tribological properties*, Wear, Vol. 267, Issues 5–8, 2009, p. 944-953;
[163] I. Hulka, D. Uţu, V. A. Şerban, *Micro-scale behaviour of HVOF sprayed WC-Co(Cr)* , Annals of faculty engineering Hunedoara – International Journal of Engineering, Tome IX, Fascicule 2, 2011;
[164] I. Hulka, V. A. Şerban, D. Uţu, *Wear resistance of WC-10Co-4Cr coatings deposited by HVAF and HVOF of thermal spray processes* , Scientific Bulletin of the

"Politehnica" University of Timisoara, Transaction of Mechanics, vol. 56(70), Iss. 2, 2011, p.13-16;
[165] V. A. Şerban, D. Uţu, I. Hulka, C. Opris, *Sliding wear behavior of different HVOF sprayed cermet coatings* , Optoelectronics and Advanced Materials, vol. 6, No 7-8, 2012, p. 764-749;
[166] D. Uţu, V. A. Şerban, H. Filipescu, *Corrosion properties of cermet coatings sprayed with high velocity oxygen fuel process*, Thomson Reuters, 4th International Conference October 23rd - 25th 2012 Hotel Voronez I, Brno, Czech Republic, 2012;
[167] V.A.Serban, C.Codrean, D. Utu, I. Hulka, *Obtaining of high performace WC-CoCr cermet coatings. Alternative Ecological Spraying Methods at Reduced Power Levels* , 6th WSEAS International Conferences on Energy, Environment, Ecosystems and Sustainable Development and landscaping, 2009, p. 188-193;
[168] M. Li, P. D. Christofides, *Multi-scale modeling and analysis of an industrial HVOF thermal spray process*, Chemical Engineering Science, Vol. 60, Issue 13, 2005, p. 3649–3669;
[169] T. Sahraoui, S. Guessasma, M. A. Jeridane, M. Hadji, *HVOF sprayed WCCo coatings: Microstructure, mechanical properties and friction moment prediction*, Materials and Design, Vol. 31, 2010, p. 1431-1437;
[170] I. Hulka, V. A. Şerban, I. Secoşan, P. Vuoristo, K. Niemi, Wear properties of CrC–37WC–18M coatings deposited by HVOF and HVAF spraying processes , Surface and Coatings Technology, Vol. 210, 2012, p. 15-20;
[171] L. M. Berger, S. Saaro, T. Naumann, M. Wiener, V. Weihnacht, S. Thiele, J. Suchánek, *Microstructure and properties of HVOF-sprayed chromium alloyed WC–Co and WC–Ni coatings*, Surface and Coatings Technology, Volume 202, Issue 18, 2008, p. 4417-4421;
[172] D.A. Stewart, P.H. Shipway, D.G. McCartney, *Abrasive wear behavior of conventional and nanocomposite HVOF sprayed WC-Co coatings*, Wear 225-229, 1999, p. 789-798;
[173] S. S. Liu, D. Sun, Z. Fan, H. Yu, H. Meng, *The influence of HVAF powder feedstock on the sliding wear behaviour of WC-NiCr coatings*, Surface and Coatings Technology, Vol. 202, 2008, p. 4893-4900;
[174] W. Fang, T. Y. Cho, J. H. Yoon, K. O. Song, S. K. Hur, S. J. Youn, H. G. Chun, *Processing optimization, surface properties and wear behavior of HVOF sprayed WC-CrC-Ni coatings*, Journal of Materials Processing Technology, Vol. 209, 2009, p. 3561-3567;
[175] J. A. Picas, A. Form, G. Matthaus, *HVOF Coatings as an alternative to hard chrome for piston and valves*, Wear, Vol. 261, 2006, p. 477-484;
[176] H. Koivuluoto, M. Honkanen, P. Vuoristo, *Cold-sprayed copper and tantalum coatings — Detailed FESEM and TEM analysis*, Surface and Coatings Technology, Vol. 204, 2010, p. 2353-2361;
[177] I. Hulka, V. A. Şerban, D. Uţu, H. Koivuluoto, P. Vuoristo, K. Niemi, *Wear behaviour of HVOF coaitngs engineered from nanostructured WC-15Co and conventional WC-10Co-4Cr powders* , Thomson Reuters, 4th International Conference October 23rd - 25th 2012 Hotel Voronez I, Brno, Czech Republic, 2012;
[178] R. C. Souza, H. J. C. Voorwald, M. O. H. Cioffi, *Fatigue strenght of HVOF sprayed Cr3C2-25NiCr and WC-10Ni on AISI 4340 steel*, Surface and Coatings Technology, Vol. 203, 2008, p.191-198;
[179] B. E. Bodger, R. T. R. Mcgram, D. A. Somerville, *The evaluation of tungsten carbide thermal spray coatings as replacements for electrodeposited chrome plating on aircraft landing gear*, Plating and Surface Finishing, Vol. 28, 1997, p. 27-31.

Table A.1 Coatings thickness

HVOF		HVAF	
Coating	Thickness [μm]	Coating	Thickness [μm]
WOKA 3654FC	300	WOKA 3654FC	310
XPT 520	303	Durmat 135lo35	253
Amperit 588	250	Durmat 251017	222
		Amperit 588	210
WOKA 7502	270	WOKA 7504	160
Amperit 618074	294	Amperit 618074	230

Table A.2 Porosity of deposited coatings

HVOF		HVAF	
Coating	Porosity vol.%	Coating	Porosity vol.%
WOKA 3654FC	0.73	WOKA 3654FC	0.93
XPT 520	1.1	Durmat 135lo35	0.92
Amperit 588	1.37	Durmat 251017	1.93
		Amperit 588	2.82
WOKA 7502	1.63	WOKA 7504	0.92
Amperit 618074	0.72	Amperit 618074	1.56

Table A.3 Roughness of as-deposited coatings

HVOF			HVAF		
Coating	Ra [μm]	Ry [μm]	Coating	Ra [μm]	Ry [μm]
WOKA 3654FC	3.64	23.49	WOKA 3654FC	4.78	36.16
XPT 520	4.54	28.49	Durmat 135lo35	3.06	22.1
Amperit 588	5.12	31.96	Durmat 251017	4.83	30.65
			Amperit 588	3.92	25.42
WOKA 7502	6.20	38.73	WOKA 7504	5.25	33.97
Amperit 618074	4.33	28.12	Amperit 618074	7.58	49.7

Table A.4 Hardness of the coatings$HV_{0.3}$

HVOF				HVAF			
Coating	Min	Max	Mean	Coating	Min	Max	Mean
WOKA 3654FC	1054	1460	1261	WOKA 3654FC	1006	1335	1152
XPT 520	834	1342	1110	Durmat 135lo35	986	1246	1148
Amperit 588	755	981	885	Durmat 251017	739	976	873
				Amperit 588	687	779	738
WOKA 7502	769	1253	769	WOKA 7504	841	1022	927
Amperit 618074	841	1218	1072	Amperit 618074	657	849	756

Table A.5 Pin-on-disk results - ball results

Coating	Ball wear scar diam [mm]	High of material removed [mm]	Ball volume loss	Ball Volumetric wear rate [mm3/(N*m)]
WOKA 3654 FC HVOF	0.466	0.004310125	3.86E-04	1.29E-08
WOKA 3654 FC HVAF	0.467	0.00432865	3.89E-04	1.30E-08
XPT 520 HVOF	0.648	0.008336945	1.44E-03	4.81E-08
Durmat 520 HVAF	1.024	0.020839547	9.02E-03	3.01E-07
Amperit 588 HVOF	0.833	0.013782715	3.95E-03	1.32E-07
Amperit 588 HVAF	0.816	0.01322531	3.63E-03	1.21E-07
Durmat 251017 HVAF	0.937	0.017444171	6.32E-03	2.11E-07
WOKA 7502 HVOF*	0.76	0.01147076	2.62E-05	
WOKA 7504 HVAF*	0.384	0.002926394	1.33E-08	
Amperit 618074 HVOF	0.485	0.004668893	4.53E-04	1.51E-08
Amperit 618074 HVAF	0.826	0.013551798	3.81E-03	1.27E-07

*tested by CSM tribometer, under 10 N normal force

Table A.6 Pin-on-disk results - coating specific wear rate

Coating	Vtot [μm^3]	Average Volumetric wear rate [$mm^3/(N*m)$]	Standard deviation of Volumetric wear rate [$mm^3/(N*m)$]
WOKA 3654 FC HVOF	3.62E-01	1.21E-05	±0.13
WOKA 3654 FC HVAF	4.15E-01	1.38E-05	±0.30
XPT 520 HVOF	2.32E-01	7.72E-06	±0.59
Durmat 520 HVAF	2.11E-02	7.05E-07	±1.90
Amperit 588 HVOF	6.40E-02	2.13E-06	±0.74
Amperit 588 HVAF	6.50E-02	2.17E-06	±0.50
Durmat 251017 HVAF	2.50E-04	4.10E-09	±2.69
WOKA 7502 HVOF*		2.62E-05	
WOKA 7504 HVAF*		2.66E-05	
Amperit 618074 HVOF	8.04E-01	4.13E-06	±0.26
Amperit 618074 HVAF	2.16E-02	7.21E-07	±1.38

*tested by CSM tribometer, under 10 N normal force